Ionospheric Imaging to Improve GPS Timing

Rose, Julian

Award date:
2011

Awarding institution:
University of Bath

Ionospheric Imaging to Improve GPS Timing

Julian Alistair Russell Rose

A thesis submitted for the degree of
Doctor of Philosophy

University of Bath
Department of Electronic and Electrical Engineering
June 2011

Abstract

Single-frequency Global Positioning System (GPS) receivers do not accurately compensate for the ionospheric delays imposed upon GPS signals. This can lead to significant errors and single-frequency systems rely upon models to compensate. This investigation applies 4D (four-dimensional) ionospheric tomography to GPS timing for the first time. The tomographic algorithm, MIDAS (Multi-Instrument Data Analysis System), is used to correct for the ionospheric delay and the results are compared to existing single and dual-frequency techniques. Days during the solar maximum years 2002, 2003 and 2004 have been chosen to display results when the ionospheric delays are large and variable. Maps of the ionospheric electron density, across Europe, are produced by using data collected from a fixed network of dual-frequency GPS receivers.

Results that improve upon the use of existing ionospheric models are achieved for fixed (static) and mobile (moving) GPS receiver scenarios. The effects of excluding all of the GPS satellites below various elevation masks, ranging from 5° to 40°, on timing solutions for fixed and mobile situations are also presented. The greatest timing accuracies when using the fixed GPS receiver technique are obtained by using the highest mask. The mobile GPS timing solutions are most accurate when satellites at lower elevations continue to be included. Furthermore, timing comparisons are made across baselines up to ~4000 km and the ionospheric errors are shown to increase with increasing baseline. GPS time transfer is then investigated and MIDAS is shown to improve the time transfer stabilities of a single-frequency GPS system. The results are comparable to the dual-frequency time transfer after ~2 hours averaging time.

Overall, the MIDAS technique provides the most accurate and most stable results (comparable to dual-frequency) for a single-frequency based GPS system. Ionospheric corrections (via MIDAS) may be broadcast to users nationally or via the internet for example, opening up the possibility of improving the accuracy and stability of single-frequency GPS systems in real-time.

Chapters at a glance

Table of Contents

List of Figures

List of Tables

List of Abbreviations

Term	Description
2D	Two Dimensional
3D	Three Dimensional
4D	Four Dimensional
ADEV	Allan Deviation
AVAR	Allan Variance
APC	Antenna Phase Center
ARP	Antenna Reference Point
AV	All in view
BBC	British Broadcasting Corporation
C/A	Coarse Acquisition code
CT	Computed Tomography
CDMA	Code Division Multiple Access
CME	Coronal Mass Ejection
CNSS	Compass Navigation Satellite System
CODE	Centre for Orbit Determination in Europe
Compass	Chinese Global Satellite Navigation System
CV	Common View
DCB	Differential Code Bias
DGPS	Differential GPS
DOP	Dilution of Precision
DSARC	Defense System Acquisition and Review Council
ECEF	Earth Centered Earth Fixed
ECI	Earth Centered Inertial
EGNOS	European Geostationary Navigation Overlay System
eLoran	Enhanced LORAN
EM	Electromagnetic
ESA	European Space Agency
EU	European Union
EUREF	Regional Reference Frame Sub-commission for Europe
EPN	European Permanent Network
FAA	Federal Aviation Administration
FDM	Frequency Division Multiplexing
FIA	Federation Internationale de l'Automobile
FM	Frequency Modulation
Galileo	European Global Satellite Navigation System
GDOP	Geometric Dilution of Precision
GEO	Geostationary Earth Orbit
GLONASS	Russian Global Navigation Satellite System
GMT	Greenwich Mean Time
GNSS	Global Navigation Satellite System
GOPE	Ondrejov, Czech Republic (IGS Station)
GPS	Global Positioning System
GPST	GPS Time
HDOP	Horizontal Dilution of Precision
HF	High Frequency
HMO	Hermanus Magnetic Observatory
ICD	Interface-Control-Document
IGRT	IGS Time (rapid product)

IGS	International GNSS Service
IGST	IGS Time (final product)
IRI	International Reference Ionosphere
KOSG	Kootwijk, Netherlands (IGS Station)
Kp	Planetary Index of geomagnetic activity
LEO	Low Earth Orbit
LORAN	Long Range Navigation System
LOS	Line of Sight
MDEV	Modified Allan Deviation
MEO	Medium Earth Orbit
MF	Medium Frequency
MIDAS	Multi-Instrument Data Analysis System
MJD	Modified Julian Day
MSAS	Multi-functional Satellite Augmentation System
NASA	National Aeronautics and Space Administration
NeQuick	Ionospheric model
NIST	National Institute of Standards and Technology
NNSS	Navy Navigation Satellite System
NOAA	National Oceanic and Atmospheric Association
NTP	Network Time Protocol
Nudet	Nuclear Detonation
ONSA	Onsala, Sweden (IGS Station)
P(Y)	Precise Code
PDOP	Position Dilution of Precision
PM	Phase Modulation
PPS	Pulse Per Second
PRN	Pseudo-random Number
PTBB	Braunschweig, Germany (IGS Station)
RINEX	Receiver Independent Exchange format
RMS	Root mean square
S4	Scintillation Index
SA	Selective Availability
SatNav	Satellite Navigation
SNR	Signal to Noise Ratio
SoL	Safety of Life
SPS	Standard Positioning Service
SV	Satellite Vehicle
TAI	International Atomic Time
TDOP	Time Dilution of Precision
TEC	Total Electron Content
TECU	TEC Units
TIC	Time Interval Counter
TOA	Time of Arrival
TOT	Time of Transmission
TW	Two-way
TWSTFT	Two-way Satellite Time and Frequency Transfer
UDP	User Defined Protocol
UK	United Kingdom
UKSSDC	UK Solar System Data Centre
URE	User Range Error
US	United States
USNDS	US Nuclear Detonation Detection System
USSR	Union of Soviet Socialist Republics
UT	Universal Time
UTC	Coordinated Universal Time
VDOP	Vertical Dilution of Precision
VHF	Very High Frequency

VILL	Villafranca, Spain (IGS Station)
VLF	Very Low Frequency
WAAS	Wide Area Augmentation System
ZECK	Zelenchukskaya, Russian Federation (IGS Station)

List of Symbols

Symbol	Description
P	Pseudorange
t_r	Time of reception (TOA)
t_t	Time of transmission (TOT)
b_{rx}	Receiver clock bias (RCB)
b_{sv}	Satellite clock bias
T_{sagn}	Sagnac bias
T_{trop}	Tropospheric delay
T_{iono}	Ionospheric delay
$\Delta_s^{1\to 2}t$	Small satellite P1 to P2 bias
$\Delta_s^1 t$	Single-frequency clock bias
$\Delta_s t$	Dual-frequency clock bias
$\vec{S}$	Antenna position
S'	Modulus of the satellite center of mass position vector
$\Delta_v S$	Vertical component of the antenna offset
$\vec{S}'$	Position vector of the satellite center of mass
Ω	Angular velocity of the Earth
$\vec{A}_i,\ \vec{B}_i$	Amplitude coefficients of the harmonic
c	Speed of light
$\dot{\lvert r \rvert}$	Rate of change of distance between satellite and receiver
Δr	Uncertainty on the range
Δt_t	Uncertainty of the transmission time
$\dot{\vec{S}}$	Satellite velocity
x, y, z	Position coordinates
$\vec{r}_i$	Receiver to satellite vector
$\hat{r}_i$	Unit vector
G	Geometry matrix
$u_{r_i}^x\ ,\ u_{r_i}^y,\ u_{r_i}^z$	Components of $\hat{r}_i$
$\vec{\Omega}$	Rotation vector of the Earth
$\vec{R}$	Receiver position vector
$T_{\pi/2,0} \approx 2.44m$	Azimuth delay at sea level
h	Receiver altitude
$\Delta_s' t$	Satellite specific error
$\Delta_s^r t$	Satellite relativistic effects
$\dot{S}$	Rate of change of distance (see S above)

N	Electron concentration
dl	Ray-path to voxel intersection
P_0	Ionosphere-free pseudorange
P_1, P_2	Pseudoranges obtained from precise P-code signal
L_1, L_2	Recorded carrier phases of the signal
λ	Carrier wavelength
$\Delta\bar{x}$	Positioning error
ρ	True geometric range between satellite and receiver
$\Delta\bar{\rho}_c$	Pseudorange errors to each satellite
σ_R^2	Variance
t_{rx1} , t_{rx2}	Timing solutions of stations 1 and 2
b_{rx1} , b_{rx2}	RCB calculated by the timing solutions for stations 1 and 2
$b_{rx1(CODE)}$, $b_{rx2(CODE)}$	RCB calculated by the CODE for stations 1 and 2
ω_p	Angular plasma frequency
ω_B	Electron gyrofrequency
e	Charge of an electron
ε_0	Permittivity of free space
m_e	Rest mass of an electron
μ_p, μ_g	Phase and group refractive indices
v_p, v_g	Phase and group velocities
ΔS_p	Carrier phase advance
ΔS_g	Group delay
t_{GPS}	GPS Time
t_A, t_B	Clock A and B
σ_y^2	Allan variance
τ	Averaging time
y_i	*i*th of M fractional frequency values averaged over τ

Acknowledgements

A PhD is a memorable journey and I must say a big thank you to all of my family and friends who have supported me along the way. I am extremely grateful to my Mother and Father, Judith and Stephen Rose, my Grandparents, Charles and Joyce Coxall and my partner, Victoria Stewart. Their strength, encouragement and great humour have fuelled my dedication over the years.

I wish to thank my supervisors; Cathryn Mitchell and Robert Watson for their outstanding friendship, advice and support throughout my time at the University of Bath. I would also like to thank Damien Allain and Jenna Tong for their general advice and tips that have helped along the way. I really value my colleagues and the light hearted and friendly atmosphere that we work in.

I am grateful to the Engineering and Physical Sciences Research Council (EPSRC) for funding this project. I would also like to thank the International GNSS (Global Navigation Satellite System) Service (IGS) and European Permanent Network (EPN) for providing valuable data. I am also grateful to Matlab, which I used throughout my PhD and to AlaVar, which I used to verify the stability results.

Chapter 1

1. Introduction

1.1 Background

Since the dawn of time the human race has endeavoured to explore and navigate the Earth. Accurate timekeeping plays a fundamental role in the navigational accuracy and throughout history various tools have been used to do it. Natural bodies such as the Sun, Moon and the stars enable rough estimates of time and position to be found. The John Harrison clock enabled world exploration to be performed to a new degree of accuracy in the eighteenth century simply by providing maritime explorers with a reference, Greenwich Mean Time (GMT).

More and more sophisticated navigation techniques were developed in the twentieth century, largely fuelled by the fight for military advantage during World Wars I and II. Radio waves were heavily exploited and their potential for all-weather positioning was realised. Several systems were developed that covered vast and even global geographical areas. The United States (US) developed Omega in 1968. Eight antenna stations and very low frequencies (VLF) were sufficient to achieve accuracies of 3 to 6 km across the globe (Larijani 1998).

In 1973 the Global Positioning System (GPS) was granted approval by the US Defense System Acquisition and Review Council (DSARC). This marked the dawn of the world's first truly global and accurate positioning system. However, it did not become fully operational until 1995. The constellation consists of roughly 30 satellites and, conservatively, navigational accuracies to within 10 m are achievable.

Signals from at least four GPS satellites are required to compute a user's four-dimensional (4D) solution (longitude, latitude, altitude and time). However, the solution is corrupted by many error sources, which may be space-based, ground-based or due to the propagation path. Most notably, before the GPS signals reach Earth, they must travel through the ionosphere. This part of the atmosphere lies between roughly 80 and 1000 km altitude and imposes one of the largest errors upon a single-frequency GPS system. The effect is dependent upon many factors: solar activity, season and time of day are just a few.

Every eleven years or so the radiation released by the sun increases and peaks at what is called solar maximum. This increase in solar activity may last for a couple of years and the rest of the so called 'solar cycle' may be denoted the solar minimum. Huge outbursts of radiation are released from the sun during solar maximum. These travel towards Earth and give rise to increased levels of free electrons and ions in the ionosphere. Correspondingly, the GPS signals suffer greater levels of refraction and retardation as they propagate through it. If left uncorrected, the ionospheric error may measure between 10 and 20 m or more.

The cheapest and most common GPS receivers are 'single-frequency' (L1), which are widely used for satellite navigation and do not adequately compensate for the ionospheric delay. These GPS receivers may be found in purpose built navigational devices, cars, mobile phones and cameras to say the least. Standard single-frequency GPS receivers use the Klobuchar model (named after its creator) to correct for this error (Klobuchar 1987). The corrections are broadcast by the GPS satellites and are designed to offer at least 50% RMS correction. The model is largely a compromise between computational requirements and accuracy. It has been shown to behave poorly during stormy ionospheric periods and there are various techniques that better compensate for this delay.

Dual-frequency GPS receivers make use of two GPS frequencies (L1 and L2) to measure the ionospheric delay. This is widely considered as the best method of ionospheric compensation. However, dual-frequency GPS receivers are much larger and more expensive than single-frequency receivers and they require calibration.

Another technique, known as ionospheric tomography, may be used to mitigate the ionospheric delay. Tomography consists of a collection of external measurements that propagate through the medium and are used to form a picture of the internal make-up of the structure. In this case, GPS data are collected from hundreds of globally distributed ground-based GPS receiver stations. These data, together with a suitable algorithm, are used image the ionosphere. Global, 4D ionospheric maps of electron density are produced in order to calculate the expected ionospheric delays. Since these systems actually monitor the ionosphere, they may be used in real-time and are shown to perform well under both stormy and quiet ionospheric conditions.

The modern world now relies upon GPS for accurate timing and navigation. Just a few of the tens of applications are as follows: mobile phone networks, seismic activity monitoring, wildlife tracking, international banking, power systems and satellite navigation.

1.2 Project Objectives

Aim: to use ionospheric imaging to improve GPS timing

Objectives:

- compare existing GPS timing solutions to a new technique that uses ionospheric tomography
- investigate the effects of various elevation masks on GPS timing accuracy
- investigate the use of ionospheric tomography in GPS time transfer

1.3 Thesis Overview

The Global Positioning System (GPS) is described in Chapter 2. To start with, the GPS constellation is explained. This is followed by information about GPS receivers and the satellites themselves. Next, the navigation message (broadcast by the satellites) is introduced. The GPS solution and pseudoranging technique are then described. In continuation, the satellite geometry, the GPS

error budget and error sources are discussed. This leads to information about the accuracy of GPS and Differential GPS (DGPS). This is followed by a discussion regarding the vulnerabilities of GPS and hence jamming and the need to provide a backup. A great number of GPS applications are then presented, before the discussion of other Global Navigation Satellite Systems (GNSS), including GLONASS, Galileo and Compass.

The Earth's atmosphere and observation techniques are discussed in Chapter 3. Following an introduction to the thermal layers of the atmosphere, is information about electromagnetic waves and how the ionosphere may be used to our advantage when it comes to high frequency communications. The Plasmasphere is then introduced, followed by more extensive information about the ionosphere, its various layers and its electron density profile. The troposphere and ground environment are then discussed. The origins of tomography are outlined, followed by information about GPS and tomography. This leads to a subsection on ionospheric imaging and consequently MIDAS (tomographic algorithm used in this project).

Information about GPS timing forms Chapter 4. Firstly, the importance of time is outlined. This is followed by descriptions of time (GPST and UTC) and includes information on how the GPS (and GPST) is managed/maintained, from a timing point of view. Finally, time transfer techniques are described in detail.

Chapter 5 is the first of three results chapters. The 4D tomographic algorithm, Multi-Instrument Data Analysis System (MIDAS), is used to mitigate the ionospheric error in a single-frequency GPS solution. This technique is compared to three other single-frequency solutions: one with no ionospheric correction, one that uses the International Reference Ionosphere (IRI) 2001 model, and finally one that uses the existing broadcast Klobuchar model. The MIDAS solution is also compared to a dual-frequency system. Maps of ionospheric electron density, across Europe, are produced for days during the solar maximum year 2002, and a famous storm in October 2003, in order to display results when ionospheric delays are large and variable. Results are presented for fixed (stationary) and mobile (moving) GPS receiver scenarios. MIDAS yields the most accurate single-frequency solutions, which are comparable to those from the dual-frequency system.

Chapter 6 builds upon the work presented in Chapter 5. MIDAS is now used, together with elevation masks, to improve the single-frequency GPS system. Signals originating from low elevation GPS satellites are often excluded from a GPS solution because they undergo greater multipath and atmospheric delays. However, their exclusion can degrade the overall satellite geometry, which can adversely affect the resulting solution. The aim is to find a balance between the choice of elevation mask and the knock-on effects of: multipath, propagation delays and satellite geometry. Three single-frequency solutions are compared (no correction, Klobuchar and MIDAS) together with the dual-frequency solution. Once again, days from 2002 and the October 2003 storm are investigated. The study focuses on Europe. Elevation masks range from 5° to 40°. MIDAS offers the most accurate and least variable single-frequency timing solutions. The most accurate results for the fixed receiver scenario are obtained using a 40° mask. For the case of the mobile receiver, a mask between 10° and 20° offers the best results.

Chapter 7 marks a natural progression from the previous work. The aim is to use MIDAS to improve the time transfer capabilities of single-frequency GPS. Periods in March 2003 and February 2004 have been used to display results when the ionospheric delays are large and variable. Five European test sites, ranging from 320 to 3760 km apart, are used to investigate ten different time transfer links. In general, the time transfer accuracies and stabilities improve with decreasing baseline. The adverse effect of the ionospheric delay is distinctly noticeable for the solutions that either have no ionospheric correction or use the Klobuchar model. MIDAS provides the most accurate and most stable single-frequency time transfers. Although the dual-frequency system tends to outperform MIDAS, their results are not dissimilar.

Conclusions from the main results and overall project are given in Chapter 8. The future directions of the work are also discussed.

Maps of Total Electron Content (TEC) are shown for several days in 2002 and 2003 in Appendix A. There are twelve maps per day, showing the TEC every two hours. Appendix B lists journal and conference publications.

Chapter 2

2. GPS

2.1 The GPS

The Global Positioning System (GPS) was granted approval by the US Defense System Acquisition and Review Council (DSARC) in December 1973. This marked the dawn of the world's first truly global and accurate positioning system.

The satellites were manufactured by Rockwell International and launched from 1978 onwards. The system began with only four satellites and so could not provide global coverage. However, four satellites are sufficient to provide a user with three a dimensional (3D) positioning solution, assuming each satellite is visible simultaneously. A single satellite failure however would have significantly compromised the solution and many more satellites were required to fulfil the goal of global coverage. Inevitably therefore, the system developed into what it is today and its basic operation remains essentially identical.

The GPS currently consists of approximately thirty satellites in Medium Earth Orbit (MEO), at an altitude of 20,200 km above sea level. They are restricted to six orbital planes, with typically four satellites in each (plus a spare), inclined at 55° to the equator. This ensures that at least four satellites are visible from virtually any location on Earth at any given time. Four satellites enable the user to solve for their longitude, latitude, altitude and time. Fewer satellites may be used provided there are fewer unknowns.

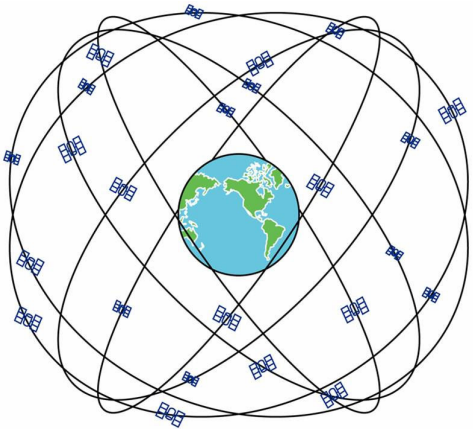

Figure 2.1 – GPS satellite constellation

GPS satellites have an orbital period of approximately 11 hrs 58 mins; passing the same point on Earth once every sidereal day. This is the time taken for the Earth to rotate about its axis ~23 hrs 56 mins 4 s. However, Choi et al., (2004) state that the satellite repeat period varies between satellites and may not be quite sidereal. They have found that the orbit repeat time is ~8 s earlier than sidereal. These findings are most relevant to high-rate GPS users, whom may achieve greater precision by taking this into account.

A network of worldwide ground stations monitors and maintains the GPS. This network provides data that enables future satellite positions to be calculated; these are crucial for calculating the GPS receiver position. The master control station uploads this information to the satellites on a daily basis, along with the satellite clock corrections in order to maintain the system as precisely as possible. Finally, the satellite positions are transmitted to the receiver via the navigation message, which, along with four pseudoranges (explained shortly), allows the receiver's position and time (x, y, z, t) to be estimated using a least squares technique.

2.2 The GPS Receiver

A GPS receiver generally uses a pseudoranging method in order to compute a solution. This is where the ranges between the GPS receiver and the satellites in view are calculated using time of arrival (TOA) techniques. The time of transmission (TOT) from the satellite is recorded within the navigation message and the receiver records the time of arrival. More specifically, the GPS receiver locally generates an identical code to that which is broadcast from the satellites. The timing alignment will differ between the received code and the locally generated code. This time difference yields the pseudorange, or distance, between the receiver and satellite (Larijani 1998). Receivers rely on time difference observations from multiple satellites for the navigation/timing solution.

2.3 GPS Satellites

The GPS satellites broadcast two frequencies, L_1 (1575.42 MHz) and L_2 (1227.6 MHz), which are generated synchronously. Dual-frequency receivers take advantage of this by computing a highly accurate ionospheric correction, since two frequencies allow the ionospheric group delay to be found (Parkinson and Spilker 1996). Most civilian receivers offer only single-frequency capabilities. Such products utilise the L_1 signal and employ a broadcast model to correct for the ionosphere (Klobuchar 1987). This model was designed with efficiency in mind; using as little computational power as possible. Klobuchar (1987) explains how the solution required a compromise between; computational complexity, the number of available coefficients, the likely application areas for single-frequency receivers and the Total Electron Content (TEC) information at the time. There were eight coefficients available for the resulting ionospheric correction algorithm, which is transmitted within the satellite message. At the time of conception, they were typically updated once every ten days. In addition, there were a number of assumptions and approximations made in order to maintain the model's simplicity. Notably, any improvements adding to the complexity failed to yield proportionally better results and thus the final model resulted in a typical 50% RMS ionospheric correction. This model continues to improve the accuracy of single-frequency GPS receivers today.

2.4 The GPS Navigation Message

The navigation message is a vital part of the GPS solution. It provides the user with the data required to achieve a navigational solution, a geodetic survey or a time transfer solution (Parkinson and Spilker 1996). The GPS ground station control segment uploads the navigation data to each satellite everyday, or sooner if the user range error (URE) lies outside the specification. Subsequently the satellites broadcast the information to the user.

The message is required to provide the user with the following:

- The precise time at which the signal is transmitted (the TOT)
- The precise satellite position at the time of transmission
- Model data for single-frequency receivers to correct for the ionosphere, given the time and user location (Klobuchar model)
- Time transfer data, by providing conversion parameters for GPS Time to Coordinated Universal Time (UTC)
- Quality and accuracy of satellite data
- Entire GPS constellation data, allowing the healthiest (most accurate) set of satellites to be included in the solution
- Data to keep track of the P(Y) code from the C/A code.

2.5 Pseudorange and the GPS Solution

The successful acquisition of the GPS navigation message enables a GPS receiver to compute a solution using pseudoranging techniques. The so called pseudorange between a given satellite and a receiver essentially represents the separation between the two, in metres. This distance is calculated using time of arrival (TOA) techniques. By obtaining and hence subtracting the GPS signal's TOA from the TOT, the propagation period remains. This value is then multiplied by the speed of light, resulting in the 'pseudorange' between satellite and receiver. A simplified example of solving for a GPS receiver's 2D position using just three satellites is shown here:

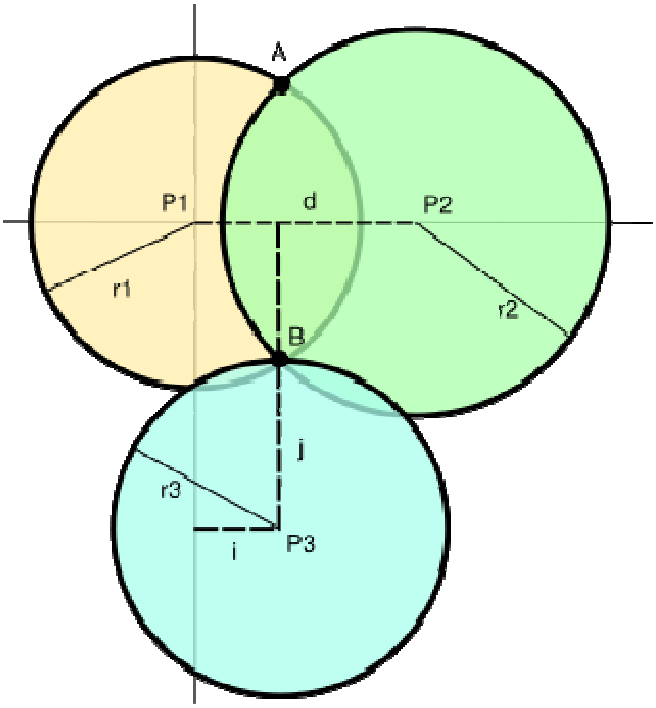

Figure 2.2 – Trilateration: intersecting pseudoranges

This method is known as trilateration. The three satellite positions are assumed to be known, together with their corresponding pseudoranges. Thus the receiver may effectively be thought to be located somewhere on the surface of an imaginary sphere, centered on each satellite. The distance between each satellite and receiver is represented by the radius. When the pseudoranges of the three satellites have been found, the receiver computes a first approximation of its 2D position. The overlapping pseudoranges intersect at the GPS receiver's location, ignoring any errors.

B represents the location of the GPS receiver. **P1, P2** and **P3** act as reference points and represent the positions of the satellites. The radius of each sphere is represented by **r1, r2** and **r3**. Measuring **r1** narrows the receiver position down to a circle. Measuring **r2** narrows it down to two points, **A** and **B**. Further still, measuring **r3** yields the receiver's coordinates at **B**. Further measurements help to reduce the error.

Additionally, as more and more satellites come into view, the receiver informatively selects the best group to use in the solution. The selection is determined by the geometric dilution of precision (GDOP), which illustrates which satellites are in the best relative positions for a good solution and those

which would provide a poor solution. Other important factors considered are as follows; multipath, the propagation path lengths through the ionosphere and the signal to noise ratio. Typically, satellites below an elevation angle of 15° may be excluded. The final solution is then found using a least squares method, resulting in the receiver coordinates and receiver clock bias. Of course the results are subject to several errors, which directly affect the quality of the GPS solution.

2.6 Satellite Geometry

The accuracy of a GPS solution greatly depends upon the ability to compensate for the errors imposed upon the signals during propagation, which can be directly affected by the geometric configuration of the satellites.

The satellite configuration is measured by the Geometric Dilution of Precision (GDOP), which corresponds to the proximity of the GPS satellites to one another. A poor GDOP is recorded when satellites are close together; making it difficult to calculate a precise location. This is directly affected by the local environment. A satellite with a building blocking its line of sight (LOS) with the receiver will hinder the GDOP, lessening the potential angular separation available between other satellites.

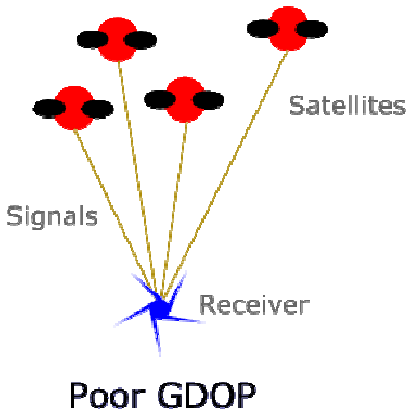

Figure 2.3 – Poor GDOP

Ideally the GDOP would be zero. But realistically a good GDOP occurs when satellites are spread-out, with wide angles of separation between them.

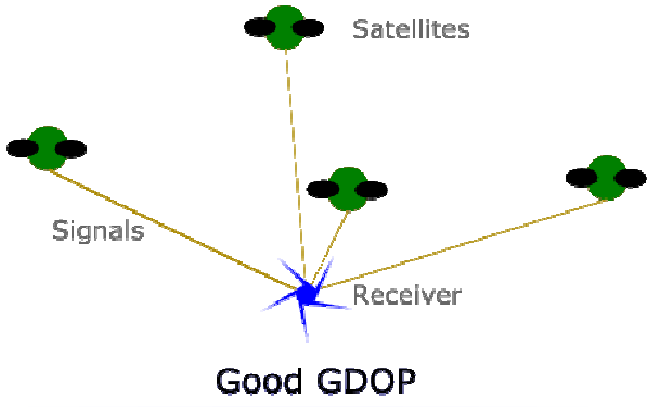

Figure 2.4 – Good GDOP

GPS receivers analyse different combinations of satellites and use the optimal configuration; the setup being recorded as GDOP. Thus the overall positioning accuracy may be estimated by multiplying the ranging accuracy by the GDOP.

2.7 GPS Error Budget

Atmospheric and environmental affects are the main contributors towards the GPS error budget (Langley 1997). For single-frequency GPS users, the ionospheric error usually dominates (Parkinson and Spilker 1996). Selective Availability (SA), the intentional degradation of the signal, used to dominate, however, SA no longer exists and was removed in May 2000. SA, according to Langley (1997), typically produced an RMS range error of 24 m. A typical GPS error budget is as follows:

ERROR SOURCE	Typical RMS error [ns]	Typical RMS range error [m]
Satellite Vehicle Clock	7	2.0
Antenna coordinates	10	3.0
Ephemeris	8	2.5
Troposphere (wet component)	2	0.7
Troposphere (dry component)	22	6.7
Ionosphere	23	7.0
Multipath	4	1.2
Receiver noise	3	0.9
Receiver software	2	0.7
Instrumental delays	2	0.7

Table 2.1 – Error Budget

These values vary slightly between sources, for example Kaplan and Hegarty (2006), nevertheless the important point to note is that the ionosphere imposes one of the most considerable errors and this project focuses on using tomography to overcome that error. The total tropospheric error is approximated using Equation 5.21.

2.8 Error Sources

Error sources may be divided into four main segments, depending upon their place of origin.

Errors at the Receiver		
1	**Antenna Phase Center Offset and Variation**	Offset between Antenna Phase Center (APC) and Antenna Reference Point (ARP). Note: signal measurement is referred to APC.
2	**Local Environment Effects (Multipath)**	Reflections from nearby structures delay and weaken signals. Attenuation depends upon reflector material, polarisation & incident angle of the GPS antenna.
3	**Receiver Noise**	Unwanted electrical signals due to switching transients and radiating electromagnetic signals.
4	**Receiver Software**	Software, adopted constants and reference frames may vary between receivers.
5	**Instrumental Delays**	Delays are imposed by hardware, such as propagation delays due to cabling, and should be calibrated for.

Table 2.2 – Errors at the GPS Receiver

Errors at the Ground Station		
1	**Solid Earth Tides**	Displace ground station coordinates.
2	**Earth Rotational Deformation**	Caused by changes in polar motion, which alter the Earth's centrifugal force and displaces the ground station position.
3	**Plate Tectonic Motion**	Can displace ground station coordinates by several cm a year.
4	**Ocean Loading**	The ocean tide and sheer mass can perturb ground station coordinates. The closer to the ocean shore, the more affected.
5	**Atmospheric Tides**	The atmosphere's varying pressure distribution produces an almost negligible affect.
6	**Antenna Eccentricity**	The measured distance between the GPS Receiver's ARP and local geodetic markers (geographic reference points) may not be exact.
7	**Sagnac**	Must account for the rotation of the Earth during signal transit.

Table 2.3 – Errors at the Ground Station

Errors during Signal Propagation		
1	**Ionospheric Delay**	Free electrons, predominantly during daytime, perturb the GPS signal. Delay is proportional to the number of electrons along the signal path. Sunspot activity, altitude, local time and season can affect the electron density.
2	**Tropospheric Delay**	Refraction due to water vapour.
3	**Relativistic Effects**	Earth's gravitational field causes the electromagnetic signal to curve in space-time, imposing a time delay; according to Einstein's theory of General Relativity. Also, due to the satellite's speed, its clock should run slower, however, it will also speed up due to a minute gravitational influence. The result is a slightly faster clock.

Table 2.4 – Errors during Signal Propagation

Errors at the Satellite		
1	**SV Center of Mass and Antenna Phase Center offset**	Ephemeris is calculated with respect to the satellites centre of mass, whereas signal measurements use the APC as a reference. An offset should hence be included if computing the range using GPS orbit information.
2	**GPS Yaw Attitude Model**	This represents the variation in rotational motion about the Z-axis, since the APC does not lie exactly on it. If the yaw attitude changes, so does the APC, with respect to a receiver.
3	**Signal Wrap Around Effect**	If the transmitter or receiver antenna orientation (reference direction) is changed, then there will be a change in the transmitted or measured phase. This affects carrier phase observables, which depend upon antenna orientations and the direction of line of sight.
4	**Satellite Clock Bias**	Satellite specific error and satellite relativistic effects.

Table 2.5 – Errors at the Satellite

To obtain the most accurate GPS results, many of the above errors should be estimated, measured or calculated. Though admittedly, several of the above are virtually small enough to be deemed negligible in many applications. More detailed definitions may be found in Byun (1998).

2.9 Accuracy and DGPS

The initial specification for the C/A standard positioning service (SPS), or civilian service as it is more commonly known, gives an expected solution accuracy of 100 m (Langley 1997). When SA was turned off, the accuracy measurably increased to between ~15 and 30 m. In contrast the higher chip-rate P(Y) signal can provide the military with approximately 30 cm accuracy.

Aircraft landing and harbour navigation applications require high degrees of accuracy and may hence use a system called Differential GPS (DGPS). This involves a reference station at a fixed known position and a remote receiver. Since the location of the reference receiver is accurately known and the remote receiver is relatively nearby (tens of km or less), several errors common to both receivers may cancel. Atmospheric errors are almost completely cancelled; the closer together the receivers, the greater the accuracy. In addition, ephemeris and satellite clock errors are completely removed. Grewal et al., (2000) comprehensively describes DGPS.

2.10 GPS Jamming and Backup

GPS signals are highly susceptible to interference because they are so weak by the time they reach Earth. This is generally true for all GNSS (e.g. Galileo and others), due to the low powered nature of the signals and their propagation paths. Interference may be intentional; 'jamming' by an enemy perhaps, or unintentional; possibly due to nearby electrical equipment. GNSS are also vulnerable to space weather events.

Thus there is a need for a backup; particularly as GPS (and GNSS in general) is used for more and more everyday applications. A ground-based system may be most suitable because it would depend upon different technology and propagation techniques when compared to space-based systems. As stated in Roth et al. (2005), an extensive study in the US confirmed that an Enhanced Loran (eLoran) system could be used for aviation, marine navigation and time and frequency applications, as well as disseminating UTC, essentially acting as

a GPS backup. Incidentally, Loran was developed not long after World War II and more information may be found in Hlavac and Stacey (2004).

eLoran signals have a 3 km wavelength; ~10,000 times greater than GPS. Antennas inside buildings and those in urban areas are therefore able to receive such signals, which is an advantage over GPS. The US and other parts of the world, such as the United Kingdom (UK) and France, have conducted performance tests, yielding results comparable to the Global Positioning System (Roth et al. 2005). However, this is only for basic time and frequency applications and is not the case for high precision functions. eLoran looks set to be a crucial system for GPS backup.

Laboratories that currently depend upon GPS for precise timing information may also employ a stable oscillator. If for example there is a GPS outage, then the oscillator will aim to maintain the delivery of accurate timing information e.g. If large timing errors are detected then the setup may allow for them to be rejected and the laboratory may then 'coast' on the oscillator until the condition is rectified (Geier et al. 1995). However, this is not always possible because the costs of a stable oscillator may be much higher than the cost of a simple GPS receiver.

In comparison to the hardware based approach above, a cheaper, software based method may be used instead to help mitigate the effects of a GPS outage. Receiver Autonomous Integrity Monitoring (RAIM) algorithms may be applied to the GPS receiver internally, which automatically detects and removes failed satellites from inclusion in the timing solution (Geier et al. 1995).

2.11 GPS Applications

GPS has provided the means for anyone to solve for their position, velocity and time at virtually any point on Earth. Inevitably the system has been exploited and applied to several areas, creating evermore GNSS applications.

Application area	*Applications*
Civilian	Navigation
Military	Precise navigation, weapon guidance systems, intelligence and reconnaissance
Safety of Life	Emergency services, search and rescue, life raft/jacket transponder
Scientific	Atmospheric science, geophysics and geology, oceanography, archaeology, wildlife monitoring
Commercial and Industrial	Telecommunications synchronisation, agriculture, cartography and surveying
Transportation	Fleet and asset tracking, vehicle theft tracking, land, sea and aircraft guidance, road pricing
Sport and Recreational	Exploration, accurate timing, competitor tracking and monitoring

Table 2.6 – GPS Application Overview

2.11.1 Satellite Navigation

Modern vehicles are equipped with satellite navigation, or so called ‘SatNav’. These systems combine mapping data, with single-frequency GPS positioning, to provide navigational assistance to the user. Cars use a discretely mounted antenna and clever software, which ‘snaps-to-road’, to provide a suitable positioning output. Therefore, even if the GPS solution suggested your vehicle was 10 m offset from the current road, placing it in a field for example, the SatNav software would simply assume you were on the closest and most likely road. The end-user only witnesses the outcome of this process and so may unwittingly rely on not so accurate GPS solutions.

It is worth bearing in mind that the forthcoming solar maximum could give rise to much larger positioning errors and the software may place the user on the wrong road entirely. Specialised SatNav devices for hiking, walking and marine exploration also exist.

2.11.2 Synchronisation

Atomic clock-level accuracy may be achieved globally with the possession of a GPS receiver (Anon 2008a). For instance, the uncertainty of a caesium fountain is 1 part in 10^{-16} at an averaging time of 10 days (after 10 days of continuous operation), according to the datasheet of a Symmetricom product: see http://www.symmetricom.com/link.cfm?lid=7832. The free availability of such a precise time measurement is sufficient in the synchronisation of financial networks, communications systems and electrical power grids. Companies take advantage of this and ultimately save money, since owning an expensive atomic clock of their own becomes unnecessary.

GPS is used to maintain synchronisation between the base stations for wireless telephone and data networks. More simply it is used to time-stamp transactions, allowing businesses to accurately record and trace such events. *GPS Time is synchronised throughout the GPS satellite constellation and so no matter where you are in the world, employing GPS for timing purposes ensures global synchronisation*, which is another reason why it is possible to accurately network computers worldwide. If signals arrived out of synch, data would become corrupt and transactions could be rendered invalid.

2.12 Other GNSS

2.12.1 GLONASS

Though this project utilises only the GPS, the same principles may be applied to the Russian Global Navigation Satellite System, GLONASS, which was created in the mid-1970's by the former USSR. GLONASS was originally intended solely for military use, however, it also offers civilian capabilities. The Russian Ministry of Defence control and operate the system, which shares similar design characteristics to GPS.

The GLONASS constellation comprises 24 satellites divided equally between three orbital planes. They orbit every 11 hrs and 15 mins at an altitude of 19,100

km above the Earth's surface, with an inclination of 64.8° to the equator. Ground stations upload-to and monitor the constellation. This system can also provide users with a 3D fix, as well as time information. In fact, the accuracies available to the Russian military and civilian users are much the same as those obtained from GPS (Kaplan and Hegarty 2006).

Nevertheless, one major difference between GPS and GLONASS is evident by the manner in which the satellite signals are multiplexed. The former uses Code Division Multiple Access (CDMA), whereas GLONASS employs Frequency Division Multiplexing (FDM). The two GLONASS carrier signals L_1 and L_2 occupy the frequency bands as follows; 1.597 GHz – 1.617 GHz and 1.240 GHz – 1.260 GHz respectively. FDM enables the C/A and P codes to be the same throughout, whereas the signal frequencies differ for each satellite.

Both the GLONASS L_1 and L_2 signals are modulated by the P code. The C/A code modulates the L_1 signal only. Unlike GPS, the GLONASS P code is freely accessible. This is particularly advantageous for time transfer because the P code pseudorange measurements are much more precise than both the GPS or GLONASS C/A code measurements and the ionospheric delays may be measured accurately using both signals (Foks 2004).

2.12.2 Galileo

The European satellite navigation system, Galileo, is another worldwide, space based radio navigation system, following GPS and GLONASS. Since the latter two systems are already operational, any problems they have encountered, common to space-based radio navigation systems, have essentially been overcome and hence provide the Galileo project with an unprecedented level of information. Such knowledge has enabled the design of Galileo to feature enhanced signals; allowing for easier tracking and acquiring of signals and increased resistance to interference (GSA 2008).

In continuation, the European Union (EU), together with the European Space Agency (ESA) run and endorse the Galileo program. In the early 1990's the EU realised the need for their own global positioning system; one which did not rely upon other nations that could stop the use of service at anytime. Galileo will be

under civilian control, which is a significant attraction in comparison to the militarily controlled American and Russian systems.

Incidentally, 2005 witnessed the launch of GIOVE-A; the first Galileo test satellite. In March 2008, the second test satellite was launched; GIOVE-B. However, the constellation will not be complete for some years. In total there will be 30 satellites, restricted to three orbital planes and inclined at 56° to the equator. Each satellite vehicle (SV) should take approximately 14 hrs to orbit the Earth and all three planes will contain one spare satellite in case of failure. The constellation should enable between 6 and 8 satellites to be visible from any location on Earth, whilst ground stations may monitor and upload data to the satellites (Anon 2007).

2.12.3 Compass

The Compass Navigation Satellite System (CNSS) is China's global satellite navigation system. It will consist of thirty MEO satellites and five geostationary Earth orbit (GEO) satellites. The latter will offer localised enhancements to the service for China-based users. Three GEO satellites are already in orbit and the first MEO satellite was launched in 2007 (Dong et al. 2008).

2.13 Summary

In conclusion, the accuracy of global navigation satellite systems (GNSS) looks set to improve. It is likely to be common place for modern receivers to use a combination of GPS, GLONASS and Galileo signals. This will increase the number of satellites in view at any given time and will improve the overall satellite geometry. This will result in a more dependable and reliable GNSS era, leading to improvements in positioning and timing accuracies.

Chapter 3

3. Earth's atmosphere, tomography and MIDAS

3.1 Introduction to the Atmosphere

The GPS satellites occupy a medium Earth orbit (MEO) set at an altitude of 20,200 km. Thus the path of a GPS signal (from SV to Earth) passes through several layers of the atmosphere. Typically, the layers are either defined by temperature profile or electron density. The former is represented by Figure 3.1 which shows the thermal characteristics of the Thermosphere, Mesosphere, Stratosphere and Troposphere.

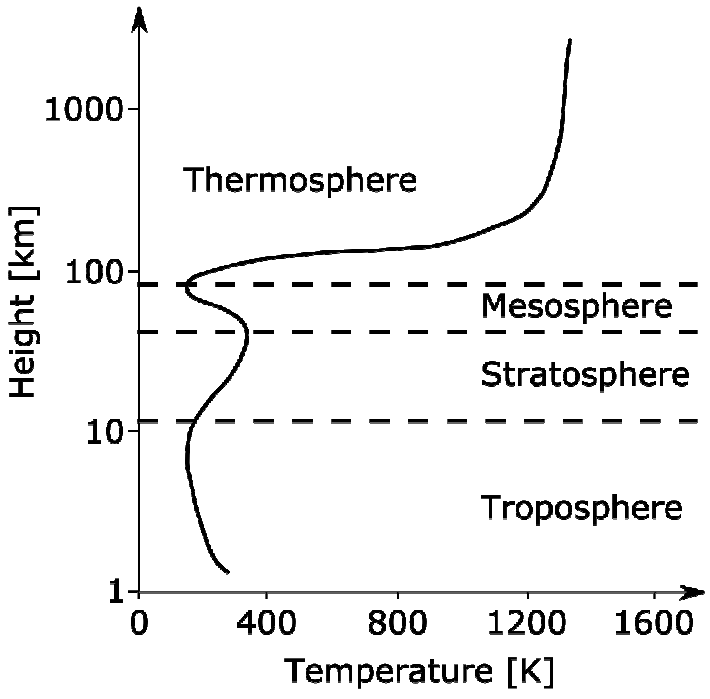

Figure 3.1 – Thermal layers of the atmosphere

However, since electromagnetic wave propagation is significantly affected by free electrons, the division of the atmosphere by electron density is most relevant here. Thus the atmosphere is divided into different layers and in conjunction with the path of a GPS signal, their names are as follows; the signal first passes through the ionised plasmasphere, followed by the ionised ionosphere and then the troposphere (affected by variable amounts of water vapour), before being subject to local environment effects at the Earth-based GPS receiver. These layers and effects are discussed in the following subsections.

3.2 The Plasmasphere

The boundaries of the plasmasphere are dependent upon solar activity and so are constantly changing, but may be considered to range from ~1000 km – ~19,000 km in altitude. The particle densities in the Plasmasphere range from $10^4/cm^3$ at 1000 km and 10-100/cm^3 at the outer edge (Tascione 1994).

The plasmasphere is not considered to have a great impact upon GPS signals and in any case, ionospheric modelling techniques can be extended to include parts of this region. For instance, the altitude of the ionospheric model could be increased. Figure 3.2, courtesy of NASA (2008), shows the Sun-Earth environment, whereby ejections from the Sun are interacting with the Earth's Magnetosphere.

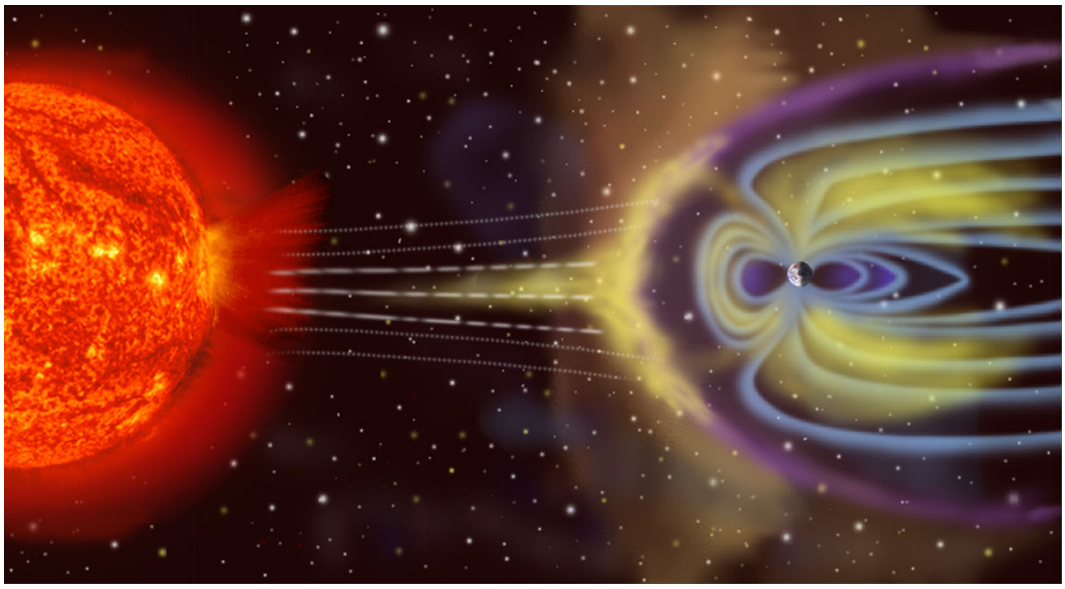

Figure 3.2 – Magnetosphere

3.3 The Ionosphere

The ionosphere has considerably greater electron content than that of the plasmasphere and thus has the greatest atmospheric effect upon GPS signals. The lower and upper boundaries are as follows; ~80 km – 1000 km altitude. This layer imposes a time delay in conjunction with refraction and phase advances. The ionisation levels are time dependent, caused by solar radiation and the resultant delay is proportional to the number of electrons along the signal path.

The radiation from the Sun ionises the neutral atoms and molecules in the upper atmosphere, resulting in free electrons during the daytime. This peaks in the early afternoon for mid-latitude areas, ~14:00 hrs local time. Such areas, together with low latitudes, are contained within the Earth's closed magnetic field lines. In contrast high latitude regions are most exposed to the solar wind, which results in a greater influence over the ionosphere (Hargreaves 1992). This is because the geomagnetic field lines in this region (polar caps) are able to reconnect with the interplanetary magnetic field, see Figure 3.2.

Sunspot activity and season can also affect the total electron content (TEC). Recombination and other electron-loss processes dominate the evening, as the Sun's radiation decreases. During night-time the Sun is absent and only the F_2 layer of the Ionosphere remains; due to the increased time taken for recombination at this higher altitude. The other layers; D, E and F_1 regions are negligible after local sunset (Tascione 1994).

The electron density profile of the ionosphere, with respect to altitude is shown by:

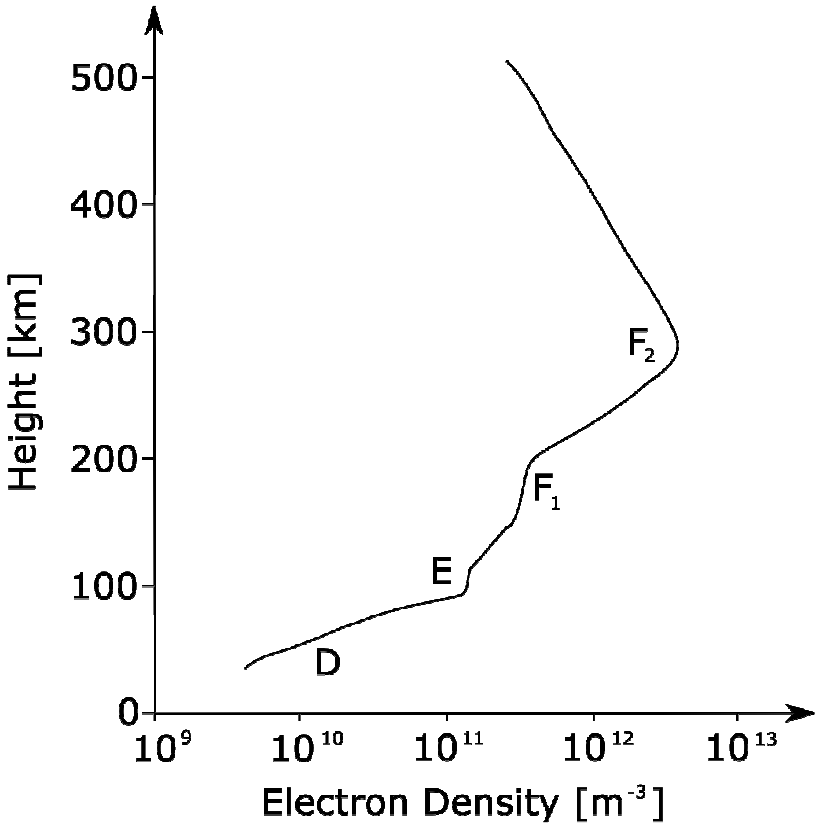

Figure 3.3 – Ionospheric electron density profile

Layer of the Ionosphere	Description
D-layer	Low rate of ionisation since the layers above absorb most of the photons. High rate of recombination due to a large molecular density. Exists only in daytime. HF pass through, LF can be refracted.
E-layer	Higher rate of ionisation. Lower molecular density, hence slower recombination, enables layer to exist for longer. Daytime refraction of HF.
F-layer(s)	High rate of ionisation. Lowest molecular density. Thus F_1 and F_2 layers exist in daytime, and continue to exist at night, merging into the F-layer.

Table 3.1 – Layers of the Ionosphere

3.4 The Troposphere

The troposphere begins at sea level and reaches ~11 km above the Earth's surface, whereby temperature decreases with height. It contains large amounts of water vapour, which refracts the GPS signals, causing a small group delay. There is also a dry delay component. Since the GPS signals are microwave in nature, the water vapour, or rain drops have a large delay effect causing errors ranging from 2.4 m for a satellite directly overhead and up to 25 m for a satellite near the horizon (Larijani 1998).

It is very difficult to predict the weather here on Earth and hence the rain density in the troposphere is challenging to account for. The rain drops cause electromagnetic waves to undergo scattering due to refraction, diffraction and absorption; weakening the GPS signals (Parkinson and Spilker 1996). The chemical composition of the troposphere leads to atmospheric fading, which is slightly easier to predict since it is less variable compared to weather. Its characteristics include refraction and absorption primarily due to water vapour and oxygen. Thus, a GPS signal propagating through the troposphere will undergo some delay due to rain and atmospheric fading. This can be corrected for by pointing a radiometer along the line of sight towards each satellite; in order to measure the water vapour quantity and hence make a correction (Larijani 1998).

3.5 Ground Environment (Blocking and Multipath)

The effects of blocking and multipath are dependent upon the physical location of the receiver. For instance, if it is placed near a tall building, then the GPS signals from satellites directly above would most likely reach the receiver. However, if a satellite is positioned on the other side of the building and close to the horizon then it's' signal will be blocked; unable to penetrate the building and reach the user. Any receiver placed at close proximity to buildings or obstructions of any kind, will receive multipath signals. These signals weaken as they are reflected off nearby obstructions, before reaching the user. The following figure illustrates blocking and multipath.

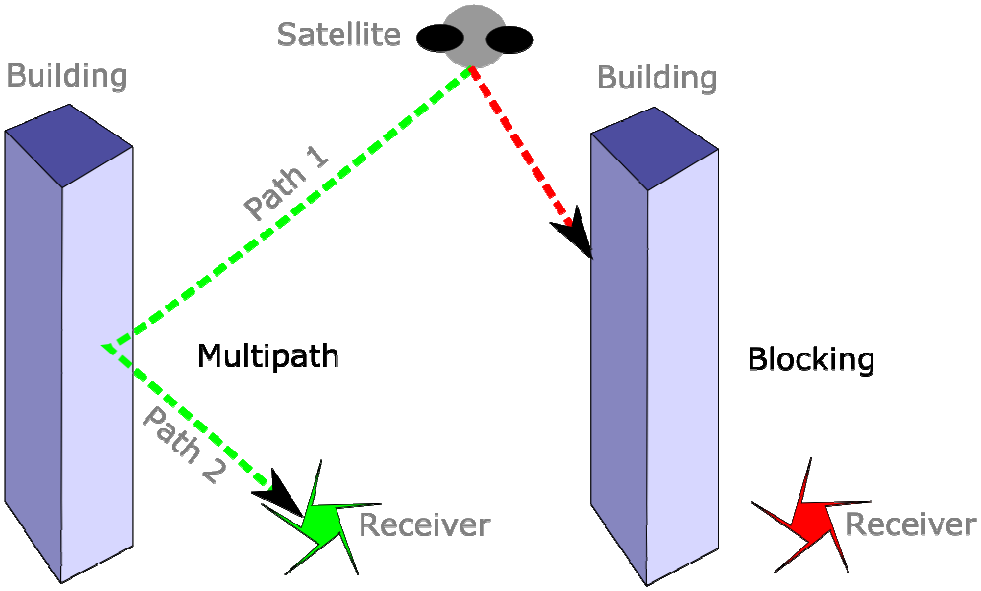

Figure 3.4 – Blocking and multipath

3.6 Radio Wave Propagation and the Ionosphere

Electromagnetic (EM) waves exhibit certain properties which allow them to propagate over extremely long distances. EM waves possess an electric field, which generates a magnetic field, in turn fuelling the electric field allowing for extensive propagation. Some EM waves are reflected by the ionosphere, whilst others propagate through it. The propagation characteristics are related to the frequency of the wave and the make up of the ionosphere.

3.6.1 Reflected Radio Waves

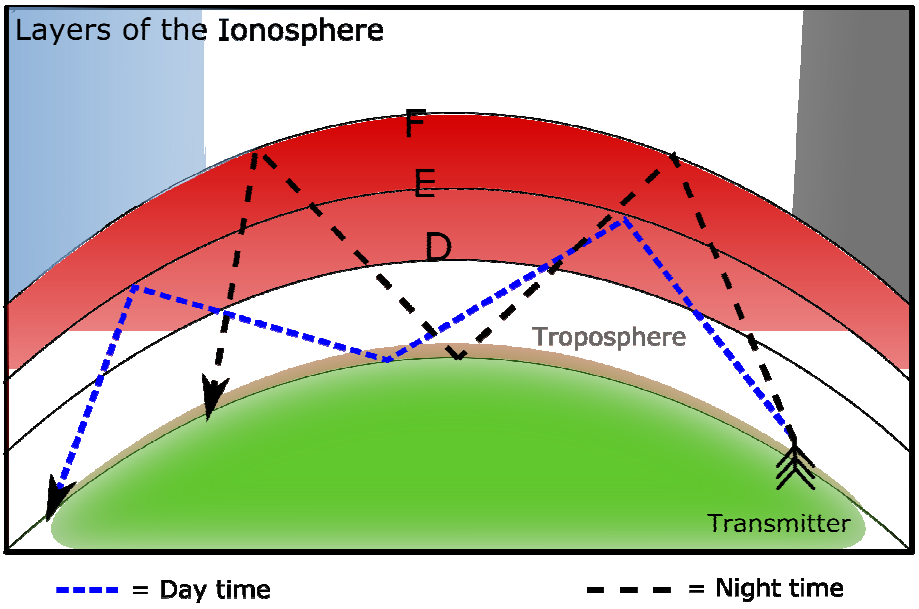

Figure 3.5 – Reflected radio waves

Figure 3.5 illustrates the reflective abilities offered by the ionosphere; whereby signals within a particular frequency (High Frequency, HF) range may be transmitted around the curvature of the Earth. The HF band covers frequencies between 3 MHz and 30 MHz, which corresponds to wavelengths between 100 m and 10 m respectively (Hargreaves 1992). Since the ionosphere is a slowly varying medium and given the size of these wavelengths, the ionospheric medium is not considered to change very much in the distance of a few wavelengths and so it may be regarded as a stack of thin slabs. Assuming that

each slab is several wavelengths thick and by applying Snell's law to each boundary, with refractive indices n_1, n_2, n_3 etc., we can see why a radio signal is reflected back from the ionosphere, according to Hargreaves (1992) page 27 as follows:

$$\begin{aligned} \sin i_0 &= n_1 \sin i_1 \\ n_1 \sin i_1 &= n_2 \sin i_2 \\ n_2 \sin i_2 &= n_3 \sin i_3 \\ &\vdots \qquad\quad \vdots \\ \underline{n_{(r-1)} \sin_{(r-1)} &= n_r} \\ \sin i_0 &= n_r \end{aligned} \tag{3.1}$$

where n is the refractive index and i is the angle of incidence.

The refractive index (n) of the ionosphere decreases with height. When n = 0, the ray is reflected and will return by a similar path, assuming the ionosphere is horizontally uniform. The ray actually returns to the ground by a process of continual refraction (bending), not reflection, within the ionosphere. However, by simplifying this process to a single reflection, accurate results are still obtained (McNamara 1991).

$$\begin{aligned} \omega_N^2 / \omega^2 &= 1 - n^2 \\ \omega_N^2 / \omega^2 &= 1 - \sin^2 i_0 \\ \omega_N^2 / \omega^2 &= \cos^2 i_0 \\ \omega_N &= \omega \cos i_0 \end{aligned} \tag{3.2}$$

where ω_N is the plasma frequency and ω is the radio signal frequency.

During the day, radio waves are reflected back down to Earth by the E-layer of the Ionosphere. At night time, the transmitted signal effectively bounces off the F-layer. This may occur several times, albeit with signal degradation. Nevertheless, a message can be received many hundreds of kilometres away using this method. A famous example was led by Marconi in 1901; achieving the successful transatlantic transmission of a signal from the UK to Canada (Kirby and Comm 1995). Notably, the Ionosphere and Troposphere are the most significant parts of the atmosphere with respect to radio wave propagation. This

is due to the former's charged state and the latter's changes in weather and density.

3.6.2 GPS Signal Propagation through the Ionosphere

Radio waves (e.g. GPS signals) travel at the speed of light, *c*, in a vacuum and in the ionosphere their velocity, *v*, is modified by the refractive index, *n*, as follows:

$$v = c/n \qquad (3.3)$$

The ionosphere both slows and refracts GPS signals as they propagate through it. The magnetised plasma, which consists of ions and free electrons, is a dispersive medium. This is because *n* depends upon the frequency of the signal passing through it. The refractive index may be found using the Appleton formula (Davies 1990):

$$n^2 = (\mu - i\chi)^2$$

$$n^2 = 1 - \frac{X}{1 - iZ - \frac{Y_T^2}{2(1 - X - iZ)} \pm \left[\frac{Y_T^4}{4(1 - X - iZ)^2} + Y_L^2 \right]^{1/2}} \qquad (3.4)$$

where *X*, *Y* and *Z* are as follows:

$$X = \omega_p^2 / \omega^2 ,$$

$$Y = \omega_B / \omega , \qquad Y_L = \omega_L / \omega , \qquad Y_T = \omega_T / \omega ,$$

$$Z = v / \omega$$

The angular plasma frequency is represented by ω_p and ω is the angular frequency. The electron gyrofrequency is represented by ω_B and it's longitudinal and transverse components are ω_L and ω_T respectively. The electron-neutral collision frequency is denoted as *v*.

In the E and F layers of the ionosphere, collisions between electrons and neutral atoms are negligible ($Z \approx 0$) because the neutral gas density is low. Absorption and the magnetic field are assumed to be negligible and so by taking the real part of *n*, Equation 3.4 may be simplified as follows:

$$\mu^2 = 1 - X \qquad (3.5)$$

At GPS frequencies, the higher order terms may be neglected and μ may be approximated as follows (Parkinson and Spilker 1996):

$$\mu \approx 1 - \frac{1}{2} X \qquad (3.6)$$

Recalling that $X = \omega_p^2 / \omega^2$ and since $f = 2\pi\omega$ we can re-write Equation 3.6 as follows:

$$\mu = 1 - \frac{1\omega_p^2}{2\omega^2} = 1 - \frac{1 f_p^2}{2 f^2} \qquad (3.7)$$

where f_p and f are the plasma and carrier frequencies respectively.

$$f_p^2 = \frac{e^2}{4\pi^2 \varepsilon_0 m_e} N \qquad (3.8)$$

$e = -1.602 \times 10^{-19}$ C, the charge of an electron

$\varepsilon_0 = 8.854 \times 10^{-12}$ F/m, the permittivity of free space

$m_e = 9.107 \times 10^{-31}$ kg, the rest mass of an electron

N is the electron concentration in electrons m^{-3}

Substituting Equation 3.8 into 3.7, together with the above constants yields:

$$\mu = 1 - \frac{40.3}{f^2} N \qquad (3.9)$$

Note that 40.3 is a constant, with units of $m^3 s^{-2}$.

The phase and group refractive indices, μ_p and μ_g respectively, may be written as follows (Kaplan and Hegarty 2006):

$$\mu_p = 1 - \frac{40.3}{f^2} N \qquad \mu_g = 1 + \frac{40.3}{f^2} N \qquad (3.10)$$

Substituting $v = c / \mu$ into the above yields the phase and group velocities, v_p and v_g respectively:

$$v_p = \frac{c}{1 - \frac{40.3}{f^2} N} \qquad v_g = \frac{c}{1 + \frac{40.3}{f^2} N} \qquad (3.11)$$

Therefore and with respect to GPS signals, the carrier phase is advanced and the navigation message and PRN codes are delayed during their journey through the ionosphere.

3.6.3 GPS Carrier Phase Advance and Group Delay

The true geometric range, ρ, between a GPS satellite, s and receiver, r, along the line of sight, is given by:

$$\rho = \int_r^s 1 \; dl \qquad (3.12)$$

Similarly, the measured range, S, is:

$$S = \int_r^s \mu \; dS \qquad (3.13)$$

Thus the path length difference, ΔS, due to the ionosphere, is as follows:

$$\Delta S = S - \rho$$
$$\Delta S = \int_r^s \mu \, dS - \int_r^s 1 \; dl \qquad (3.14)$$

The carrier phase advance, ΔS_p, is then found by substituting the phase refractive index from Equation 3.10 into 3.14:

$$\Delta S_p = \int_r^s \left(1 - \frac{40.3}{f^2} N\right) dS - \int_r^s 1 \; dl \qquad (3.15)$$

Now by integrating along the line of sight path and by changing *dS* to *dl*, the carrier phase advance (in metres) is as follows:

$$\Delta S_p = -\frac{40.3}{f^2} \int_r^s N \; dl \qquad (3.16)$$

Likewise, the group delay, ΔS_g, may be expressed (in metres) as:

$$\Delta S_g = +\frac{40.3}{f^2} \int_r^s N \; dl \qquad (3.17)$$

Noting that the Total Electron Content (TEC) may be expressed (in electrons m^{-2}) as:

$$I = \int N dl \qquad (3.18)$$

Then the carrier phase advance (Equation 3.16) and group delay (Equation 3.17), respectively, may be re-written as:

$$\Delta S_p = -\frac{40.3}{f^2} I \qquad \text{and} \qquad \Delta S_g = \frac{40.3}{f^2} I \qquad (3.19)$$

3.6.4 Dual-frequency TEC Measurements

There are two main positioning signals provided by the GPS: L1 (1575.42 MHz) and L2 (1227.6 MHz). The former is modulated with a coarse acquisition (C/A) code and a precise (P) code. The latter is modulated by the P code.

On the L1 frequency, the C/A code (C1) is unencrypted and so the corresponding P code (P1) may be used by all GPS receivers. However, in order to use it, the C/A code must first be tracked, due to the high frequency of the P code. On the L2 frequency, the P code (P2) is encrypted and may be used by tracking it with the P1 code (Allain 2009).

Most GPS receivers are 'single-frequency' (i.e. can only use the L1 signal). However, 'dual-frequency' GPS receivers, which are more expensive and heavier, can use both the L1 and L2 signals, as explained in the previous paragraph. Such receivers are used for high accuracy applications, such as geodetic positioning, surveying and also by the International GNSS Service (IGS), which is explained in Chapter 5.

RINEX files (discussed in Chapter 5) are recorded by these receivers and contain these observables:

$$P_1 = P_0 + \frac{I}{f_1^2} + \varepsilon_1 \qquad (3.20)$$

$$P_2 = P_0 + \frac{I}{f_2^2} + \varepsilon_2 \qquad (3.21)$$

$$L_1 = P_0 - \frac{I}{f_1^2} + n_1\lambda_1 \qquad (3.22)$$

$$L_2 = P_0 - \frac{I}{f_2^2} + n_2\lambda_2 \qquad (3.23)$$

The pseudoranges from the precise P code are denoted by P_1 and P_2. The carrier phases of the signal (in metres) are given by L_1 and L_2. The ionosphere-free pseudorange is P_0, n is the integer ambiguity and λ is the carrier wavelength. The TEC and carrier frequency are given by I and f respectively.

Differencing the code and phase ranges, gives two expressions for I:

$$\frac{P_1 - P_2}{f_1^2 - f_2^2} = I + \frac{\varepsilon_1 - \varepsilon_2}{f_1^2 - f_2^2} \qquad (3.24)$$

$$\frac{L_1 - L_2}{f_1^2 - f_2^2} = -I + \frac{n_1\lambda_1 - n_2\lambda_2}{f_1^2 - f_2^2} \qquad (3.25)$$

Using Equation 3.24, I may be found together with a noise term. Equation 3.25 gives I with an offset term from the integer ambiguity, which is constant whilst the satellite is visible (ignoring sudden or large changes in cycle slips). Note that large cycle slips are easy detectable. By substituting Equation 3.25 into 3.24, I may be calculated. The weighted mean of the differences between Equations 3.24 and 3.25 is used to find the offset between cycle slips. The weights are correlated with the signal to noise ratio (Allain 2009).

The line integral of the electron density gives the TEC, which is derived using dual-frequency measurements. Images of the TEC may then be formed using tomography.

3.7 Tomography

'Tomo' comes from the Greek word for a slice and the term 'tomography' represents the process by which a two dimensional image of a section or slice of a three dimensional object is obtained. The 'tomograph' is the apparatus and the 'tomogram' is the picture (Anon 2008b).

The process is performed by externally subjecting the 3D object to penetrative electromagnetic waves. The resulting representation of the internal make-up of the structure is obtained after an inversion of the line-integral measurements. Computed Tomography (CT) scanning is the most commonly used form of tomography and may be referred to as X-ray computed tomography (RCR 2008).

The technique was applied to radio astronomy in 1956, Bracewell (1956) presents the notion of creating a complete and full reconstruction from a finite number of scans in all directions. In 1988 tomography was first applied to ionospheric imaging (Austen et al. 1988). This is known as 'ray tomography' and is becoming increasingly common; providing images of the electron density in the upper atmosphere.

3.8 GPS and Tomography

GPS signals penetrate the atmosphere from well above the upper ionospheric boundary and progress all the way through the ionosphere before reaching the surface of the Earth. This is due to the altitude and setup of the GPS constellation; whereby the satellites orbit and encompass the whole globe. The vast array of fixed ground-based GPS receivers and LEO-based receivers thus allow the measurements to be recorded and communicated for computation. But why is this data important? Radio signal propagation is directly affected by electron density and so a comprehensive real-time understanding of the ionosphere is highly sought after. Two main effects of this phenomenon are described below.

Firstly, international high frequency radio communications links exploit the ionosphere, by using it to refract transmitted signals back down towards Earth over the horizon. The instantaneous path of refraction is dependent upon the electron density. Contrastingly, scintillation in the ionosphere can cause disruption to communications signals. Scintillation can impose an unknown time delay upon GNSS signals. The increased dependence upon such systems requires a more accurate technique to account for all of the effects imposed by the ionosphere. The following two resources provide a wealth of information regarding radio signals and the ionosphere, Davies (1990) and McNamara (1991).

3.9 Ionospheric Imaging

Certainly, ionospheric imaging unlocks the potential to accurately map and track the electron density across the world in real-time. As explained in Section 3.3 The Ionosphere, the amount of *electron density depends upon: the time of day, the season, the amount of solar activity and the geographic location*. Of course there are other ionospheric transient parameters, but the most crucial to this application is the electron density. *The integral of the density between each satellite-to-receiver path is known as the Total Electron Content (TEC)*, which is fundamental to ionospheric tomography.

Initially, the ionosphere was imaged using 2D maps, yet as the research matured, 3D imaging became possible and was shown to produce a threefold improvement over the former method, see Meggs and Mitchell (2006). This study reinforces an earlier comparison between different TEC mapping methods for mid-latitude regions (Meggs et al. 2004). Several algorithms and techniques created to continuously monitor the ionosphere are reviewed by Bust and Mitchell (2008). This acts as a very valuable resource by not only reviewing the history, but the present state and future directions of ionospheric imaging as well.

3.10 MIDAS

The foundation of this project is based upon a three-dimensional time-dependent algorithm for ionospheric imaging using GPS (Mitchell and Spencer 2003). This resulted in a Multi-Instrument Data Analysis System (MIDAS), able to essentially produce a 4D movie of the evolving electron-concentration distribution. A snapshot example of this system is shown by Figure 3.6.

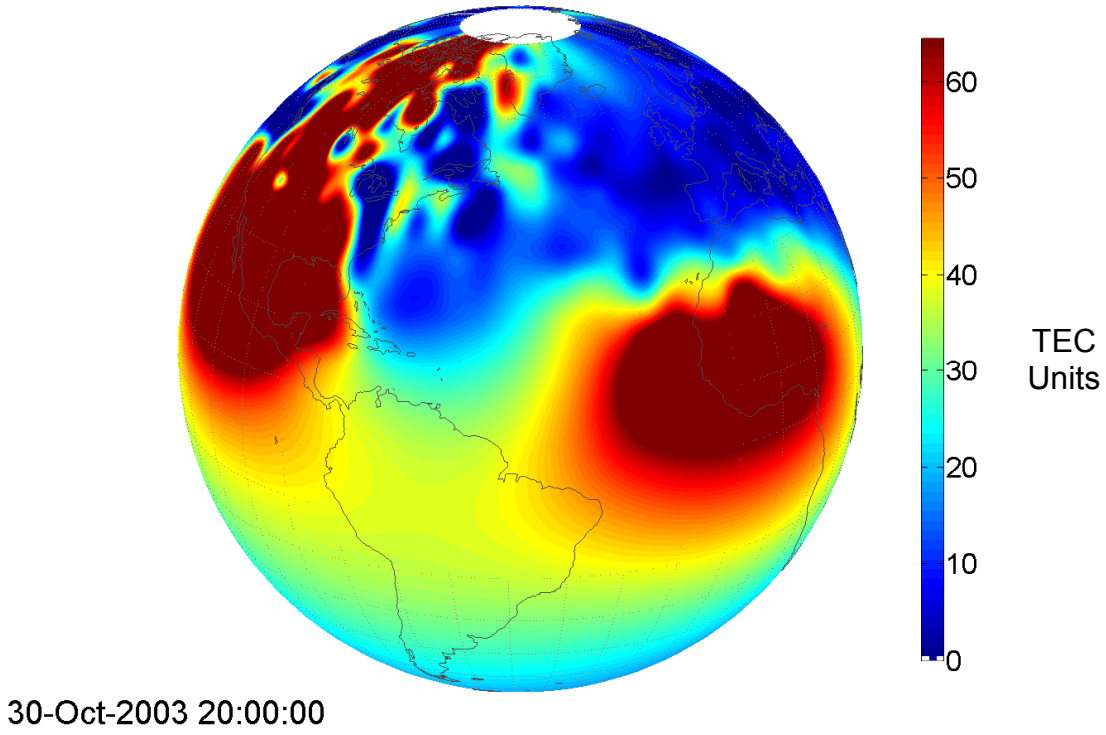

Figure 3.6 – MIDAS TEC map

Figure 3.6 represents the vertical total electron content (TEC) measured at 20:00 hrs on the 30th October 2003; a snapshot of time during the so called 'Halloween Storm'. TEC provides a means of quantifying the number of electrons along a path between two points. The deep red patches indicate the highest amounts of TEC and are seen over North America and Northwest Africa at this time. The vast blue areas represent weaker amounts of TEC, whilst green-yellow patches portray medium-high TEC. More precisely the colours correspond to TEC Units (TECU): the larger the value, the greater the total electron content. Subsequent images would portray the movement of this plasma across the globe.

Note: 1 TECU = 10^{16} electrons/m^2.

Tomography based GPS corrections are a suitable technique to correct for ionospheric delays. This is because the electron densities are constantly changing and a predictive model is not sufficient to account for the transient nature of the ionosphere for precise applications. Thus constant monitoring and imaging will continue to mature.

The MIDAS algorithm is explained by Mitchell and Spencer (2003) and Spencer and Mitchell (2007) .

Chapter 4

4. GPS Timing

4.1 Importance of Time

Scientific, commercial and industrial applications are increasingly taking advantage of GPS and it's ability to disseminate time. The vast amount of applications doing so is a good measure of how important precise timing has become. Without it, many 'everyday' applications would suffer. Mobile phone base stations, data networks and electrical power grids are synchronised using GPS. Crucially, GPST is available worldwide and should not differ between locations.

4.2 Time, GPST and UTC

GPST began at 00:00 hrs on the 6th January 1980. This was in fact a Sunday, which is defined as Day 0 and marked the beginning of GPS Week 0. Monday is denoted by Day 1, Tuesday by Day 2 and so on until Day 6, Saturday. Thereafter, the GPS Week number is incremented at the beginning of every Sunday and the days continue to be numbered from 0 to 6. Therefore, every day since GPST began may be identified by a unique week number and specific day number.

GPST is a continuous timescale and though similar to UTC it does not include leap seconds. UTC, an atomic timescale, has introduced leap seconds since 1972 in order to keep it in approximate step with the Earth's rotation (Parkinson and Spilker 1996). Leap seconds are usually added or removed on the 30th June or 31st December of any particular year. This is the fundamental difference

between GPST and UTC, since they run at the same rate. More information may be found from the following resources: Parkinson and Spilker (1996) and Borre (2007).

The GPS Control Segment compares GPS Time to each SV clock and provides corrections as and when required. It consists of a network of strategically placed stations across the globe, monitoring and maintaining the whole system (including GPST) as follows:

#	***Location***	***Responsibility***
1	Falcon Air Force Base Colorado Springs, Colorado, USA	Master Control Station & Monitor station
2	Hawaii	Monitor station
3	Cape Canaveral Florida, USA	Monitor station
4	Ascension Island Atlantic Ocean, UK	Monitor station & Ground antenna
5	Diego Garcia Indian Ocean	Monitor station & Ground antenna
6	Kwajalein Island South Pacific Ocean	Monitor station & Ground antenna

Table 4.1 – GPS control stations

The Master Control Station is responsible for the overall management of the network. It provides the GPS ephemeris data, which is a collection of SV computed positions, velocities, derived right ascensions and declinations of SV's at specific times (FAA 2007). Information regarding the accuracy and consistency of the broadcast ephemeris data is presented in a 2000 study (Jefferson and Bar-Sever 2000). Furthermore, the network of monitoring stations check the; exact altitude, position, speed and health of each satellite twice a day; as the SV's complete their orbit around the Earth. This allows the behaviour of each satellite's orbit and clock data to be predicted. Such behaviour is maintained to within an acceptable limit by the GPS Control Segment (Parkinson and Spilker 1996).

The ephemeris data is uploaded to the SV's, where it is then re-transmitted to the user. Communication with each SV can be achieved due to the strategic locations of the stations. Transmissions are made using the ground antennas,

whilst they monitor the satellites from horizon to horizon. The Federal Aviation Administration (FAA) provides a valuable resource for this section (FAA 2007).

The GPS Space Segment not only refers to the actual satellites, but also to the rockets that launched them. Relevant information related to the space segment and timing is provided here. Four atomic clocks are contained within each GPS satellite. Three act as a backup, whilst only one operates at any given time (Larijani 1998). Atomic clocks are used because they are very accurate, with an uncertainty of 1 second over tens or even hundreds of thousands of years. An error of 1 microsecond would result in a ranging error of ~300 m for example.

4.3 GPS Time Transfer

4.3.1 GPS Time Transfer Overview

Various methods of time transfer are discussed in this section. Time transfer is the process of comparing the time and frequency offset between clocks at two distant locations. Typically, a time measurement comes from a reference source (such as the GPS system) and is transmitted, or transferred, to a different location (or several locations) in order to synchronise a network or system. The GPS provides the global, reliable and precise time standard that is required to synchronise communications systems, computer networks and electrical power transmission lines for example. GPS is the source of the time.

4.3.2 Basic Pseudoranging Technique

GPS satellites are synchronised to GPST. Their orbits and ephemeris data are known and a GPS receiver records the local time of arrival (TOA) of a GPS signal. Each received navigation message includes the time at which the SV broadcast the signal, the time of transmission (the TOT). The TOA minus the TOT results in the time of transit, which yields the pseudorange. Thus, when the pseudoranges (or time differences) between several satellite-receiver paths are found, the positional solution at the receiver, as well as the time, may be computed. Note that receivers vary and may measure the GPS code and/or phase.

4.3.3 Direct-Reference Time Measurement

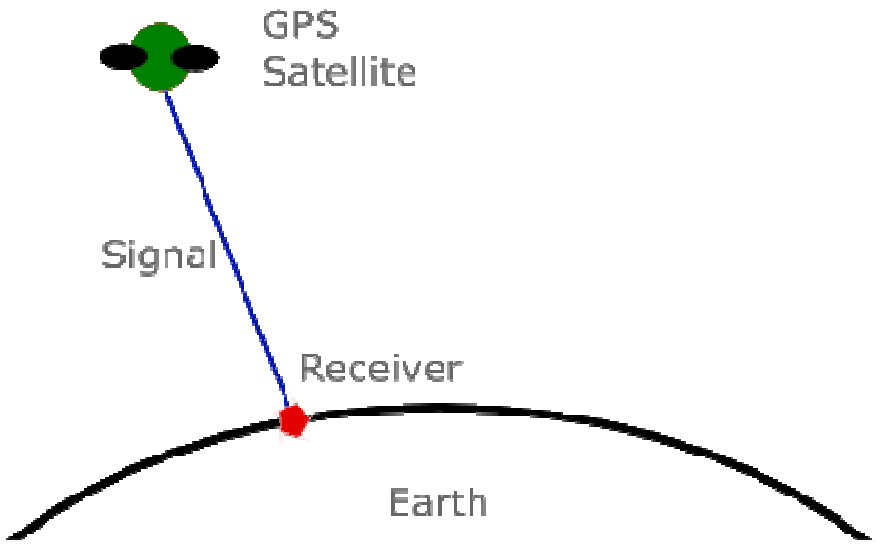

Figure 4.1 – Direct reference time transfer

This is the simplest and least accurate method of GPS time transfer, but has global coverage. Suppose a GPS receiver is at a fixed, known position then GPST (or UTC) may be obtained by tracking just one satellite. To compute the solution, the receiver coordinates must be provided, together with data from just one GPS satellite. Specialised timekeeping GPS receivers with modified algorithms are available to do this.

However, it is important to note that relying solely on just one GPS satellite is dangerous because it is not possible for the GPS Control Segment to remove a bad satellite from the constellation immediately. The process would in fact take between 5 and 45 mins (Geier et al. 1995). Geier et al. (1995) state that by using GPS, relative timing accuracies of the order of 1 to 10 ms are easily achieved. For example, Global System for Mobile Communication (GSM), which uses Time Division Multiple Access (TDMA), requires at least these accuracies to maximise the use of the allocated spectrum.

Accuracies of a few tens of nanoseconds are typically achievable (Kaplan and Hegarty 2006). During the implementation of SA, accuracies within 100 ns were expected (Dana 1997). Please see Figure 4.1 and Lewandowski et al., (1999) for more information.

4.3.4 Common View and All in View Techniques

Supposing two clocks (can be more), A and B, are each controlled by a GPS receiver station and are separated by some distance; a baseline, then given that GPS satellites broadcast GPST and ensuring both stations receive signals from the same specific satellite(s) simultaneously; a value for GPST can be obtained. This value is available at both locations and originates from the common signal(s). It is then communicated between the stations to compare their clocks. Ideally, it would be exactly the same at each station, but the signals succumb to several errors.

However, the Common View (CV) technique is advantageous because the satellite clock error contributes nothing to the solution, as GPST drops out when comparing the difference between the two clocks. The differential accuracy is said to be ~10 ns or better according to Allan and Weiss (1980) and Lewandowski and Thomas (1991).

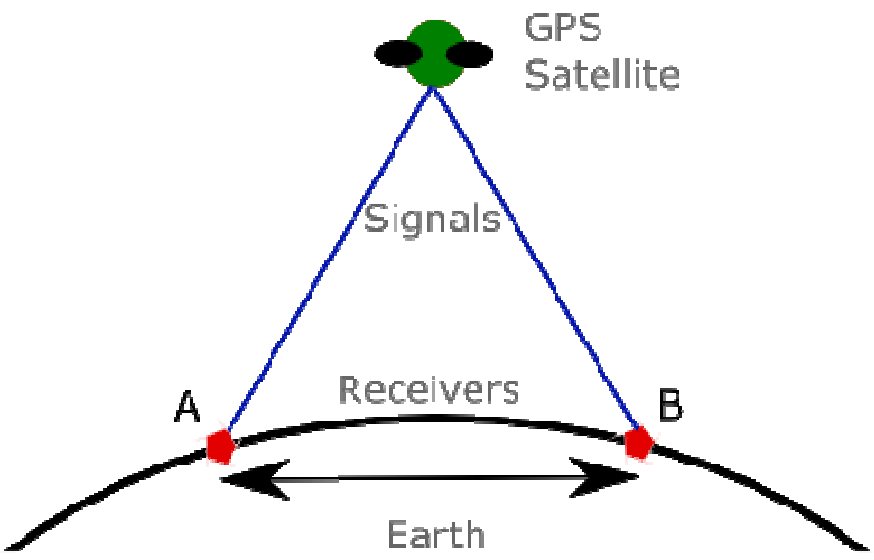

Figure 4.2 – Common view time transfer

In comparison, advances in acquiring clock parameters and precise satellite orbits have led to the replacement of CV by the All in View (AV) method (Petit and Jiang 2008). All available measurements, from all of the satellites in view, are used and averaged to obtain a reference time. In 2005, Weiss et al. (2005)

stated that if the errors in the satellite clock estimates were sufficiently small, then AV would have an important advantage and since 2006, the AV method has been used towards International Atomic Time (TAI) computation, rather than CV.

AV enables time comparisons to be made globally, as the same satellites do not have to be observed simultaneously between stations. Furthermore, AV enables satellites at higher elevations to be used: GPS measurements originating from such satellites typically leads to a reduction in errors at the receiver, due to reduced ionospheric and tropospheric delays and less multipath (Weiss et al. 2005).

4.3.5 Carrier Phase Method

The GPS signal carrier phase can be used as an alternative to using purely the C/A code measurements. Four simultaneous measurements are required for geodetic analysis, which include the code and phase measured at both carrier frequencies for each satellite observed (Dach et al. 2006).

To quantify the carrier phase, a receiver will measure the difference between the phase of the received carrier signal (SV generated) and the phase of the locally generated signal (produced by the receiver), see Larson and Levine (1999). However, there is an uncertainty with respect to defining which carrier phase cycle is being tracked by the receiver, see Dach et al., (2003). This is known as the carrier phase ambiguity and may be solved for with the help of the much noisier code measurements. “Averaging the code data over some interval and fitting the resulting data as to best match the carrier phase data is the method most commonly used to resolve for this carrier phase ambiguity” (Brown et al. 2000). Brown et al., (2000) state that accuracies using carrier phase methods have the potential to be more accurate than C/A code methods since the carrier frequency is ~1000 times greater, which provides an increased resolution.

Defraigne and Petit (2003) state that there is an improvement by a factor of two when using a geodetic receiver, as opposed to using just measurements based on the C/A code, for long baselines e.g. a transatlantic time link. Geodetic receivers are capable of measuring the carrier phase. Over short baselines the

carrier phase technique is however comparable to measurements based solely on the C/A code (Defraigne and Petit 2003).

4.4 TWSTFT

Note that Two-way Satellite Time and Frequency Transfer (TWSTFT), or 'Two-Way' (TW), does not use GPS.

Imagine two stations once again separated by some baseline and suppose a geostationary telecommunications satellite exists ideally at the midpoint separating the two stations. Both stations communicate with this satellite to determine the absolute time difference between them and hence achieve a stable and accurate time transfer. This is achievable because propagation delays largely cancel-out due to symmetry; as the satellite-receiver path lengths are essentially common to each receiver, as stated by Takahashi et al. (1993) and Kirchner (1991). The Sagnac effect must also be accounted for.

A satellite was first used in 1962 to carry out a timing comparison between the US and the UK. The satellite was called Telstar I, which was a low orbiting communications satellite (Steele et al. 1964). The satellite link achieved an accuracy of 1 μs and 20 μs for the complete link; which includes the Earth-based stations and timekeeping institutions. Ever since, time transfer experiments have endeavoured to develop a reliable and inexpensive method of operation. Over time there has been rapid growth in satellite communications and costs have decreased (Kirchner 1991).

In TWSTFT, time signals are transmitted (uploaded and downloaded) between the two stations (transceivers) *via the communications satellite*, hence the 'two-way' element to this method. In contrast the aforementioned GPS methods are 'one-way' techniques, since they only receive signals from the satellite. Therefore, an extra complication for TWSTFT is that both stations need transmit-receive hardware, which increases the cost. Time Interval Counters (TIC's) are used at each station to take time interval measurements. A pulse from the local clock causes the TIC to start, and a pulse from the remote clock stops them. As the TIC begins it is simultaneously transmitted to the other

station. A 1PPS (Pulse Per Second) signal is typically used. Both stations record the time interval data, which is then exchanged and differenced. This technique can effectively be used in real-time, since there is usually a large bandwidth available, allowing for the data to be transferred concurrently with the transmission of timing pulses. The time interval data recorded at each station includes the propagation delays and the clock differences, as shown below (NIST 2008b):

$$TIC(A) = A - B + T_A + t_{s\text{-}A} \tag{4.1}$$

$$TIC(B) = B - A + T_B + t_{s\text{-}B} \tag{4.2}$$

The time interval counter readings are represented by *TIC(A)* and *TIC(B)*, the respective clock times are *A* and *B* and the propagation and Sagnac delays are represented by T_X and $t_{s\text{-}X}$ respectively. The time difference between clocks A and B is found from Equations (4.1) and (4.2) by differencing the individual simultaneous TIC readings. The path delays tend to cancel, but not perfectly since the 'transmit and receive' equipment are physically different pieces of hardware and impose different delays. This is a major source of inaccuracy and instability for TWSTFT. Any satellite delay perfectly cancels if the same satellite transponder is used for both directions.

Additionally, the up and downlink frequencies tend to be different. For example, for Ku-band communications the uplink and downlink frequencies are normally 14 GHz and 11 GHz respectively and so the ionospheric delay will differ depending upon the mode; uplink or downlink. This is because the refractive index for the ionosphere varies with frequency, due to the ionised gases. The velocity (v) of propagation changes according to the refractive index (n), $n = c/v$, where c is the speed of light and v is related to frequency (f) and wavelength (λ) as follows: $v = f\lambda$. Thus different frequencies have different refractive indices. The tropospheric delay mostly cancels because it does not depend upon frequency (NIST 2008b). This technique improves signal-to-noise ratio (SNR) and multipath may be lessened using highly directional antennas. Hanson (1989) presents a wealth of information regarding TWSTFT.

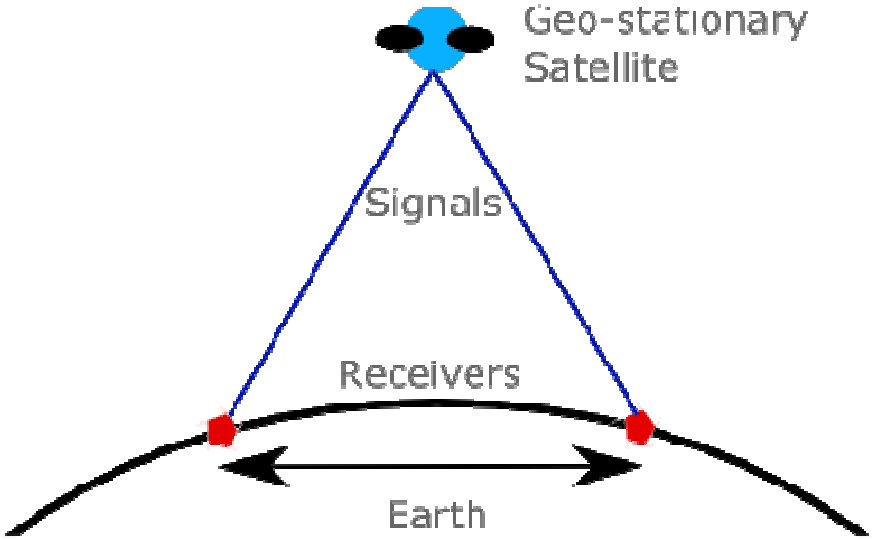

Figure 4.3 – Two-way time transfer

4.5 Time Transfer - Discussion

TWSTFT is a good method of verifying the time transfers made using GPS common view, because it is independent and has low measurement noise (Davis et al. 1996). Kirchner (1991) states that since 1988 precisions of 100 ps and expected accuracies of at least 1 ns were achieved using domestic communications satellites for two-way time transfers between USNO (United States Naval Observatory) and NIST (National Institute of Standards and Technology). This is of course after having calibrated the station delays.

For accurate time transfers, it is crucial to measure hardware delays and calibrate the equipment. Shemar and Davis (1999) have shown that delays incurred during transmission through cables, are more stable at lower frequencies. For example, significantly lower outdoor temperature coefficients are achieved when transmitting through cables at 70 MHz or L-band, rather than Ku-band. The clock stabilities of the stations involved also have a significant impact on time transfers: caesium clocks are known to exhibit relatively large instabilities when compared to Hydrogen masers. Clock noise due to caesium clocks noticeably impacts the Allan Variance calculations between laboratories (Davis 1996).

Clarke et al. (1999) show hardware, rather than GPS signals, are the limitation for short baselines e.g. only 5 m. The use of temperature controlled GPS antennae and cables, with low temperature coefficients should improve the situation. Over long baselines, such as 750 km for example, hardware delays must not be ignored, however Braasch and Dierendonck (1999) state that most errors are not under the control of the receiver, since they are typically related to the path of propagation, or the SV itself. Undeniably the most significant factors affecting the accuracy are; the ionosphere, troposphere, multipath and hardware delays, as stated by Petit and Thomas (1996). For example, the propagation paths may vary significantly over longer baselines. Another resource states how there are “inadequacies in the models of the ionosphere and troposphere” (NIST 2008a). This reinforces the work of this project, which uses tomography to provide a more accurate method to represent the ionosphere.

For frequency transfer, it is preferable to use the phase measurements, rather than the code observations (Dach et al. 2006). Carrier phase measurements yield much less noise, in contrast to using just the C/A code, and they are intrinsically less noisy. Note that phase multipath is around a thousand times smaller than code multipath (Clarke et al. 1998).

GPS AV is now regarded as advantageous over CV. By making use of every GPS satellite in view for the calculations, direct comparisons can be made between stations across the globe, whereas CV requires that the stations observe the same satellite(s). AV also allows for improved dilutions of precision and reduced propagation delays and multipath (Weiss et al. 2005).

Senior and Ray (2001) concur that more accurate time transfer results may be obtained by using carrier phase measurements and antenna cables with small temperature coefficients. Interestingly they also state that older generation dual-frequency receivers cannot track the L2 signal during periods of high ionospheric activity. This is part of the motivation behind this project, whereby tomography is coupled with a single-frequency system (L1).

GPS is used for many timing applications because it can provide atomic clock accuracy at the lesser cost of just a receiver. It is difficult to obtain accurate time from a cheap, portable single-frequency GPS receiver during stormy ionospheric conditions, however, MIDAS helps towards making that possible.

Chapter 5

5. Ionospheric tomography applied to GPS timing

5.1 Introduction

The work in this Chapter is presented in Rose et al. (2009) and I would like to thank the co-authors for their general advice.

The Global Positioning System (GPS) allows a user to solve for their position and time virtually anywhere in the world. GPS receivers use Time Difference of Arrival (TDOA) techniques to measure the time of signal propagation between each satellite in view and the receiver, together with the knowledge of the satellite positions, to compute a solution. When the GPS signals propagate through the ionosphere they are both slowed and refracted which directly affects the accuracy of the solution. This effect is proportional to the line integral of the ionospheric electron density, the Total Electron Content (TEC), which is dependent upon several factors: season, time of day, solar activity and latitude, to name but a few. Hence, an unknown, highly variable propagation delay is imposed upon the signals (Davies 1990).

Civilians commonly use GPS receivers for satellite navigation. They operate on a single-frequency, the L1 channel and are now compact and affordable. However, their accuracy is hindered by the ionospheric delay, which is the cause of the largest error in a single-frequency solution (Langley 1997). This delay is largely removed by dual-frequency GPS receivers, which hence provide more accurate solutions and are used by the scientific community towards atmospheric monitoring for example. However, dual-frequency receivers are

more expensive than standard single-frequency receivers and in extreme ionospheric conditions, are susceptible to losses of lock on the L2 signal, which corrupts the GPS solution.

There are ionospheric models available to single-frequency users that compensate for this delay. The GPS satellites broadcast the Klobuchar model coefficients via the GPS navigation message (Klobuchar 1987). This aims to provide at least a 50% Root Mean Square (RMS) correction for the ionospheric time delay. Similarly, ionospheric correction coefficients will be broadcast via the Galileo navigation message, for single-frequency users (Hochegger et al. 2000). Future development of the NeQuick ionospheric model (Radicella and Leitinger 2001) will provide an alternative to that of Klobuchar (1987).

Another model, known as the International Reference Ionosphere (IRI), is available (Bilitza 2001), but not in real-time to GPS users. Furthermore, geostationary satellite systems approximate the ionosphere to a thin shell (2D) and broadcast real-time ionospheric mapping information to complement the GPS solution. North America, Europe and Asia employ the: Wide Area Augmentation System (WAAS) (El-Arini et al. 1995), European Geostationary Navigation Overlay Service (EGNOS) (Hein 2000) and Multi-functional Satellite Augmentation System (MSAS) (Matsunaga et al. 2003) respectively.

Single-frequency GPS receivers, coupled with the 4D tomographic algorithm, Multi-Instrument Data Analysis System (MIDAS) (Mitchell and Spencer 2003), present a cheaper alternative to dual-frequency receivers and a more accurate alternative to standard single-frequency receivers. Tomographic imaging allows for a realistic estimate of the ionosphere to be created, see for example the review by Bust and Mitchell (2008). This real-time mapping system, MIDAS, provides the ionospheric delay by producing electron density images (maps), which have been proven to provide more accurate representations of the ionosphere than 2D shell approximations (e.g. WAAS) which introduce mapping function errors (Meggs and Mitchell 2006). Smith et al. (2008) state that thin shell models fail to describe the TEC of a slanted ray path because they do not contain any information regarding the vertical structure of the ionosphere. The MIDAS maps show the time evolution of plasma across the ionosphere, allowing real-time corrections to be made.

A large network of GPS receivers is required over the area of interest in order to monitor and track the plasma. This is already in place within Europe through the International GNSS (Global Navigation Satellite System) Service (IGS) and the Regional Reference Frame Sub-Commission for Europe (EUREF) Permanent Network (EPN). The IGS and EPN are voluntary services and collectively consist of hundreds of fixed GNSS stations that provide high precision products.

This study focuses on Europe and it is important to note that the behaviour of the ionosphere varies according to geographic location. Solar tides and horizontal geomagnetic field lines dominate the evolution of the ionosphere at low latitudes. Electron precipitation and the solar wind govern the ionospheric dynamic at high latitudes (Mitchell et al. 2005), whereas at mid-latitudes, neutral winds and the inner magnetosphere drive the dynamics (Kintner et al. 2007).

The aim of this work is to show that the accuracy of a single-frequency GPS timing solution can be improved by using 4D tomographic mapping to reduce the ionospheric delay. Results are presented to this effect by including comparisons between timing solutions that are obtained using different ionospheric corrections. The figures show solutions for fixed and mobile receivers with: no correction, the Klobuchar model, the IRI 2001 model, the real-time MIDAS maps and dual-frequency corrections. The latter is taken as the benchmark timing solution because it essentially removes the ionospheric delay by providing a direct means of measuring it.

It should be noted from the outset that these results represent the GPS solutions for a free-running GPS timing device, regardless of location and show how accurately the error may be bound. This is analogous to a navigational solution that is relative to the center of the Earth, as opposed to a solution that is relative to a known, fixed and local point. In systems such as the latter, Differential GPS (DGPS) for example, common errors are cancelled out, which greatly enhances the solution accuracy. The dual-frequency results presented here should not be compared to precise time transfer techniques, such as Two-Way Satellite Time and Frequency Transfer (TWSTFT), which can obtain 1 ns accuracy (0.1 ns precision) and is expensive to operate as it requires a dedicated satellite link (Ray and Senior 2003). This is because results are presented as instantaneous solutions for fixed and mobile GPS receivers and do not use common view geostationary or CV GPS satellites to synchronise two clocks at different

locations, nor are these results averaged over any lengthy time periods. Averaging over several days can improve the accuracy by smoothing-out noise in time transfers (Lewandowski and Azoubib 2000). Therefore, this research does not aim to compete with high precision time transfer techniques, but instead focuses on improving the accuracy of existing single-frequency GPS timing solutions that are *globally obtainable from the standard GPS constellation*.

The results are in the form of a receiver clock bias; this is the offset between the GPS receiver clock and GPS Time (GPST), which is referenced to the receiver clock bias as calculated by the Centre for Orbit Determination in Europe (CODE) (Beutler et al. 1999). From this point on, the Receiver Clock Bias shall be referred to as the RCB. The CODE, an IGS Analysis Center, uses the GPS code and phase measurements, together with atomic clock references to calculate their clock solutions (Kouba and Springer 2001). This yields a precise timing solution at the test station and is taken as the 'truth', to give an independent and fair comparison between methods. These receiver clock products are computed daily and are freely available to download from the IGS (Dow et al. 2005). The RCB, calculated by each of the timing solutions, are presented relative to the bias as calculated by CODE.

An offset exists between these solutions and the solution provided by CODE due to differences in filtering to remove multipath: the CODE solution is obtained using integer ambiguity resolution, whereas the presented timing solutions are obtained using phase filtering only (Rose et al. 2009). Ambiguity filtering is not used because it is not feasible for the timing methods presented in this thesis. The integer ambiguity is constant as long as the received power is sufficient. The presented timing solutions, for both the fixed and mobile cases, are calculated instantaneously at each sampling point, without relying on historic or averaged data and produce a solution without prior knowledge of the local multipath effects. The phase filtering yields the sum of the integer ambiguity and of the small multipath average, offering improvements over raw multipath error and noise. The offset is location/site specific and in the case of GPS, is repeated every sidereal day.

5.2 Method

5.2.1 Overview

The method described in this section is similar to the method presented by Allain and Mitchell (2009), which involves using tomography to correct for the ionosphere and measures its impact upon GPS positioning. In contrast this work is concerned with *fixed and mobile* single-frequency GPS receiver *timing* solutions, each of which incorporates a different ionospheric correction technique.

In order to represent different geophysical conditions both quiet and stormy days have been selected for this study from the year 2002, along with a stormy period during October 2003. The selection was based upon Kp index, which ranges from 0-9 and gives a measure of the disturbance in the Earth's magnetic field. The Kp values were obtained from the UK Solar System Data Centre (UKSSDC), see http://www.ukssdc.ac.uk/.

5.2.2 IGS/EPN Stations, Map and MIDAS

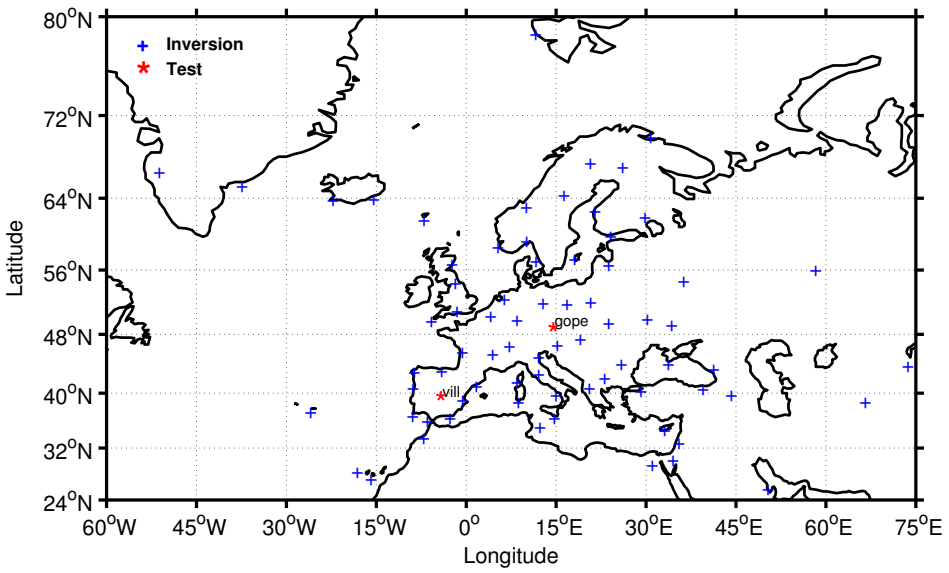

Figure 5.1 – Map of Europe, showing the test stations and those used for the inversion

Data from dual-frequency GPS receiver sites across mainland Europe have been obtained from the IGS (Dow et al. 2005) and the EPN (Bruyninx 2004) for this study. The data at each site is recorded at 30 s intervals in Receiver Independent Exchange (RINEX) format (Gurtner 2002). Stations in close proximity to each other were not chosen because they fail to provide any additional data about the ionosphere for that region. As a result 74 stations located across Europe were used to create ionospheric maps.

Two IGS stations, based in different areas of Europe, are used as test stations. Single-frequency GPS data from these sites are used to illustrate the performance of a single-frequency GPS receiver with: no ionospheric correction, the Klobuchar ionospheric correction, the IRI 2001 correction and finally the MIDAS correction. The dual-frequency data, available from these test sites, are then included in the resulting figures to enable direct comparisons between a wide range of GPS timing solutions. The data from these test stations does not contribute to the ionospheric mapping since independent single-frequency solutions are desired. The test stations are VILL (Villafranca, Spain) and GOPE (Ondrejov, Czech Republic). Figure 5.1 shows the location of the test stations and those used for the imaging (or 'inversion'), by representing each site with a red and blue marker respectively.

The tomographic grid is centered on Europe at 50°N 15°E. The longitude and latitude ranges from -44° to +44° in steps of 4°. The altitude ranges from 100 km to 1500 km in steps of 50 km. The MIDAS inversions use three empirical orthonormal functions, to represent the vertical basis functions and are computed from a range of Epstein functions. For a detailed description of the MIDAS tomographic algorithms please see Mitchell and Spencer (2003) and Spencer and Mitchell (2007).

5.2.3 Timing solution overview

GPS satellites are synchronised to GPST and their positions are provided by the IGS. The GPS receiver records the local Time of Arrival (TOA), or 'time of reception', of a GPS signal according to its clock. Each received navigation message incorporates the time at which the Satellite Vehicle (SV) broadcast the signal, the Time of Transmission (TOT). Thus the pseudorange between each

satellite and the receiver may be computed. However, it is not that simple. Parkinson and Spilker (1996) state that the *pseudorange may be defined as the difference between the satellite clock time and the receiver clock time*, but it is corrupted by the receiver's clock bias which must be estimated and removed. Additionally, there are several biases and propagation errors which are imposed upon the GPS signal and system as a whole and so several corrections are applied to the pseudorange equation, before the ionospheric correction, that are fundamental and common to each of the GPS timing solution techniques presented in this thesis.

If the GPS receiver is at a known position then the receiver clock bias, b_{rx}, can be obtained from a single satellite. The fundamental and common corrections (described in section 5.2.5) may be calculated from the outset using the known position. This yields the RCB and as there are typically several satellites in view, a more accurate b_{rx} value is obtained by averaging all of the values of b_{rx} for all of the satellites in view at each instant in time.

In contrast, if the GPS receiver is at an unknown position it must track at least four satellites, to form at least four pseudorange equations, to solve for its position coordinates *x*, *y*, *z* and its RCB, using a least squares technique. The fundamental and common corrections must first be estimated using an approximation of the receiver coordinates. More accurate pseudorange equations may then be formed and applied to the least squares technique for a second time in order to output more accurate receiver coordinates. This process is repeated to obtain an increasingly accurate *x, y, z* and b_{rx}.

The RCB represents the receiver clock's offset from actual GPS system time. Therefore, once this value has been found, the GPST at the receiver's location is known and may be converted to Coordinated Universal Time (UTC) using the specific broadcast conversion parameter. GPST is not converted in this study. This technique is employed by each of the GPS timing solutions, together with the common corrections and the only difference between them is the method by which the ionospheric delay is accounted for. Each solution yields the RCB at the receiver, which is then presented relative to the bias as calculated by CODE.

5.2.4 Pseudorange

The pseudorange, *P*, is the difference between the satellite clock time and receiver clock time and in the idealised error-free condition is as follows, in seconds:

$$P = t_r - t_t \qquad (5.1)$$

where t_r is the GPST at the receiver (time of reception) and t_t is the GPST at the satellite (time of transmission). But it is also corrupted by the clock in the GPS receiver, the 'RCB', b_{rx}:

$$P = (t_r - t_t) + b_{rx} \qquad (5.2)$$

Realistically, there are propagation errors, relativistic effects and various other biases and noise effects and so the pseudorange, as measured by the GPS receiver, becomes (in seconds):

$$P = (t_r - t_t) + b_{rx} + b_{sv} + T_{sagn} + T_{trop} + T_{iono} + \varepsilon \qquad (5.3)$$

where T_{sagn} is the Sagnac bias, T_{trop} is the tropospheric delay, T_{iono} is the delay imposed by the ionosphere, b_{sv} is the satellite clock bias (accounts for the satellite specific bias and relativistic effects) and ε represents any unmodelled errors (which are ignored). Several corrections are applied to each of the timing solutions to account for the above delays or biases, but before they can be calculated several other fundamental corrections and calculations must be performed.

5.2.5 Fundamental corrections and calculations

This section describes the fundamental corrections and calculations which are necessary in order to compute the GPS solution (Allain and Mitchell 2009).

5.2.5.1 Differential Code Bias (DCB)

The two codes, modulated onto the L1 and L2 frequencies, have different electrical path lengths at the transmitter/receiver, which results in the so called Differential Code Bias (DCB), which are specific to each satellite and receiver and are provided by the CODE. The satellites show a small P1 to P2 bias, $\Delta_s^{1\to 2}t$, which gives a different clock bias for each frequency, f_1 and f_2. For time transfer, the absolute measurement of P1 and P2 is required. The single-frequency clock bias, $\Delta_s^1 t$ is offset from the dual-frequency clock bias, $\Delta_s t$ (which is given in the ephemeris data) as follows:

$$\Delta_s^1 t = \Delta_s t + \frac{f_1^{-2}}{f_1^{-2} - f_2^{-2}} \Delta_s^{1\to 2} t \qquad (5.4)$$

5.2.5.2 Antenna Offsets

The ephemeris data are calculated with respect to the satellite's centre of mass, whereas signal measurements are made with respect to the Antenna Phase Center (APC). These offsets are calculated by Schmid et al. (2007) for each satellite. The position of the antenna is found as follows:

$$\vec{S} \simeq \frac{S' - \Delta_v S}{S'} \vec{S}' \qquad (5.5)$$

where $\vec{S}$ is the antenna position, S' is the modulus of the satellite center of mass position vector, $\Delta_v S$ is the vertical component of the antenna offset and $\vec{S}'$ is the position vector of the satellite center of mass. The horizontal satellite

antenna offsets are neglected because they are extremely complicated to take into account and have an insignificant impact upon the range.

5.2.5.3 Satellite position, $\vec{S}$ and Time of transmission, t_t

The satellite positions are given by the ephemeris data and are presented in Earth-Centered Earth-Fixed (ECEF) frame coordinates at intervals of 15 min (Dow et al. 2005). The antenna coordinates are interpolated from the ephemeris (with the antenna offsets applied) at the TOT. Trigonometric interpolation, with 4 harmonics in the ECEF frame, is used as follows:

$$\vec{S} \simeq \sum_{i=1}^{4} \vec{A}_i \sin i\Omega t + \vec{B}_i \cos i\Omega t \qquad (5.6)$$

where $\vec{S}$ is the satellite position, *i* is the index of the harmonic, *Ω* is the angular velocity of the Earth, *t* is the time and $\vec{A}_i$ and $\vec{B}_i$ are the amplitude coefficients of the harmonic.

However, t_t is not explicitly recorded in the RINEX file and so iterative methods are used to extract it. It can be calculated provided the time of reception, t_r (recorded in the RINEX file) and the range between the satellite and receiver *r* are known:

$$t_t = t_r - r/c \qquad (5.7)$$

where *c* is the speed of light and the range can be calculated from the receiver and satellite coordinates, *R* and *S* respectively. But since *S* is a function of transmission time an iterative approach is required to find it. A first approximation of the receiver coordinates, *R*, may be found using the least squares method, described later.

The rate at which the distance between a GPS satellite and a ground-based receiver changes is:

$$|\dot{r}| < 800 ms^{-1} \qquad (5.8)$$

The uncertainty on the range, Δr, and the uncertainty of the transmission time, Δt_t, are related as follows:

$$\Delta r = |\dot{r}| \Delta t_t \text{ and } \Delta t_t < c^{-1} \Delta r \qquad (5.9)$$

The computation converges quickly towards the solution because each iteration multiplies the uncertainty on the range by:

$$c^{-1} |\dot{r}| < 2.7 \times 10^{-6} \qquad (5.10)$$

The range, r, between a GPS satellite and a ground based receiver must lie between 20.2 $\times$ 10^6 m and ~26.6 $\times$ 10^6 m, ignoring any delays, as follows (in metres):

$$r = (23.4 \pm 3.2) \times 10^6 \qquad (5.11)$$

The aim is to achieve an uncertainty of Δr < 0.1 m, which leads to the number of iterations required, 2, as follows:

$$\frac{\ln(0.1/3.2 \times 10^6)}{\ln(|\dot{r}|/c)} \leq 2 \qquad (5.12)$$

Results with an uncertainty of approximately 0.04 m RMS and a maximum of 0.15 m were achieved.

5.2.5.4 Satellite velocity, $\dot{\vec{S}}$

Satellite velocities are found by multiplying the coefficients, found from the position interpolation, with the derivatives of the trigonometric functions, also used in the interpolation of the satellite positions:

$$\dot{\vec{S}} \simeq \sum_{i=1}^{4} i\Omega\left(-\vec{A}_i \sin i\Omega t + \vec{B}_i \cos i\Omega t \right) \qquad (5.13)$$

where $\dot{\vec{S}}$ is the satellite velocity and the other terms are as described previously under the heading 'satellite position'. The precise satellite positions and velocities are hence used to calculate the relativistic clock bias of the satellites and the Sagnac bias.

5.2.6 Least squares technique

A least squares technique is used to solve for the position (*x*, *y*, *z*) and clock bias (b_{rx}) of a GPS receiver. The method shown below originates from Parkinson and Spilker (1996) and is used by Allain and Mitchell (2009).

If each satellite is given a number, *n*, and *r* is the range between satellite and receiver, then for n ≥ 4 satellites, taking a receiver of position *R* and satellite of position S_i, with 1 ≤ *i* ≤ n, then the pseudorange between a specific satellite, *i*, and receiver, ignoring errors, is as follows (in metres):

$$P_i = cb_{rx} + r_i \qquad (5.14)$$

where *c* is the speed of light and r_i is the range between satellite *i* and the receiver.

By rewriting r_i with the receiver to satellite vector, $\vec{r}_i$ and its unit vector, $\hat{r}_i$ and by using the position vectors of the satellite and receiver, $\vec{S}_i$ and $\vec{R}$ respectively, the pseudorange is as follows:

$$P_i = cb_{rx} + \hat{r}_i \bullet \vec{S}_i - \hat{r}_i \bullet \vec{R} \qquad (5.15)$$

The geometry matrix of the satellite constellation, *G*, is as follows:

$$G = \begin{pmatrix} u_{r_1}^x & u_{r_1}^y & u_{r_1}^z & -1 \\ \vdots & \vdots & \vdots & \vdots \\ u_{r_n}^x & u_{r_n}^y & u_{r_n}^z & -1 \end{pmatrix} \qquad (5.16)$$

where $u_{r_i}^x$, $u_{r_i}^y$ and $u_{r_i}^z$ are components of $\hat{r}_i$ and n represents the satellite number, for n ≥ 4.

Now by re-arranging Eq. 5.15:

$$\hat{r}_i \bullet \vec{R} - cb_{rx} = \hat{r}_i \bullet \vec{S}_i - P_i \qquad (5.17)$$

and by using the same notation, *G* becomes:

$$G \begin{pmatrix} x \\ y \\ z \\ cb_{rx} \end{pmatrix} = \begin{pmatrix} \hat{r}_1 \bullet \vec{S}_1 - P_1 \\ \vdots \\ \hat{r}_n \bullet \vec{S}_n - P_n \end{pmatrix} \qquad (5.18)$$

The solution to Eq. 5.18 is then found by taking the generalised inverse of *G*, $(G^T G)^{-1} G^T$ as follows:

$$\begin{pmatrix} x \\ y \\ z \\ cb_{rx} \end{pmatrix} \simeq (G^T G)^{-1} G^T \begin{pmatrix} \hat{r}_1 \bullet \vec{S}_1 - P_1 \\ \vdots \\ \hat{r}_n \bullet \vec{S}_n - P_n \end{pmatrix} \qquad (5.19)$$

The receiver coordinates are initially unknowns, yet are needed to find a solution. Therefore, iteration is necessary and a guess, such as the centre of the Earth, must be given at the start. Four or five iterations will yield a solution.

5.2.7 Common Pseudorange Corrections

The following corrections, from Parkinson and Spilker (1996), are applied to each of the timing solutions to account for the Sagnac effect, the tropospheric delay and the satellite clock bias.

5.2.7.1 The Sagnac bias, T_{sagn}

The Sagnac bias, T_{sagn} is calculated to account for the Earth's rotation during the propagation time of the GPS signal. The receiver coordinates must be known (or approximated) beforehand.

$$T_{sagn} \simeq c^{-1} \vec{\Omega} \cdot \vec{S} \times \vec{R} \qquad (5.20)$$

Where *c*, $\vec{\Omega}$, $\vec{S}$ and $\vec{R}$ represent the speed of light, the rotation vector of the Earth, the satellite position vector and the receiver position vector respectively.

5.2.7.2 Tropospheric delay, T_{trop}

The error imposed upon the GPS signal as it propagates through the troposphere, is approximated and corrected for as follows (wet and dry components):

$$T_{trop} \simeq T_{\pi/2,0} \frac{1.0121 \times e^{-0.133 \times 10^{-3} h}}{\sin \phi + 0.0121} \qquad (5.21)$$

The azimuth delay at sea level, the receiver altitude and the elevation angle of the satellite are represented as follows; $T_{\pi/2,0} \approx 2.44m$, *h* and ϕ respectively.

5.2.7.3 Satellite clock bias, b_{sv}

The satellite clock bias b_{sv} accounts for the satellite specific error $\Delta_s^{'}t$ and the satellite relativistic effects $\Delta_s^{r}t$ and is corrected for according to Kouba and Heroux (2001) as follows:

$$c\Delta_s^{r}t = 2S\dot{S}c^{-1} \Rightarrow cb_{sv} = c\Delta_s^{'}t + 2S\dot{S}c^{-1} \qquad (5.22)$$

where S and $\dot{S}$ represent the distance between the satellite and center of the reference frame and the rate of change of this distance respectively.

The product of these fundamental and common corrections results in a set of partially corrected pseudorange equations for each satellite-to-receiver ray path, which lays the foundation for each GPS timing solution. Only the method by which the ionospheric delay is to be accounted for remains.

5.2.8 Ionospheric corrections and the five timing solutions

The method of ionospheric compensation employed by each of the five timing solutions is now described below.

5.2.8.1 Single-frequency solution and no ionospheric correction

A single-frequency solution is obtained by extracting the P1 code from the RINEX file. This represents the first GPS timing solution and does not include any correction for the ionosphere (only the common pseudorange corrections) and illustrates the sheer magnitude of the ionospheric delay.

5.2.8.2 Single-frequency solution and the Klobuchar model

The second technique incorporates the Klobuchar model for ionospheric correction. This is a global model of the ionosphere and is represented by 8

coefficients, which are broadcast along with the GPS navigation message. Standard single-frequency GPS receivers use this model to correct for the ionosphere in real-time, via a receiver based algorithm. This solution portrays the current accuracy of such receivers. The data are recorded within the RINEX navigation file and are obtained from the IGS. Typically, a minimum of 50% RMS correction is obtained. Please refer to Klobuchar (1987) for more information.

5.2.8.3 Single-frequency solution with IRI model

The IRI 2001 model (Bilitza 2001) offers a global, 3D description of the electron density, given the solar activity and a particular date/time. This model is not available for real-time applications. Forward integration along slant paths of the model provide an estimate of the ionospheric delay imposed upon an L1 signal, using Eq. 5.23 below:

$$T_{iono} = \frac{40.3}{cf^2} \int Ndl \qquad (5.23)$$

where *c* is the speed of light, *f* is the frequency of the GPS signal (L1, 1575.42 MHz), *N* is the electron concentration, provided by the model and *dl* is the ray-path to voxel intersection.

5.2.8.4 Single-frequency solution with MIDAS

MIDAS, together with the pure single-frequency solution, represents a new approach to GPS timing solutions. MIDAS was first presented by Mitchell and Spencer (2003) and has since been upgraded (Spencer and Mitchell 2007). Data is input from the IGS/EPN network of dual-frequency receivers, based across Europe, in order to produce 4D real-time ionospheric maps. The ionospheric (group) delay may be found as follows:

$$T_{iono} = \frac{40.3}{cf^2} \int Ndl \qquad (5.24)$$

where $\int Ndl$ is the TEC in electrons per squared metre. The TEC is given by the line integral of the electron density between the satellite-to-receiver ray-path, which is provided by MIDAS.

5.2.8.5 Dual-frequency solution

Lastly, the dual-frequency solution is used to act as a benchmark. Two GPS signals with differing frequencies are used to measure the ionospheric delay, thus this method represents what is widely considered as the best ionospheric compensation technique, provided that accurate DCB data are obtained.

The ionosphere-free pseudorange, called P_0 here, is used to calculate the dual-frequency solution. P_0 is computed from four observables, P_1 and P_2, which represent the pseudoranges obtained from the precise P-code signal and L_1 and L_2, which are the recorded carrier phases of the signal, in terms of distance:

$$\begin{aligned} P_1 &= P_0 + T_{iono} f_1^{-2} + \varepsilon_1 \\ P_2 &= P_0 + T_{iono} f_2^{-2} + \varepsilon_2 \\ L_1 &= P_0 - T_{iono} f_1^{-2} + n_1\lambda_1 \\ L_2 &= P_0 - T_{iono} f_2^{-2} + n_2\lambda_2 \end{aligned} \qquad (5.25)$$

Where, ε_1 and ε_2 represent the noise, n represents the integer ambiguity and λ represents the carrier wavelength. Thus the following expressions for T_{iono} may be obtained from dual-frequency data:

$$\frac{P_1 - P_2}{f_1^2 - f_2^2} = T_{iono} + \frac{\varepsilon_1 - \varepsilon_2}{f_1^2 - f_2^2} \qquad (5.26)$$

$$\frac{L_1 - L_2}{f_1^2 - f_2^2} = -T_{iono} + \frac{n_1\lambda_1 - n_2\lambda_2}{f_1^2 - f_2^2} \qquad (5.27)$$

The first expression illustrates the ionospheric delay plus a noise term, whilst the second includes the integer ambiguity term, along with T_{iono}. Whilst a given satellite is visible, the ambiguity does not change. However, large and sudden changes can occur due to cycle slips, but these are detectable. T_{iono} is hence found by fitting Eq. 5.27 into Eq. 5.26 to yield:

$$P_1 - T_{iono} f_1^{-2} = P_0 + \varepsilon \qquad (5.28)$$

$$L_1 + T_{iono} f_1^{-2} = P_0 + n_1 \lambda_1 \qquad (5.29)$$

Fitting Eq. 5.29 into Eq. 5.28 then gives P_0. This forms part of the dual-frequency timing solution.

5.3 Results

Figures 5.2 to 5.5 inclusive show the diurnal variation in RCB for geomagnetically quiet and disturbed days selected from 2002, for GOPE and VILL. The minimum and maximum values for the Kp indices measured on each day are quoted in each corresponding figure caption. Kp values between 0-4 and 5-9 represent geomagnetically quiet and stormy days respectively. For reference, TEC maps are shown for certain days in Appendix A. Each figure consists of two plots, (a) and (b), which represent the fixed and mobile receiver techniques respectively. These figures illustrate the performance of MIDAS in comparison to other GPS timing solutions and in increasing order, the general accuracy is: no correction, Klobuchar, IRI 2001, MIDAS and dual-frequency.

Figures 5.2 to 5.5 inclusive show that the uncorrected solution gives the worst results because it always exhibits a significant peak around midday (as expected due to the Sun's ionizing radiation). During the night-time this solution generally provides a more stable and reduced RCB, but this is not so evident in Fig. 5.5 and the other solutions always perform better. The Klobuchar solution also exhibits a diurnal peak, which is either positive or negative and represents the model's tendency to undercompensate or overcompensate, respectively, for the ionospheric delay. This solution provides a steady night-time result and overall, a lower RCB than the solution with no ionospheric correction, but it is still highly variable. Generally, the IRI solution displays a small diurnal peak and despite its variability, it yields an improved RCB at night-time and daytime, with respect to the Klobuchar and uncorrected solutions.

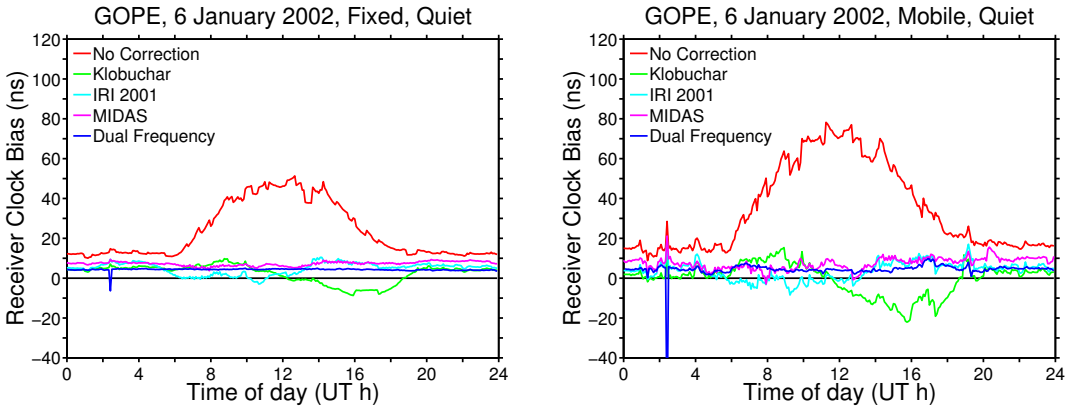

(a) (b)

Figure 5.2 – Receiver clock bias referenced to the receiver clock bias from CODE for GOPE 6 January 2002, for a quiet ionosphere (Kp index 0-1.3) using a fixed **(a)** and mobile **(b)** GPS receiver solution

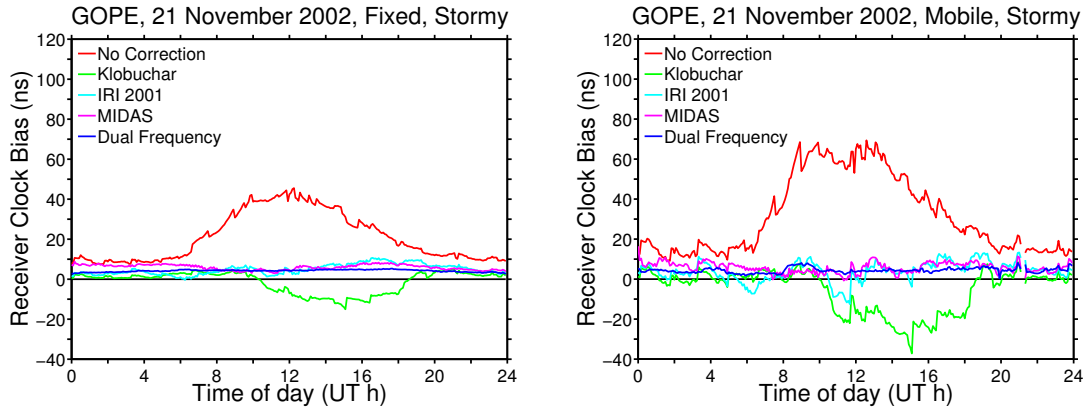

(a) (b)

Figure 5.3 – Receiver clock bias referenced to the receiver clock bias from CODE for GOPE 21 November 2002, for a stormy ionosphere (Kp index 4.3-6.7) using a fixed **(a)** and mobile **(b)** GPS receiver solution

MIDAS offers the most accurate and least variable single-frequency solution throughout the whole day. It eliminates the diurnal peak and is highly comparable to the benchmark dual-frequency solution. This yields a virtually constant RCB of 5 ns, largely irrespective of the time of day.

The solution characteristics described above are typical of both the quiet and stormy days. Figures 5.2a and 5.2b exhibit a negative-looking spike at around 02:00 UT for the dual-frequency solution. This is due to losses of lock on both frequencies at the receiver and shows that the MIDAS solution performs better under these conditions, because it is not vulnerable to isolated losses of lock on the L2 signal.

By comparing the results for a fixed receiver (see Figures 5.2a to 5.5a inclusive) to those for a mobile receiver (see Figures 5.2b to 5.5b inclusive), it is clear that the solutions become more variable and that the magnitude of the RCB generally increases. This is most evident for the following solutions: no correction, Klobuchar and IRI 2001, which is to be expected because the receiver is constantly moving and so an approximation of its position is regularly being made, which directly affects the accuracy of the fundamental calculations and corrections described in the Method. However, the MIDAS and dual-frequency solutions continue to yield a RCB of typically 10 ns or less, whilst the stability of the latter solution is slightly better than that of MIDAS.

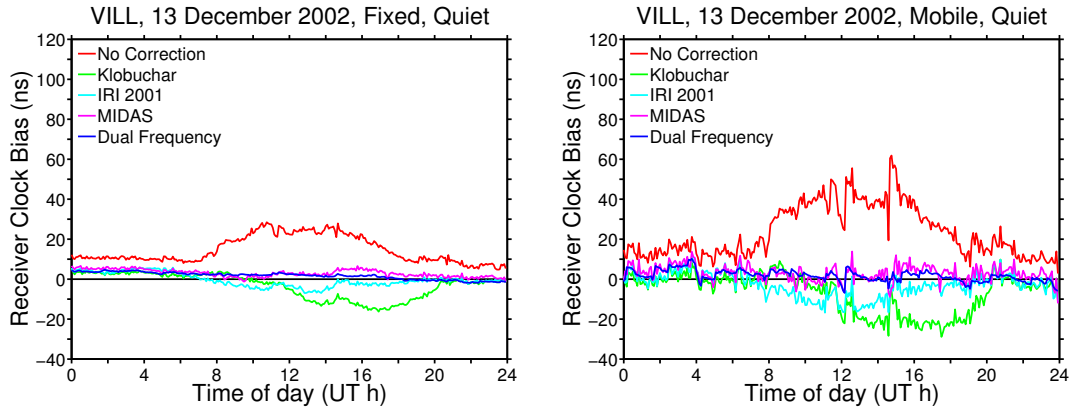

Figure 5.4 – Receiver clock bias referenced to the receiver clock bias from CODE for VILL 13 December 2002, for a quiet ionosphere (Kp index 0.3-1.7) using a fixed **(a)** and mobile **(b)** GPS receiver solution

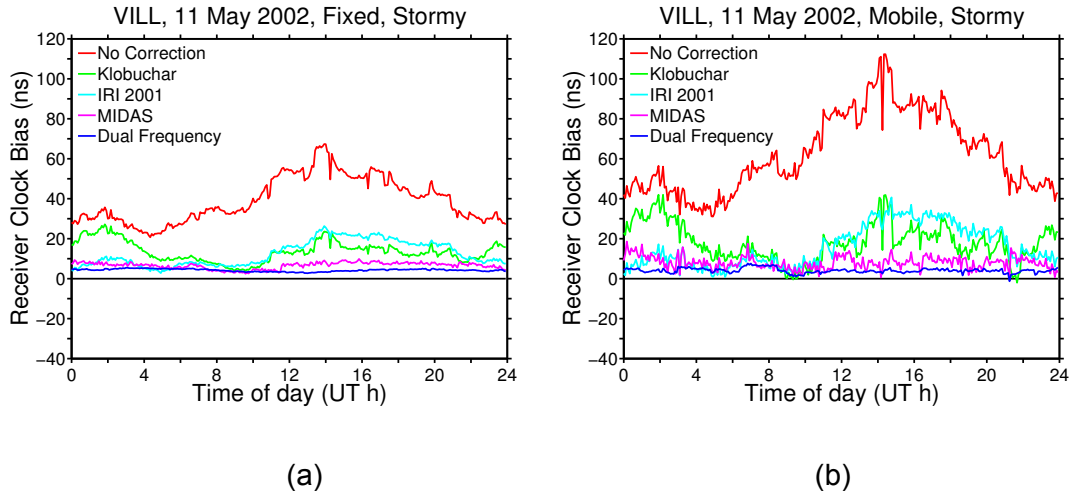

Figure 5.5 – Receiver clock bias referenced to the receiver clock bias from CODE for VILL 11 May 2002, for a stormy ionosphere (Kp index 0.7-6.7) using a fixed **(a)** and mobile **(b)** GPS receiver solution

Figures 5.6a and 5.6b illustrate the RCB at 12:00 UT (midday) for one quiet and one stormy day, respectively, from each month in 2002, for each timing solution, at VILL. The RCB have not been included for September due to data quality. Table 5.1 summarizes the RMS midday RCB for both the quiet and stormy days selected from 2002 at VILL. These figures, together with Table 5.1, reinforce the fact that the solution *accuracies, in increasing order are as follows: no correction, Klobuchar, IRI 2001, MIDAS and dual-frequency*. The solution with no correction is the worst and MIDAS gives the best single-frequency GPS timing solution, which is virtually on par with the dual-frequency solution.

Figures 5.6a and 5.6b also show a seasonal variation. The midday peak in RCB for the uncorrected solution tends to be larger in the autumn and winter months in comparison to the spring and summer months. The same is true for the Klobuchar and IRI 2001 solutions, which yield similar results to each-other. These models undercompensate at the beginning of the year (winter-spring) and compensate best during the summer, whilst overcompensating in the autumn. MIDAS and the dual-frequency solutions are very similar and the former performs slightly better in March 2002. According to the RMS values for the quiet days from Table 5.1, for each solution, MIDAS is shown to achieve an 86% and 37% RMS improvement with respect to the uncorrected and Klobuchar solutions correspondingly. The Klobuchar solution achieves its design goal of providing a minimum 50% RMS ionospheric correction.

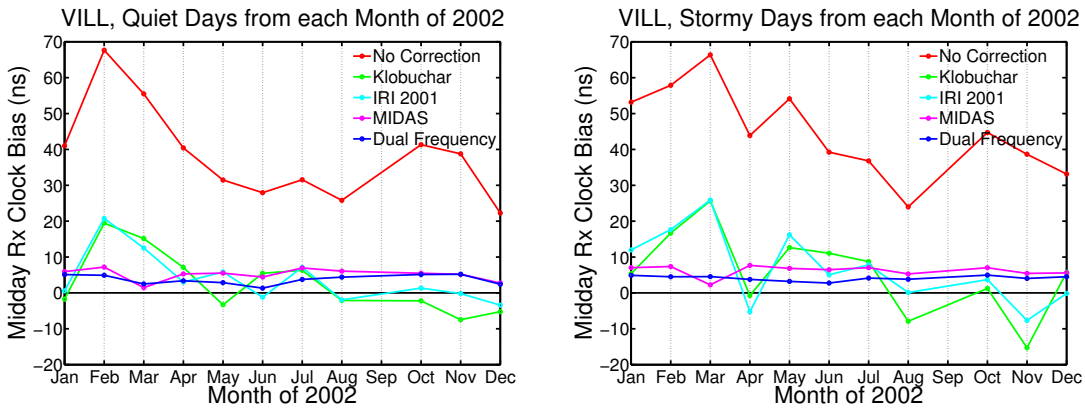

(a) (b)

Figure 5.6 – Midday (12:00 UT) receiver clock bias referenced to the receiver clock bias from CODE (using the fixed receiver solution) for one quiet day **(a)** and one stormy day **(b)** from each month of 2002 at VILL, excluding September due to data quality

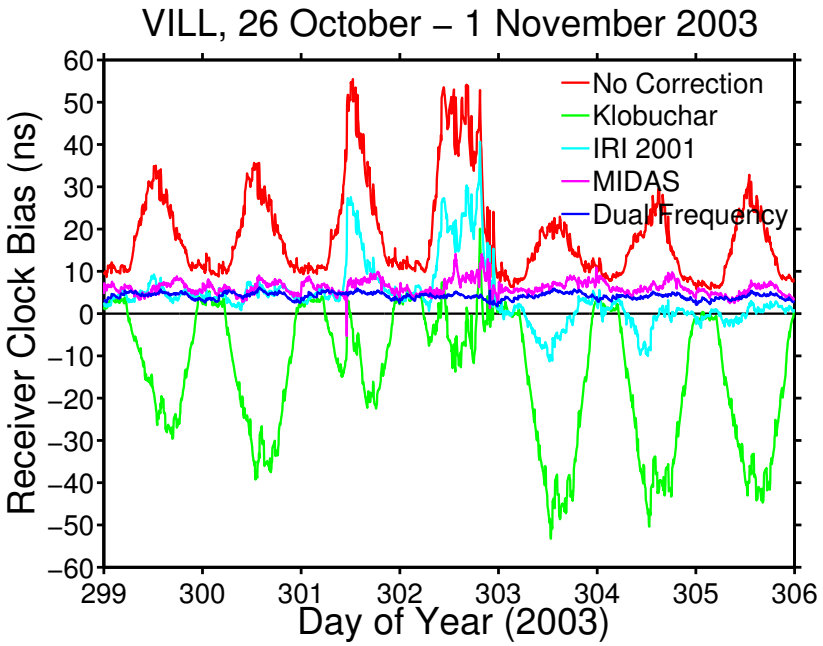

(a)

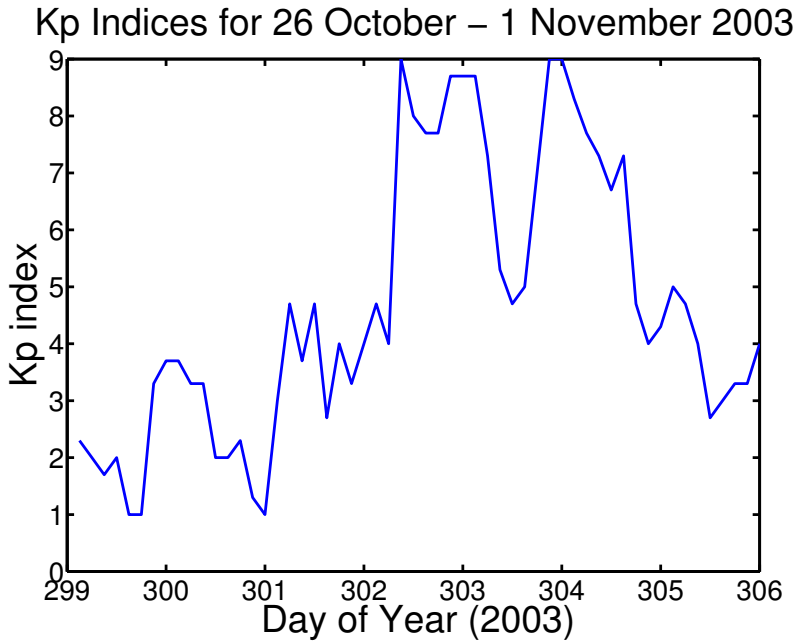

(b)

Figure 5.7 – Receiver clock bias referenced to the receiver clock bias from CODE for VILL before, during and after the October 2003 ionospheric storm, using a fixed GPS receiver solution **(a)** and corresponding Kp indices **(b)**

GPS Timing Solution	RMS receiver clock bias (ns)	
	Quiet days	Stormy days
No correction	40.6	46.0
Klobuchar	8.7	12.3
IRI 2001	8.0	12
MIDAS	5.4	6.4
Dual-frequency	4.0	4.2

Table 5.1 – RMS midday (12:00 UT) receiver clock bias (ns) referenced to the receiver clock bias from CODE (using the fixed receiver solution) for the quiet and stormy days selected from each month of 2002 at VILL, excluding September due to data quality

Figure 5.7a shows the variation in RCB for several GPS timing solutions over the period 26 October (day 299 of 2003) to 1 November 2003 (day 305 of 2003) inclusive, at VILL, using a fixed receiver solution. Two Coronal Mass Ejections (CME) were detected on days 302 and 303 (Skoug et al. 2004). This led to global and intense geomagnetic storms, as reflected by the corresponding high Kp indices in Fig. 5.7b. VILL is in Spain and it is important to note that days 302 and 303 mark the positive and negative phases of the storm respectively, across this region. Figure 5.7b shows that days 299 and 300 mark a depression in the ionosphere and are essentially quiet, which is reinforced by the corresponding low peak of about 35 ns in RCB in Fig. 5.7a, for the solution with no correction. In contrast, day 301 is moderately disturbed and with reference to Figures 5.2 to 5.5 inclusive, a midday peak in RCB of about 55 ns for the solution with no correction is not unusual, as seen on day 301 in Fig. 5.7a. Days 304 and 305 show the RCB after the storm. Figure 5.7a shows that the Klobuchar solution always overcompensates for the ionospheric delay and would indeed make the resultant timing solution worse on days 300, 303, 304 and 305, in comparison to the solution with no ionospheric correction. This was when the ionosphere is in negative storm and/or with very low TEC. A prolonged and highly variable RCB peak is seen in Fig. 5.7a on day 302, for the curve with no correction and is due to the intensely disturbed ionosphere, which exists not only during the daytime but continues deep into the night because of the positive phase of the storm. The same curve for day 303 exhibits a much lower peak than normal, at about 22 ns and is due to the negative phase of the storm, which causes a depression in the ionosphere. Overall, the IRI model is unstable and exhibits significant midday peaks. In contrast, the MIDAS and dual-frequency solutions provide fairly stable and comparable solutions throughout the intense period.

5.4 Conclusions and Discussion

A new single-frequency GPS timing solution that uses tomography to correct for the ionospheric delay has been presented and compared to various other GPS timing solutions in this thesis. Results were produced using fixed and mobile based receiver techniques for two IGS stations, VILL (Spain) and GOPE (Czech Republic).

In increasing order, the general timing accuracy is: no correction, Klobuchar, IRI 2001, MIDAS and dual-frequency. It should be noted that in certain circumstances the Klobuchar solution can produce a worse result than if there were no ionospheric correction at all, as seen by the extreme ionospheric conditions presented in Fig. 5.7a. MIDAS offers the best single-frequency solution because it is typically very stable and eliminates the large RCB seen at midday by the other single-frequency solutions. These characteristics are true for the fixed and mobile receiver solutions. The RMS RCB of the GPS timing solutions with no ionospheric correction, the Klobuchar model and the IRI model noticeably increase and become more variable under stormy conditions, as opposed to quiet conditions. This is in contrast to the MIDAS and dual-frequency solutions which continue to provide stable and accurate results under variable ionospheric conditions.

Overall MIDAS is shown to achieve accuracies comparable to those from the dual-frequency system presented here and is in some cases more robust as it is not vulnerable to L2 losses of lock. For stormy days, MIDAS provides a stable GPS timing solution accurate to within 6.4 ns RMS, typically correcting 86% of the error imposed by the ionosphere (according to the solution with no correction). In comparison, the broadcast Klobuchar model exhibits a 73% reduction in the ionospheric error, but as Figures 5.2 to 5.7 inclusive show, it can be highly variable (over the course of a few minutes to a few hours) and unreliable in severe conditions.

Chapter 6

6. Elevation masks, tomography and GPS timing

6.1 Introduction

The work in this Chapter is presented in Rose et al. (2011). I am grateful to the co-authors for providing general advice.

Some GPS receivers, built specifically for timing, may rely on a single GPS satellite for a timing solution. When a GPS receiver's position is already known, such a method is perfectly feasible. This however could lead to a highly unreliable solution, due to environmental, atmospheric and satellite specific errors. Contrastingly, for navigation receivers, when the receiver's position is unknown, signals from at least four GPS satellites are required to compute the user's 3D position and time. However, any errors in the measurements used to estimate the position will propagate into the timing solution. If navigation receivers are to be used for timing purposes then improved accuracies (relative to fixed timing receivers) may be obtained when placed in a fixed position over time; allowing the positional solution to improve over averaging and smoothing times of a few hours or more. Both fixed and mobile receiver scenarios are considered in this chapter and described later.

Signals from GPS satellites at high elevations (or directly overhead at zenith) travel through smaller portions of the ionosphere on their journey towards Earth and so contribute smaller errors to the GPS solution, in contrast to signals from GPS satellites at low elevations (near the horizon). Low elevation signals travel through a larger part of the ionosphere, are subject to more multipath and are

hence delayed by a larger and unknown amount when compared to high elevation signals. Satellite geometry plays an important role with respect to a GPS navigation/timing solution and may be measured by the Dilution of Precision (DOP). A good DOP is most likely to occur when there are wide angles of separation between the satellites, allowing more accurate horizontal and vertical positioning solutions, and hence timing solutions, to be found. A poor DOP is most likely when there are small angles of separation between the satellites. Overall, the future combination of the Galileo and GPS constellations will lead to greater performance, enhanced satellite geometry and a more dependable GNSS service (Feng 2003). More signals and measurements will be available, resulting in more accurate GNSS solutions and could lead to improved ionospheric modelling techniques (Hernández-Pajares et al. 2003).

The satellite geometry is investigated by enforcing various elevation masks, which begin at 5° and increase in steps of 5° up until 40°. Masks beyond this value are not employed due to the limited number of satellites available above 40°. Signals from GPS satellites originating from below the value of the elevation mask are excluded from the solution. For a mobile GPS receiver, signals from both high and low elevation satellites are required to calculate a good positioning and hence timing solution. Therefore, there is a trade-off to be made between excluding extremely low elevation satellites whilst still including some in order to calculate an accurate position. In contrast and since fixed GPS receivers only require at least one GPS satellite to calculate a timing solution, signals from a high elevation satellite are desirable, as they would be expected to contribute less ionospheric and multipath errors into the solution.

The aim is to minimise multipath, DOP and the ionospheric delay by finding a balance between the elevation mask and satellite geometry. Ionospheric tomography is also used towards producing a more accurate single-frequency GPS timing solution. In total, four separate GPS timing solutions are presented in the results, each with a different method of ionospheric compensation. The solutions are presented for fixed and mobile GPS receivers with: no ionospheric correction, the Klobuchar model, MIDAS and dual-frequency corrections. The first three are single-frequency solutions. The solution with no correction illustrates the sheer magnitude of the ionospheric delay, whilst the Klobuchar solution demonstrates the current capability of single-frequency receivers. The 4D tomographic real-time mapping system, MIDAS, portrays the capability of an

ionospheric tomography system. The dual-frequency solution provides a direct means of measuring the first order ionospheric delay and is hence a benchmark solution.

6.2 Method

6.2.1 Overview

The method described in Chapter 5 is built upon in this chapter to investigate the relationship between satellite geometry and GPS timing accuracy (Rose et al. 2009). Ionospheric tomography and elevation masks are the key focus points. Results are presented for fixed and mobile receiver situations. Allain and Mitchell (2009) use similar techniques to investigate the relationship between various ionospheric models and GPS positioning.

Geophysically quiet and stormy days from the year 2002 and a stormy period in October 2003 have been included in this study in order to represent diverse geophysical conditions. As GPS signals propagate through the ionosphere during 'quiet' periods such as solar minimum (a period of reduced ionospheric activity) they are delayed by smaller amounts. This is in contrast to periods of high ionospheric activity, which is more common during solar maximum conditions and can lead to significant delays upon GPS signals. It is relevant to present results during both quiet and stormy conditions because they are both equally valid situations.

Furthermore, it is important to illustrate the performance of MIDAS under challenging geophysical conditions. Days were chosen according to the Kp index, which measures the disturbances in the Earth's magnetic field and ranges from 0-9. It is important not to depend solely upon the Kp index to indicate the local geophysical conditions, but simply to use it as a general indication that a higher Kp is more likely to correspond to an enhancement in the ionosphere, but perhaps not over the particular area of interest. TEC maps may be plotted over these areas to illustrate the local ionospheric activity.

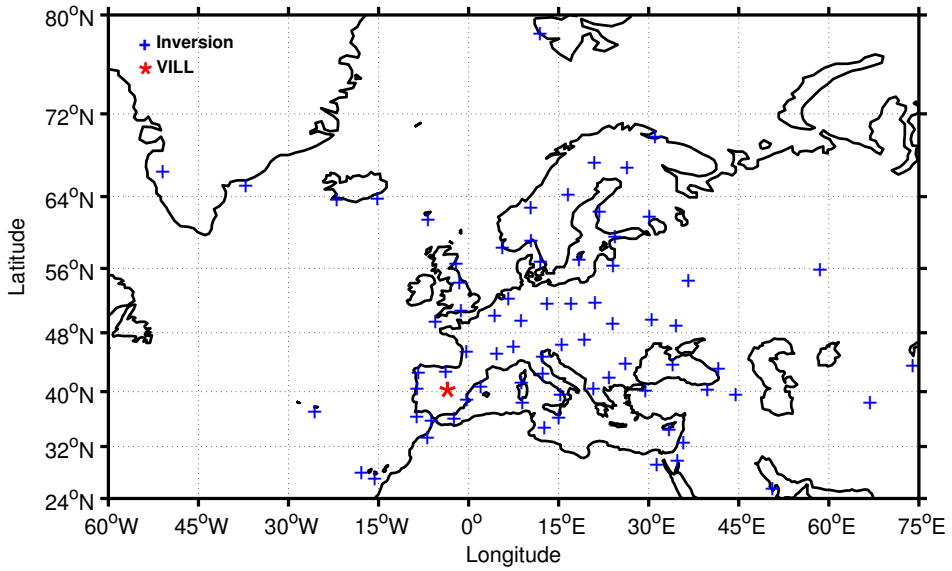

Figure 6.1 – Map of Europe, showing the test station VILL and those used for the inversion

Collectively, data from 74 IGS (Dow et al. 2009) and EPN (Bruyninx 2004) sites across mainland Europe are used in this study. These, together with MIDAS, are used to create the 4D real-time ionospheric maps, which are then employed to mitigate the ionospheric delay imposed upon the GPS signals. The tomographic grid ranges from -44° to +44° in steps of 4° in longitude and latitude and is centered on Europe at 50°N 15°E (see Figure 6.1). The altitude ranges from 100 km to 1500 km in steps of 50 km.

An additional IGS station was chosen as a test site; VILL (Villafranca, Spain), to demonstrate the performance of a single-frequency GPS receiver with: no ionospheric correction, the Klobuchar ionospheric correction and finally the MIDAS correction. Dual-frequency data are included in the resulting figures to enable direct comparisons between various GPS timing solutions. The IRI model is no longer included in these results as it is not available in real-time.

6.2.2 GPS timing solution, pseudorange and corrections

The timing solutions presented in this Chapter are described in Sections 5.2.3-8, along with the common/fundamental corrections and ionospheric compensation techniques. Similarly, each type of timing solution yields the RCB at the receiver,

which is presented relative to the precise bias as calculated by the Centre for Orbit Determination in Europe (CODE).

Note that if there are less than 4 satellites in view, due to the enforcement of a high elevation mask perhaps, the mobile GPS timing solution presented here will fail. This method is used to demonstrate that high elevation masks are not suited to mobile GPS receiver applications, albeit that in reality if less than 4 satellites are in view GPS receivers may have some memory of their previous position and so may be able to continue providing a solution for a short while, however, as time passes, the more degraded and unreliable the solution would become. Incidentally, the combination of the Galileo and GPS constellations will make more satellites available at higher elevations at any given time.

6.2.3 Multipath

Various elevation masks are employed with the aim of limiting multipath, but whilst maintaining reasonably good satellite geometry for the calculations. It is beyond the scope of this thesis to focus on techniques that attempt to significantly remove multipath from a GPS solution. In precise GNSS applications, and due to reflections from the local environment, multipath may be considered as one of the most limiting factors (Axelrad et al. 1996). Multipath is similar from one sidereal day (23 h 56 m 04 s) to the next, due to the repeatability of the GPS satellite ground-tracks (Choi et al. 2004). Sidereal filtering takes advantage of this repetition and may be used to help reduce the errors due to multipath in GNSS solutions (Ragheb et al. 2007). For sidereal filtering, data is required from at least two consecutive orbits. Following the estimation of 1 Hz positions for day one, high-frequency noise (unrelated to the satellite-receiver geometry) is removed via a low-pass filter. These positions are then shifted by the sidereal period and subtracted from the estimated positions on the second day (Choi et al. 2004). Multipath may be identified in the results by analysing the GPS timing accuracies over consecutive days: if there is a significant error in timing accuracy, due to multipath, on one particular day then it should also be evident the following sidereal day.

6.2.4 Satellite Geometry and DOP

GPS satellite positions may be described by azimuth and elevation angles, which are important when investigating the relationship between satellite geometry and GPS timing accuracy. The elevation angles at the horizon and at zenith are 0° and 90° respectively. North, East, South and West are represented by azimuth angles of 0°, 90°, 180° and 270° respectively. The ranging accuracy, multiplied by a dilution factor (that depends solely on geometry) may be used to estimate the positioning accuracy (Parkinson and Spilker 1996).

The number of GPS satellites in view also plays an important role; the more satellites there are, the more likely a good DOP will be obtained. The Position DOP (PDOP) gives a measure of the positioning accuracy (vertical and horizontal), while more specifically, the Horizontal and Vertical DOP are measured by the HDOP and VDOP respectively. Time DOP (TDOP) may be used as an indicator of timing accuracy and the Geometric DOP (GDOP) includes PDOP and TDOP. In general, a DOP greater than 6 represents poor satellite geometry and the worldwide PDOP median is roughly 2.5 according to Parkinson and Spilker (1996). The satellite geometry directly impacts the accuracy of the horizontal and vertical positioning solutions. The vertical positioning errors are correlated with the timing errors (explained below) and are therefore presented in the results, along with the TDOP. Note that in the case of a fixed receiver, when its position is already known, a good DOP is not so crucial. The following shows the relationship between the satellite geometry and the positioning error (Parkinson and Spilker 1996):

$$\Delta\bar{\boldsymbol{x}} = \boldsymbol{G}^{-1}\Delta\bar{\rho}_c \qquad (6.1)$$

where $\Delta\bar{\boldsymbol{x}}$ is the positioning error, $\boldsymbol{G}$ is the geometry matrix and $\Delta\bar{\rho}_c$ represents the pseudorange errors to each satellite. The satellite elevation and azimuth angles θ and ϕ respectively, can be translated into the east, north, up coordinate frame. The geometry matrix, for four satellites, is shown below:

$$G = \begin{bmatrix} \cos\theta_1 \sin\phi_1 & \cos\theta_1 \sin\phi_1 & \sin\theta_1 & 1 \\ \cos\theta_2 \sin\phi_2 & \cos\theta_2 \sin\phi_2 & \sin\theta_2 & 1 \\ \cos\theta_3 \sin\phi_3 & \cos\theta_3 \sin\phi_3 & \sin\theta_3 & 1 \\ \cos\theta_4 \sin\phi_4 & \cos\theta_4 \sin\phi_4 & \sin\theta_4 & 1 \end{bmatrix} \quad (6.2)$$

The covariance matrix of the solution may be expressed as follows (in m^2):

$$\mathrm{cov}(solution) = \sigma_R^2 \begin{bmatrix} (EDOP)^2 & & & \\ & (NDOP)^2 & & \\ & & (VDOP)^2 & \\ & & & (TDOP)^2 \end{bmatrix} \quad (6.3)$$

where σ_R^2 is the variance, EDOP and NDOP are the East and North DOP respectively, which make up the HDOP. The GDOP is the square root of the trace of the GDOP matrix and may be found as follows:

$$GDOP = \sqrt{(EDOP)^2 + (NDOP)^2 + (VDOP)^2 + (TDOP)^2} \quad (6.4)$$

Negative correlation between vertical positioning errors and timing errors are shown by an example in Parkinson and Spilker (1996) that yields non-zero off diagonal terms in the covariance of position matrix. Accordingly, a positive timing error will typically correspond with a negative vertical positioning error and vice versa. In general, vertical positioning and timing errors largely correlate and with opposite signs.

6.2.5 Elevation Masks

An elevation mask of 20° means that signals from all of the GPS satellites below this value will be ignored and only signals from those above it will be included in the timing solution. The masks range from 5° to 40° in steps of 5°. Lower elevation masks are most likely to yield better DOP's than high elevation masks. This is because there are fewer satellites in view at higher elevations, which reduces the likelihood of good angles of separations between them. High elevation satellite signals are less prone to multipath and ionospheric delays in comparison to signals originating from low elevation satellites. GPS satellite

elevation angles are linked to multipath (Jin and de Jong 1996), whereas satellite azimuth angles are not crucial to this investigation, but may aid towards specifically locating multipath sources if desired.

6.3 Results

GPS timing solutions for fixed and mobile GPS receiver situations are presented that employ various elevation masks and different ionospheric compensation techniques. The figure titles specify the: receiver name, date(s), type of solution (fixed/mobile, where relevant) and elevation mask. The figure captions include the minimum and maximum Kp indices measured for the particular period. These results are representative of solar maximum conditions. For reference, TEC maps are shown for certain days in Appendix A.

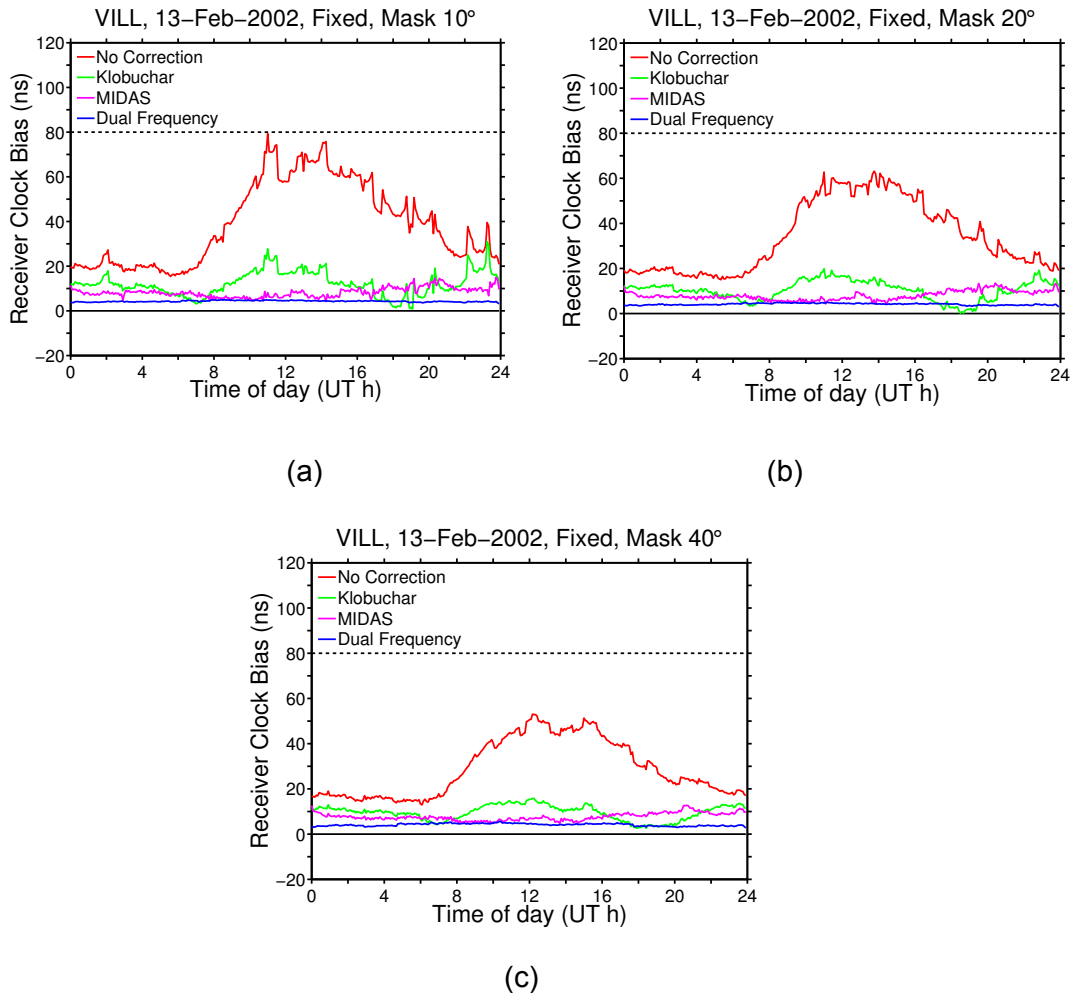

Figure 6.2 – Receiver clock bias referenced to the receiver clock bias from CODE for VILL 13 February 2002 (Kp index 1.0-3.7) using a fixed receiver solution at an elevation mask of **(a)** 10° **(b)** 20° **(c)** 40°. Dashed horizontal line at 80 ns aids the comparison between elevation masks

Figures 6.2a-c represent the diurnal variation in RCB for 13 February 2002, at VILL, using the *fixed* receiver solution. A dashed horizontal line is fixed at 80 ns RCB to help compare the reduction in the diurnal peak of RCB when using a 20° or 40° elevation mask, as opposed to a 10° mask. These figures imply that the accuracy of a GPS timing solution, for a *fixed* receiver, improves as satellites at lower elevations are excluded. The 'no correction' curves effectively illustrate the magnitude of the ionospheric error and this clearly reduces as the elevation mask increases from 10° to 40°: the curve peaks at approximately 80 ns in Fig. 6.2a and at roughly 55 ns in Fig. 6.2c respectively. Table 6.1 summarizes the RMS RCB for both the geophysically quiet and stormy days selected from 2002, at VILL (using the fixed solution). The data includes one quiet and stormy day from each month, excluding September due to data quality. Table 6.2 summarizes the standard deviations over the same period.

GPS Timing Solution	**RMS receiver clock bias (ns)**			
	5° mask	**15° mask**	**20° mask**	**40° mask**
No correction	34.9	30.8	28.9	24.4
Klobuchar	11.0	9.4	8.8	7.8
MIDAS	6.7	6.3	6.3	6.1
Dual-frequency	4.4	4.3	4.3	4.2

Table 6.1 – RMS receiver clock bias (ns) referenced to the receiver clock bias from CODE (using the fixed receiver solution at VILL) with 5°, 15°, 20° and 40° elevation masks, for Geophysically quiet and stormy days selected from each month of 2002, excluding September due to data quality

GPS Timing Solution	**Standard deviation of the receiver clock biases (ns)**			
	5° mask	**15° mask**	**20° mask**	**40° mask**
No correction	15.3	13.1	12	9.7
Klobuchar	8.9	7.8	7.3	6.2
MIDAS	2.2	2.1	2.1	2.0
Dual-frequency	1.8	2.0	2.0	1.7

Table 6.2 – Standard deviation (ns) (using the fixed receiver solution at VILL) with 5°, 15°, 20° and 40° elevation masks, for Geophysically quiet and stormy days selected from each month of 2002, excluding September due to data quality

According to Table 6.1, the most accurate solutions are obtained by employing the highest elevation mask tested, 40°, as opposed to the lowest elevation mask, 5°. By comparing these masks, the greatest improvements in timing accuracy are shown by the no correction and Klobuchar solutions: 30% and 29% respectively. The MIDAS and dual-frequency timing solutions improve by only 9% and 5% respectively under the same circumstances. These reductions are most likely due to both the decrease in propagation delay and multipath when using the 40° mask.

Overall, Table 6.2 indicates that the higher the elevation mask, the less variable the timing solution becomes. This table shows that the timing solution with no ionospheric correction has a standard deviation of 13.1 ns when an elevation mask of 15° is employed. This solution improves by 26% when a 40° mask is used. The Klobuchar solution is shown to be less variable and improves by 20% when using a 40° mask as opposed to a 15° mask. The MIDAS and dual-frequency solutions have lower and similar standard deviations than the other solutions, so much so that the changes in elevation mask have little effect. In fact, one would expect that as the elevation mask is increased, the dual-frequency solution would become less variable. This is true when comparing only the 40° mask with the 5° mask, however the standard deviations for the 15° and 20° mask are both 0.2 ns higher than the standard deviation obtained using a 5° mask. Though these changes are relatively small, it does suggest that there are other accuracy-limiting factors such as multipath.

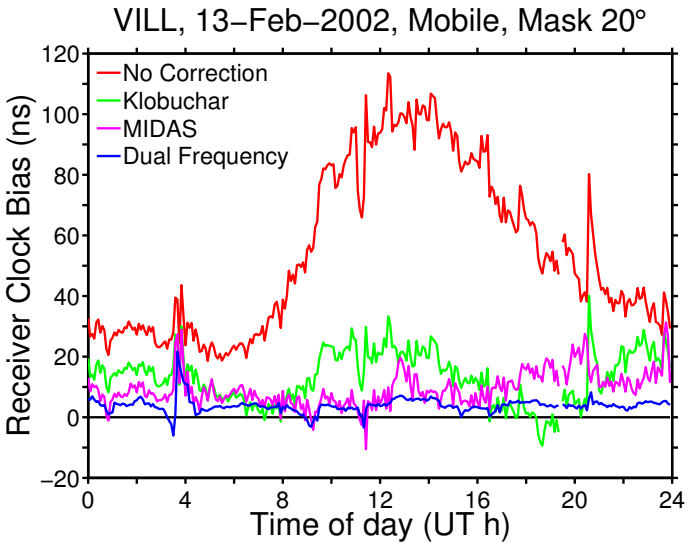
VILL, 13–Feb–2002, Mobile, Mask 20°
No Correction
Klobuchar
MIDAS
Dual Frequency
Receiver Clock Bias (ns)
Time of day (UT h)

(a)

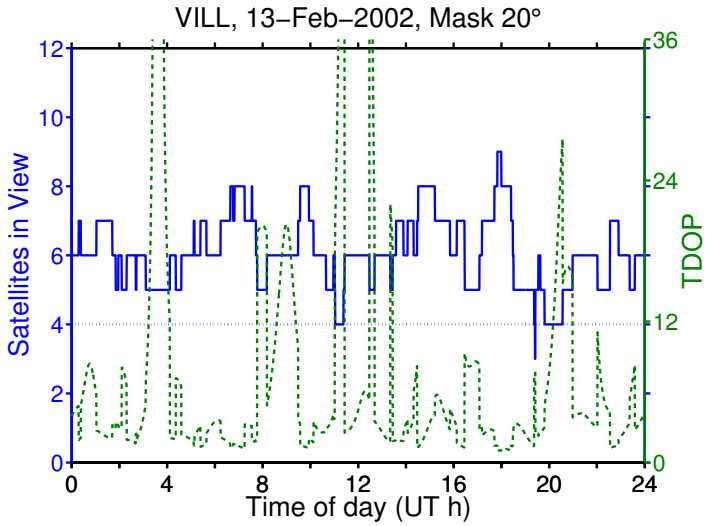
VILL, 13–Feb–2002, Mask 20°
Satellites in View
TDOP
Time of day (UT h)

(b)

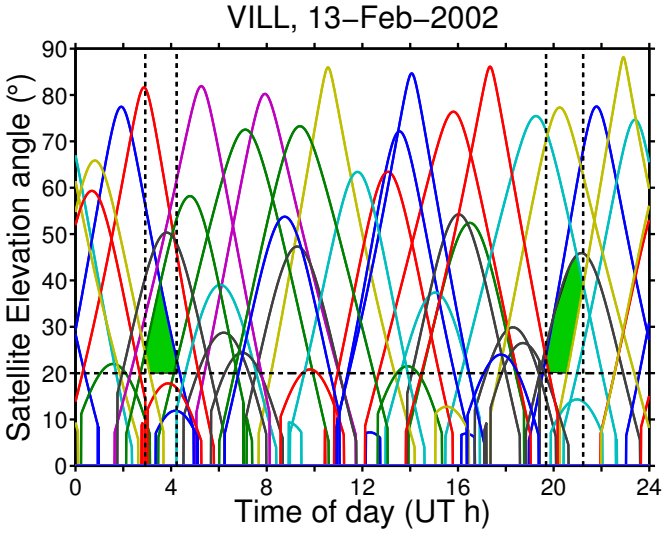
VILL, 13–Feb–2002
Satellite Elevation angle (°)
Time of day (UT h)

(c)

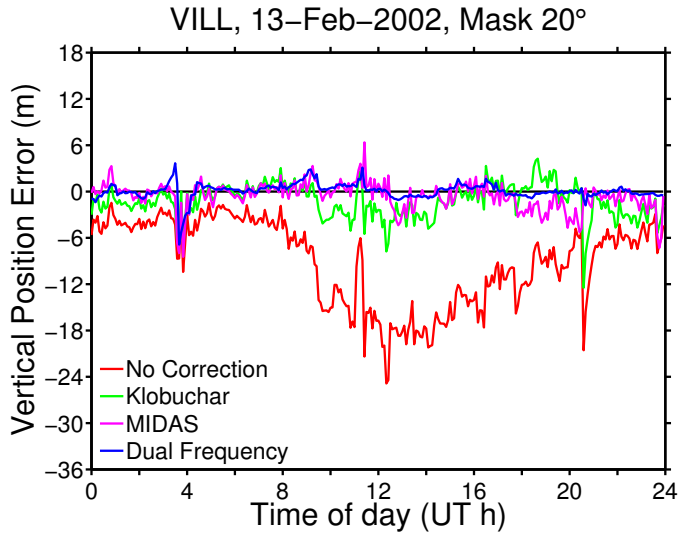

(d)

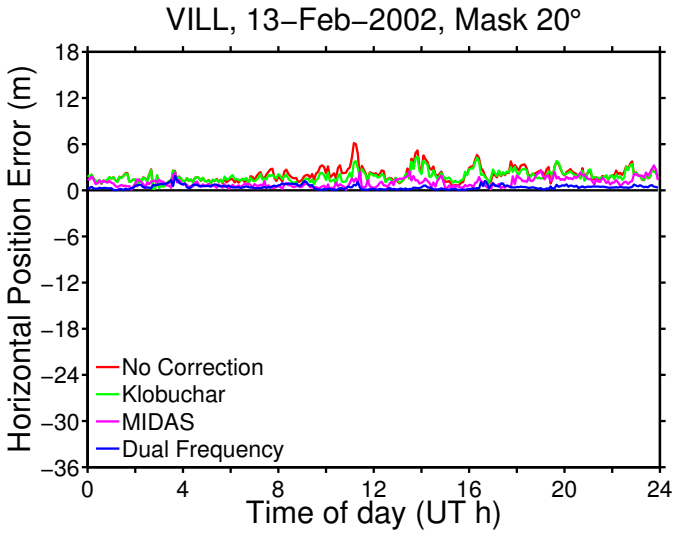

(e)

Figure 6.3 – Various results for 13 February 2002, at VILL, using a mobile receiver solution and an elevation mask of 20° (Kp index 1.0-3.7), as follows: **(a)** Receiver clock bias referenced to the receiver clock bias from CODE, **(b)** the number of satellites in view and the TDOP, **(c)** the satellite elevation angles (the vertical dashed lines highlight the time periods of interest and the patches define the area more specifically), **(d)** the vertical positioning errors, **(e)** the horizontal positioning errors

Figure 6.3a shows the diurnal variation in RCB for 13 February 2002, at VILL, using the *mobile* receiver solution and an elevation mask of 20°. Figures 6.3b-e are presented to explain particular anomalies. Figures 6.3b and 6.5b illustrate the number of satellites in view and the TDOP. A dotted horizontal line marks the threshold at which there are only 4 satellites in view. When the number of satellites falls below this threshold, the corresponding mobile timing solution is unavailable because at least 4 satellites are required for a 4D solution. Two prominent examples of error in the timing solution are shown at approximately 04:00 UT h and 20:00 UT h (see the large spikes) in Fig. 6.3a. Figure 6.3b shows that just before 04:00 UT h the number of satellites in view dropped from 6 to 5, which was followed by an increase in the TDOP.

Additionally, just before 20:00 UT h, the number of satellites in view momentarily dropped from 5 to 3 (see the slight data gap in Fig. 6.3a) before settling at 4 in view, which is accompanied by a rise in TDOP. Figures 6.3c and 6.5c show the satellite elevation angles of all of the satellites in view on the day in question, each curve represents a particular satellite. A dashed horizontal line has been placed at the satellite elevation angle of 20° on Fig. 6.3c. The satellite tracks above/below this line represent those that are available/unavailable when a 20° elevation mask is implemented. The dashed vertical lines in Figures 6.3c and 6.5c highlight particular periods of interest, whilst the green patches illustrate instances when only satellites at high elevations are available (around 30-40° for example). For the purpose of this investigation, it is not necessary to show which curve corresponds to which GPS satellite. Figure 6.3c shows that at around 04:00 UT h and above 20° elevation, there is a period when only satellites at even higher elevations were available. This is akin to an even higher elevation mask that varies between ~20° and ~40°.

Figures 6.3d and 6.3e show that the vertical positioning errors are much larger than the horizontal positioning errors. By analysing the no correction curves: the midday peak in vertical positioning error reaches approximately -28 m, which is equivalent to roughly 93 ns and the midday peak in RCB is roughly +112 ns (see Fig. 6.3a). This agrees with the relationship explained in the Method (see section 6.2.4), whereby the vertical positioning errors are most likely to correlate with the timing errors and with opposite signs.

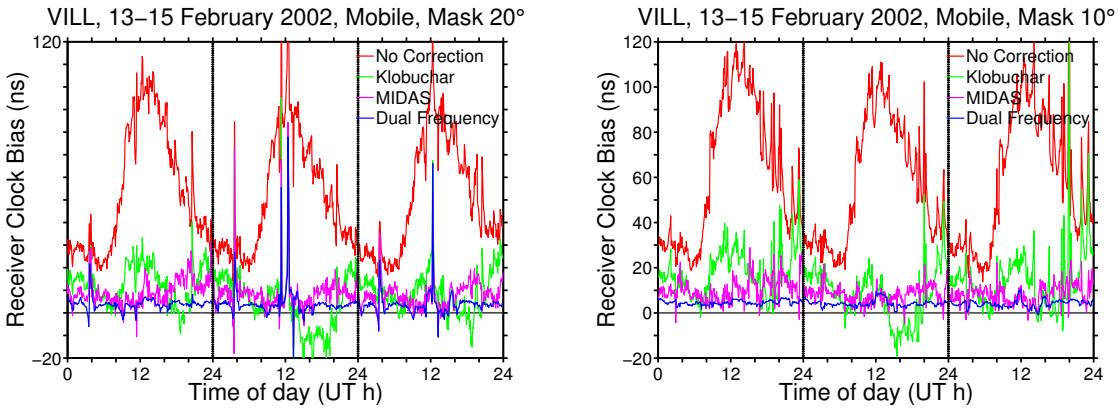

(a) (b)

Figure 6.4 – Receiver clock bias referenced to the receiver clock bias from CODE for VILL 13-15 February 2002 (Kp index 0-3.7) using a mobile receiver solution at an elevation mask **(a)** 20° **(b)** 10°

Figure 6.4a shows the variation in RCB using a 20° mask over a consecutive three day period, 13-15 February 2002 inclusive. A dashed vertical line is shown to represent the boundary line between each consecutive day. The previously discussed anomalies from Fig. 6.3a are now of course evident in the first day shown in Fig. 6.4a and are repeated on the following two days. See the spikes at around 04:00 and 20:00 UT h. By analysing these consecutive days, the most likely cause of the anomalies is due to the satellite geometry. More specifically, as the number of satellites in view decreases there is a reduced likelihood of a good DOP, as is the case here, whereby only high elevation satellites are in view. This prevents an accurate positioning solution from being calculated, which in turn causes a large TDOP and results in a degraded timing solution.

Similarly, distinctive anomalies exist at around 11:00, 12:00 and 13:00 UT h for the 14 and 15 February 2002 in Fig. 6.4a (see the large spikes). They are also evident for 13 February 2002, though on a smaller scale. Fig. 6.3b shows that at these times the TDOP increases significantly and the number of satellites in view changes rapidly at around 11:00 to 12:00 UT h and fluctuates between 6 and 5 at 13:00 UT h. Figure 6.4b shows the variation in RCB using a 10° mask over the same period. By comparing Figures 6.4a and 6.4b, the single-frequency solutions show less variability in Fig. 6.4a (20° mask) when compared to Fig. 6.4b (10° mask), most notably from midday onwards. The dual-frequency solution however becomes more variable. Furthermore, there are more anomalies when using a 20° elevation mask, rather than the 10° mask. This

indicates that there is a trade-off between the size of the elevation mask and the timing accuracy. When the elevation mask is too high, there is a bad effect on satellite geometry and TDOP (see Fig. 6.3b-c).

The single-frequency and even the dual-frequency solutions exhibit a clear anomaly between ~03:00 and ~04:00 UT h in Fig. 6.5a. Figure 6.5c illustrates that the most likely cause is due to a lack of GPS satellites between 0° and ~40° elevation at particular instances during this period (see highlighted area). Figure 6.5b shows that at this time the number of satellites in view drops to 6 and there is an increase in TDOP. Large increases in TDOP at 11:00 and 14:00 UT h coincide with setting satellites and correspond to slight anomalies in Fig. 6.5a at these times (see the small downward spikes).

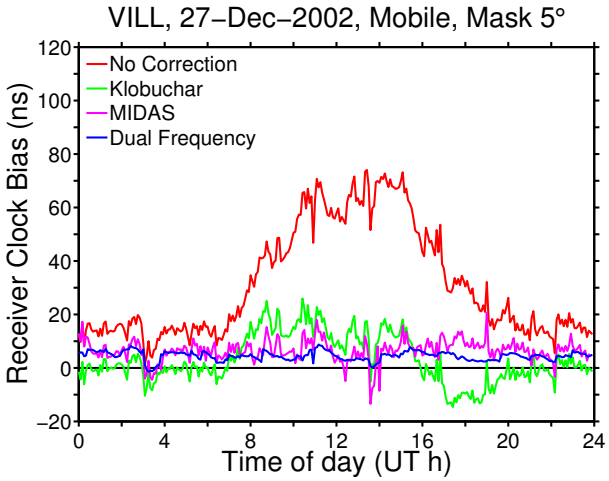

(a)

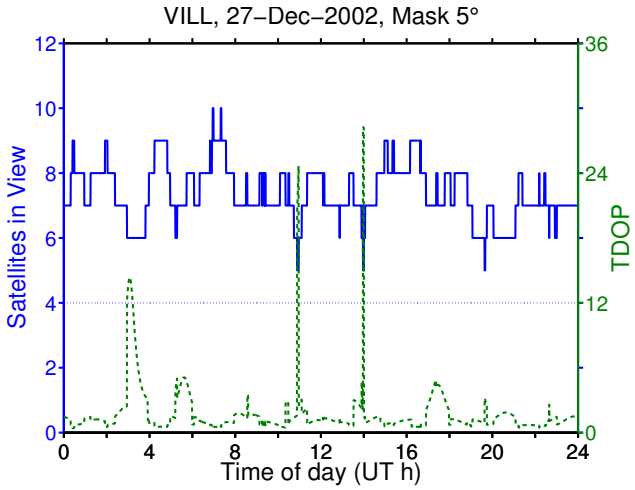

(b)

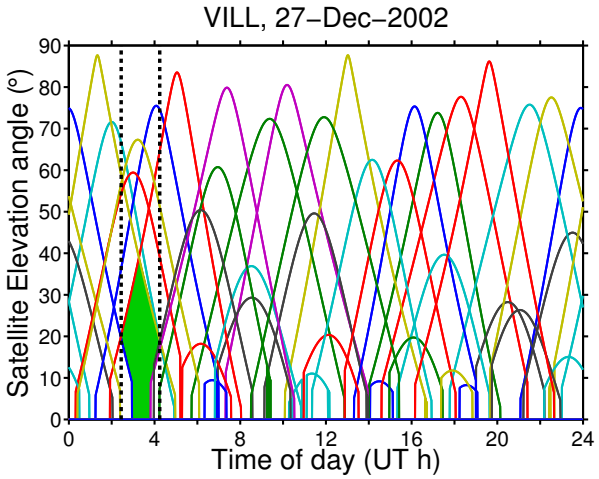

(c)

Figure 6.5 – Various results for 27 December 2002, at VILL, using a mobile receiver solution and an elevation mask of 5° (Kp index 3.3-6.0), as follows: **(a)** Receiver clock bias referenced to the receiver clock bias from CODE, **(b)** the number of satellites in view and the TDOP, **(c)** the satellite elevation angles (the vertical dashed lines highlight the time periods of interest and the patch defines the area more specifically)

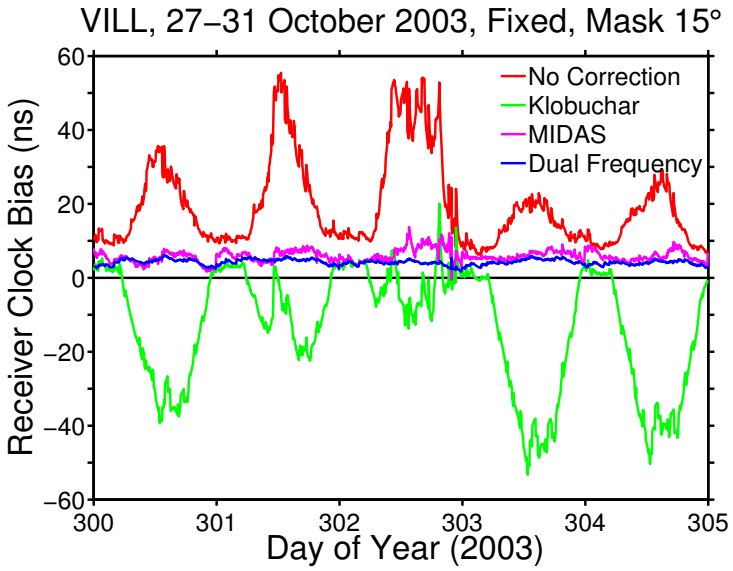

(a)

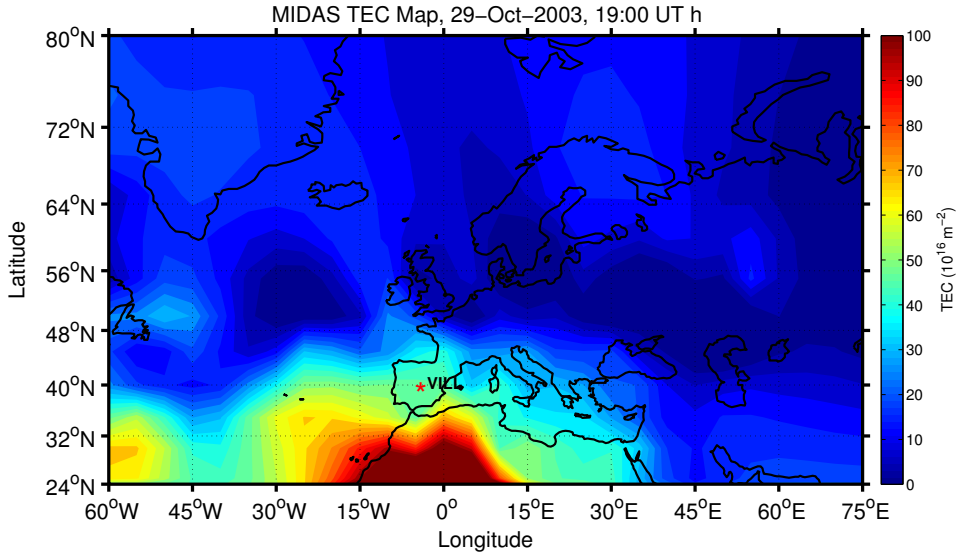

(b)

Figure 6.6 – Results for October 2003: **(a)** Receiver clock bias referenced to the receiver clock bias from CODE for VILL 27-31 October 2003 (Kp index 1.0-9.0) using a fixed receiver solution at an elevation mask of 15°, **(b)** MIDAS TEC map for 29 October 2003 at 19:00 UT h

Figure 6.6a shows the variation in RCB (using a 15° mask and the fixed timing solution) over a consecutive five day period, 27-31 October 2003 inclusive. Two Coronal Mass Ejections (CME) were detected on days 302 and 303, which led to global and intense geomagnetic storms. These two days mark the positive and negative phases of the storm respectively, across the European region. A snapshot of the ionosphere across Europe on the 29 October 2003 (day 302) at 19:00 UT h is shown by Fig. 6.6b. This figure was produced using MIDAS and shows the spatial distribution of vertical TEC. TEC Units ranging between 40-60 are apparent across VILL at this time and correspond to the highly variable peak in RCB, which continues deep into the night, shown by the no correction curve in Fig. 6.6a. The negative phase of the storm causes a depression in the ionosphere, resulting in the lower than average RCB for the curve with no correction on day 303 (Fig. 6.6a). Table 6.3 summarizes the RMS RCB for 27-31 October 2003, at VILL (using the fixed solution).

GPS Timing Solution	**RMS receiver clock bias (ns)**			
	5° mask	**15° mask**	**20° mask**	**40° mask**
No correction	25.2	22.8	21.4	18.1
Klobuchar	22.5	20.7	19.5	15.2
MIDAS	6.3	6.1	6.1	5.9
Dual-frequency	4.4	4.3	4.2	4.2

Table 6.3 – RMS receiver clock bias (ns) referenced to the receiver clock bias from CODE (using the fixed receiver solution at VILL) with 5, 15°, 20° and 40° elevation masks, calculated over a geophysically stormy period between 27 and 31 October 2003

GPS Timing Solution	**Standard deviation of the receiver clock biases (ns)**			
	5° mask	**15° mask**	**20° mask**	**40° mask**
No correction	13.1	11.9	11	8.9
Klobuchar	17.3	16.0	15	11.9
MIDAS	1.8	1.6	1.6	1.6
Dual-frequency	0.7	0.8	0.8	0.9

Table 6.4 – Standard deviation (ns) (using the fixed receiver solution at VILL) with 5, 15°, 20° and 40° elevation masks, calculated over a geophysically stormy period between 27 and 31 October 2003

Table 6.4 summarizes the standard deviations over the same period. According to Table 6.3, the most accurate solutions are achieved when the highest elevation mask (40°) is employed. Notably the no correction and Klobuchar RMS RCB values differ by less than 3 ns, whichever mask is used. The latter solution performs only slightly better. The MIDAS and dual-frequency RMS RCB values are comparable, differing by less than 2 ns irrespective of elevation mask. Table 6.4 shows that the no correction and Klobuchar solutions are least variable when the highest elevation mask is used. The variability of the MIDAS and dual-frequency solutions remains largely constant irrespective of elevation mask. Interestingly, Table 6.4 shows that the Klobuchar solution is roughly 32-36% more variable than the solution with no ionospheric correction, whichever elevation mask is used. This along with Fig. 6.6a (see days 300, 303 and 304) show that during intense geomagnetic storms it may be better not to employ the broadcast Klobuchar corrections. According to Table 6.4, and with a 15° mask, the standard deviations of the RCB for the MIDAS and dual-frequency solutions are 1.6 ns and 0.8 ns respectively. MIDAS and the dual-frequency solutions yield a 90% and 95% improvement respectively when compared to the Klobuchar solution.

6.4 Conclusions and Discussion

Ionospheric tomography and elevation masks have been used to reduce the overall timing error and produce a new single-frequency GPS timing solution. This is compared to other timing solutions produced for the IGS station, VILL (Spain), using fixed and mobile based receiver techniques. Results were produced using data from the previous solar maximum in 2002 and a particular stormy period in October 2003.

The tomographic mapping system, MIDAS, provides the most accurate and least variable single-frequency GPS timing solutions. Using MIDAS, accuracies to within 10 ns are achievable in fixed GPS receiver situations, even during periods of intense geomagnetic activity. In general and in increasing order the timing accuracy is as follows: no correction, Klobuchar, MIDAS and dual-frequency. However, during intense storms the Klobuchar solution may produce a worse timing solution than if there were no ionospheric correction at all. The method of ionospheric error compensation is integral to an accurate timing solution.

This research indicates that for fixed GPS receivers, the greater the elevation mask; the less variable and more accurate the timing solution will be. This relationship continues up to and including the 40° elevation mask, (masks beyond 40° have not been tested). This is because signals from satellites at high elevations are typically subject to less multipath and less ionospheric delays. Good satellite geometry is not crucial to a fixed timing solution and a balance between the number of available satellites and those at high elevations should be found. On the other hand, an elevation mask of 40° typically reduces the number of satellites in view to around 2 or 3 at any given time and since the average of all of the RCB's (calculated from all of the satellites in view) forms the fixed GPS timing solution, if just one of the satellites used is subject to a fault/error then it has the potential to seriously degrade the overall solution.

Relying on just one satellite, or too few, can make it difficult to detect and remove satellite specific errors. Therefore, it would be prudent to employ some sort of warning/alarm system that could detect large anomalies and not only prevent the erroneous satellite from being included in the solution but also

dynamically lower the elevation mask to increase the number of satellites in view. In continuation, a potential solution to this might be to perform TDOP analyses. By using the known receiver position (or trajectory of a mobile receiver) along with the satellite ephemeris data, the covariance matrix (from which the TDOP is calculated) may be computed prior to the actual data collection. This technique may be employed to give an advanced warning of the potential degradation in timing accuracy that could be due to changes in satellite geometry.

For mobile GPS receivers (unknown position) the timing solutions improve as the elevation mask is increased from 5° to 10°. Multipath appears to be reduced by using at least a 10° elevation mask. However, as the mask is increased from 10° to 20° some errors can be exasperated, due to the degradation of satellite geometry, that actually worsen the overall solution (whereas errors due to multipath and the ionosphere are expected to decrease with higher elevation masks). The best choice of elevation mask for a mobile receiver lies between: 10° and 20°. Nonetheless, even a 20° elevation mask can lead to times when there are less than 4 satellites in view.

Although it may be crude to assume that as soon as there are less than 4 satellites are in view, the mobile GPS timing solution will fail; this method does suitably demonstrate that high elevation masks are not suited to mobile GPS receiver applications. There are occasions when there are not any low elevation satellites in view at all, say between 0° and 40°. These periods have been shown to adversely affect the mobile timing solution. A balance must be struck between elevation mask and its effect on satellite geometry to minimise the propagation delays and optimise the timing solution, depending upon application. The rising/setting of satellites can improve/worsen the overall geometry, but the effects of acquiring/losing a satellite signal can lead to momentary fluctuations in timing accuracy and increases in TDOP.

The Galileo constellation will consist of 30 satellites and several new signals. These, together with the GPS constellation (and its forthcoming modernization) will lead to a much larger number of satellites in view at any given time and will improve the overall satellite geometry. This will result in a more dependable and reliable GNSS era, leading to improvements in positioning and timing

accuracies. Please see http://www.esa.int/esaNA/galileo.html for more information.

MIDAS is currently used to generate real-time ionospheric corrections, which are available via the internet. The corrections are created using GPS data, which are available from an existing infrastructure and are processed at the University of Bath. The corrections could be broadcast to actual GPS end-users in the field, in real-time, using a radio signal. This would enable more accurate GPS timing solutions to be obtained from a low-cost single-frequency GPS receiver, than is currently possible using the broadcast ionospheric corrections, albeit with a modification to enable them to receive and interpret the MIDAS data. It is intended that these real-time ionospheric corrections, for Europe, will be broadcast across the UK in the near future. Two or more free running devices may be synchronised anywhere in the world, using GPS, to within 10 ns using the MIDAS system proposed here. This system could also help to reduce the risks of poor synchronisation during highly variable ionospheric conditions and in particular during the impending solar maximum.

Chapter 7

7. Baseline comparisons and GPS time transfer with tomography

7.1 Introduction

Supposing two GPS receivers were collocated and assuming everything is equal (hardware and setup for example), then the GPS timing solutions according to each receiver should be identical, assuming all of the errors are equal. If both receivers are then separated by a baseline of tens or hundreds of kilometres, then the timing solutions would be expected to differ, because some components of timing errors depend upon the length of the baseline. This is because some of the largest errors in GPS solutions may be due to the propagation paths travelled by the GPS signals and these errors are more likely to differ as the distance between each receiver, or 'station', increases. For instance, the ionosphere between London and Edinburgh is likely to differ by a greater amount than the ionosphere between London and Reading.

The effects of the ionosphere on GPS timing, across baselines ranging from 320 km to 3760 km, are investigated in the first part of this chapter. Four GPS timing solutions are presented in the corresponding results, similar to those presented in Chapter 6. Recalling that these timing solutions were presented in the form of the calculated RCB, with respect to the RCB calculated by CODE, the results presented in the first part of this chapter show the differences between the above as calculated for station 1 and station 2. This is not a time transfer, but simply a comparison between the error in the timing solution calculated at

station 1 and the error calculated at station 2. The difference between these errors is presented and is expected to increase as the baseline increases.

This study takes place over Europe and uses data from March 2003 (a period of high solar activity) and February 2004 (lower solar activity). Approximately 70 IGS/EPN stations are used to provide data towards the construction of 4D ionospheric maps (for MIDAS) and 5 additional stations are used as test stations. The aim of this work is to show how the ionosphere affects GPS timing accuracy and how that affect increases with increasing baseline and that MIDAS can reduce that affect.

The second part of this chapter investigates the use of MIDAS in GPS time transfer and the potential improvements in accuracy and stability that it may offer over the other single-frequency and dual-frequency methods presented. Data from March 2003 and 2 test stations are used.

Accurate timing and synchronisation are essential to modern infrastructure. Power transmission systems, the internet, television/radio and mobile phone networks are just a few of the telecommunications applications that require accurate timing and synchronisation. The Global Positioning System (GPS) provides access to atomic clock accuracy at the cost of a GPS receiver and is available worldwide. For these reasons, GPS is widely employed for synchronisation purposes.

Several methods of time transfer exist, for example: direct-reference, CV, AV and TW, which are described in Chapter 4, and there are various costs and accuracies attributed to each method. Time transfer is the process of transmitting time and frequency measurements from one point to another, which are then compared. The GPS acts as a reference source for time. The satellites are synchronised to GPS Time (GPST), which differs from UTC by an integer number of seconds, and the GPST may be transmitted to different locations across the world, using a GPS Receiver.

The AV method is used in this chapter. This is where all available measurements from all of the satellites in view are averaged to obtain a reference time. AV is advantageous because it makes use of all available satellites; enabling data from high elevation satellites to be included which

provide more accurate results in comparison to low elevation satellites (Rose et al. 2011). AV also allows time transfers to be done anywhere in the world using a GNSS system.

The aim of this work is to show that single-frequency GPS receivers, together with an ionospheric tomography system, may be used to produce improved time transfer results when compared to existing single-frequency techniques and also produce results that are not dissimilar to those produced by a dual-frequency system. Compared to a single-frequency system, dual-frequency systems are much more expensive, cumbersome and have to be calibrated, and in time transfer, a single-frequency system requires fewer calibrations than a dual-frequency system.

7.2 Method

7.2.1 Overview

The application of 4D ionospheric tomography to GPS timing. described by Rose et al. (2009), is used here to investigate the effects of the ionosphere across various baselines and GPS time transfer accuracy and stability. Ionospheric tomography is a key focus point. Diverse geophysical conditions are represented by an 18 day period during solar maximum conditions, in March 2003 and an 18 day period of decreased solar activity in February 2004.

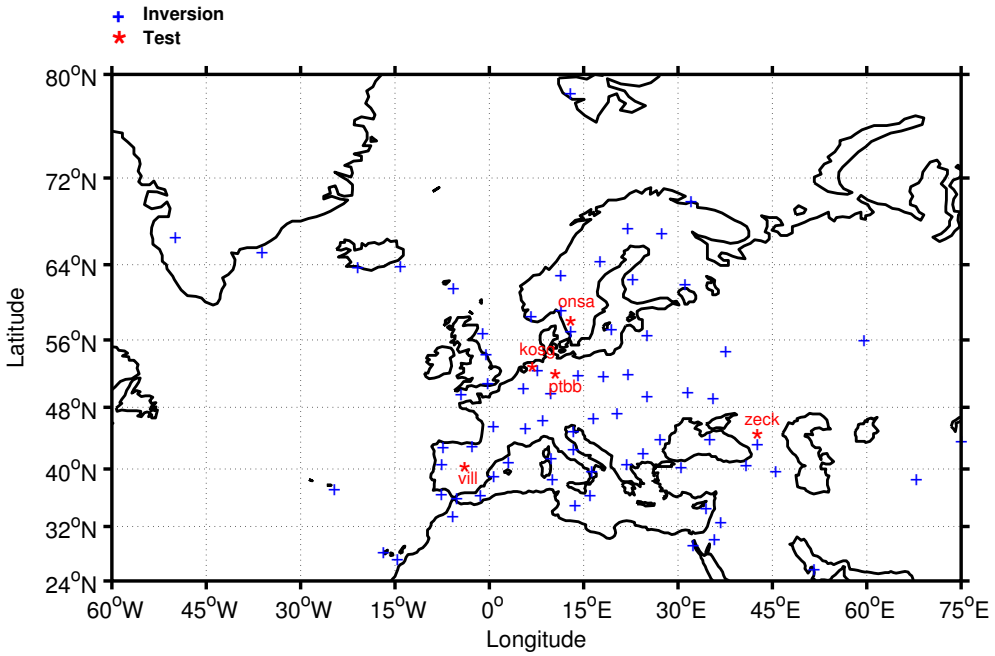

Figure 7.1 – Map of Europe, showing the test stations and those used for the inversion

Receiver Independent Exchange (RINEX) data (Gurtner 2002) for all of the IGS/EPN stations, used in this study, are collected from the IGS/EPN and used towards computing the timing solutions and maps. The 4D real-time ionospheric maps are created using data from around 70 IGS/EPN sites, situated across mainland Europe. The maps are used to mitigate the ionospheric delay imposed upon GPS signals. The tomographic grid is centred on Europe at 50°N 15°E, the longitude and latitude both range from -44° to +44° in steps of 4°. The altitude ranges from 100 to 1500 km in steps of 50 km.

The data from the test sites are used to demonstrate the performance of single-frequency GPS receivers with: no ionospheric correction, the Klobuchar ionospheric correction and finally the MIDAS correction. Dual-frequency data are also included in the results for direct comparisons. The five test stations are as follows: KOSG (Kootwijk, Netherlands), ONSA (Onsala, Sweden), PTBB (Braunschweig, Germany), VILL (Villafranca, Spain) and ZECK (Zelenchukskaya, Russian Federation). There are ten different links between the five test stations, the shortest baseline is KOSG-PTBB (320 km) and the longest is VILL-ZECK (3760 km).

7.2.2 GPS timing solution, pseudorange and corrections

The timing solutions, fundamental corrections and ionospheric compensation techniques presented in this chapter are calculated according to the methodology described in Sections 5.2.3-8. Note that all of the satellites in view, above an elevation angle of 15° are used to compute the solutions presented in this chapter.

7.2.3 Baseline comparisons

The effects of the ionosphere on GPS timing across various baselines are investigated. The GPS AV method is used: all of the satellites in view at each of the five test stations are used towards calculating the timing solutions. The timing solutions are calculated instantaneously at each sampling point, without relying on historic or averaged data. The RCB is calculated at each of the five test stations using each of the four timing solution techniques. The differences between these RCB and the precise RCB (calculated by the CODE) are then computed. It is these results that are then compared between two stations, station 1 and station 2, over an 18 day period in March 2003 and an 18 day period in February 2004. The differences between stations 1 and 2 are presented in the results, which illustrates the error due to the ionospheric component between the solutions at each station.

For this part of the results, the differences (in nanoseconds) between station 1 (t_{rx1}) and station 2 (t_{rx2}) are given by:

$$t_{rx1} - t_{rx2} = (b_{rx1} - b_{rx1(CODE)}) - (b_{rx2} - b_{rx2(CODE)}) \qquad (7.1)$$

where b_{rx1} and b_{rx2} are the RCB calculated by the timing solution techniques for stations 1 and 2 respectively. The RCB computed by the CODE are represented by $b_{rx1(CODE)}$ and $b_{rx2(CODE)}$ for stations 1 and 2 respectively. These results do not represent a time transfer.

The impact of the ionospheric error is a key focus point. As the baseline increases, the ionospheric error is more likely to differ by a larger amount between the two stations and so the presented differences should increase. The timing solution techniques that least adequately account for the ionospheric delays are most likely to exhibit these characteristics.

7.2.4 GPS time transfer

Two stations, PTBB and ONSA, are used to investigate GPS time transfer over the 18 day period in March 2003. PTBB and ONSA are separated by a baseline of 580 km and both are equipped with hydrogen masers. Transfer noise is expected to dominate for averaging times up to and in excess of one day. The results include the three single-frequency techniques: 'no correction', Klobuchar and MIDAS, in addition to the dual-frequency method.

The GPS Time minus the station clock (clock A for PTBB and clock B for ONSA), according to each of the four timing solutions, for March 2003, is presented in the results. The Modified Julian Day (MJD), instead of day of year, is used in these figures as it is widely used when computing time transfers. The MJD which started at 00:00, 17 November 1858 and each day is represented by a unique number. Correspondingly, plots of the modified Allan deviation (MDEV), described shortly, are then shown to investigate the ionospheric impact on the instabilities of the timing solutions.

Stability gives an indication of how well an oscillator can produce the same frequency offset, or time, for a given period (Lombardi 2002). Frequency stability is commonly measured using the Allan variance (AVAR) (Allan 1966). This is a measure of the fractional frequency fluctuations and though similar to the standard variance, it is instead convergent for most types of clock noise. The standard variance is not suited to measure stability in this case because it only converges when used with stationary data. When measured in the time domain clock noise is not a stationary process.

However, the data used in this study contains time dependent noise and is non-stationary and so would not converge to any particular values. In contrast, the AVAR transforms a non-stationary clock noise data set to one that is stationary using the transforms $z = (y_{i+1} - y_i)$ for frequency measurements and $z = (x_{i+2} - 2x_{i+1} + x_i)$ for time measurements. AVAR may be defined as:

$$\sigma_y^2(\tau) = \frac{1}{2(M-1)} \sum_{i=1}^{M-1} [y_{i+1} - y_i]^2 \qquad (7.2)$$

where τ is the averaging time, y_i is the *i*th of M fractional frequency values averaged over the averaging time τ (Riley 2008). AVAR converges to a value for divergent noise types, such as flicker noise.

The term AVAR is typically used to refer to the overlapping Allan variance, which increases the number of degrees of freedom and improves the confidence. At each averaging time the overlapping AVAR forms all possible overlapping samples, making maximum use of the data set:

$$\sigma_y^2(\tau) = \frac{1}{2m^2(M-2m+1)} \sum_{j=1}^{M-2m+1} \left\{ \sum_{i=j}^{j+m-1} [y_{i+m} - y_i] \right\}^2 \qquad (7.3)$$

where *m* is the averaging factor and the averaging time is $\tau = m\tau_0$ and τ_0 is the basic averaging time (Riley 2008).

The modified Allan variance (MVAR) is also commonly used to measure frequency stability (Allan and Barnes 1981) and may be defined as (Riley 2008):

$$Mod\sigma_y^2(\tau) = \frac{1}{2m^4(M-3m+2)} \sum_{j=1}^{M-3m+2} \left\{ \sum_{i=j}^{j+m-1} \left(\sum_{k=i}^{i+m-1} [y_{k+m} - y_k] \right) \right\}^2 \qquad (7.4)$$

MVAR is advantageous over AVAR because it can help to distinguish between white and flicker Phase Modulation (PM) noise, it also includes an additional phase averaging operation. Note that MVAR is usually expressed as the square root, the MDEV. The analysis focuses on the ionospheric impact on the instabilities. Information regarding frequency stability may be found in Riley (2008).

Subsequently, the differences between the 'GPS Time (t_{GPS}) minus clock A (t_A)' and the 'GPS Time (t_{GPS}) minus clock B (t_B)' are presented to illustrate the time transfer accuracy between PTBB and ONSA respectively:

$$PTBB - ONSA = (t_{GPS} - t_A) - (t_{GPS} - t_B) \qquad (7.5)$$

The corresponding MDEV is then shown to illustrate the impact of the ionosphere on the instabilities of the time transfer.

7.3 Results

7.3.1 Baseline comparisons

Five GPS receiver stations, situated across Europe, have been used to allow ten different timing comparisons to be made between various pairs of stations. The baselines between the stations range from 320 to 3760 km in length. Four different timing solutions were computed at each station and then compared to the corresponding solutions across the various baselines.

Figures 7.2a-b illustrate the differences between the shortest baseline and the longest baseline respectively for the 18 day period in March 2003. This period coincides with solar maximum. Tables 7.1 and 7.2 show the RMS and standard deviations, respectively, of the differences for each baseline and each of the four solution techniques for March 2003.

Note that the term ‘accuracy’, used in this section, refers to the RMS values of the differences between the two stations – for example, the method (no correction, Klobuchar, MIDAS or dual-frequency) is said to be most accurate when the RMS values are smallest i.e. when the ionospheric component is smallest, in comparison to the other methods. Also note that the percentage improvements quoted in this section (for Figures 7.2a-d) are with respect to the corresponding ‘no correction’ results.

Figure 7.2a shows the results for the smallest baseline, 320 km, between KOSG and PTBB. The largest differences belong to the comparison derived from the solutions with ‘no correction’. The corresponding RMS is 2.16 ns. The Klobuchar results offer a 17% improvement in accuracy over the no correction results, with an RMS of 1.79 ns. The MIDAS results offer a 60% improvement, with an RMS of 0.86 ns. An improvement of 77% is achieved using the dual-frequency technique, which has an RMS of 0.49 ns. The differences in order of least to most accurate technique are: no correction, Klobuchar, MIDAS and dual-frequency. Similarly, the standard deviations, presented in Table 7.2, show the same pattern, the corresponding standard deviations are as follows: 2.15, 1.71, 0.85 and 0.49 ns respectively.

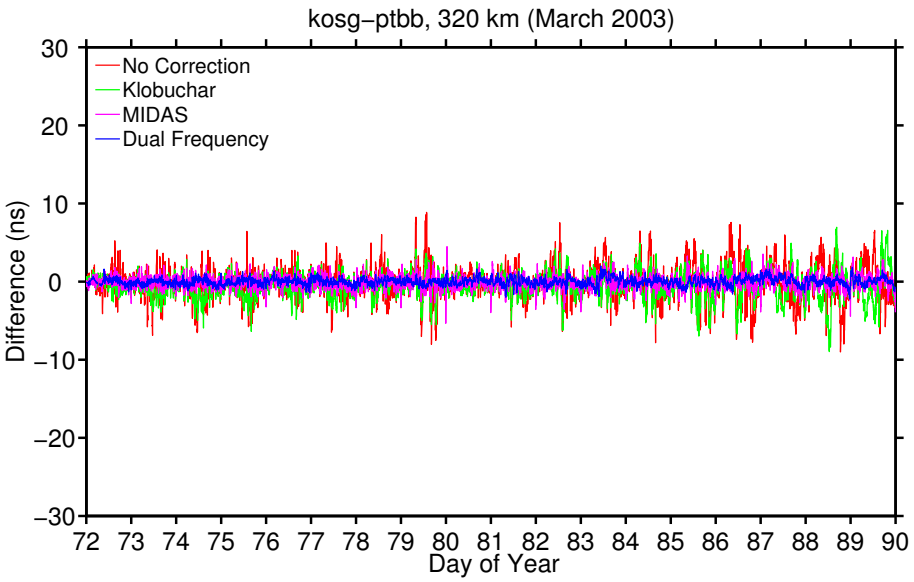
kosg–ptbb, 320 km (March 2003)
No Correction
Klobuchar
MIDAS
Dual Frequency
Difference (ns)
30
20
10
0
–10
–20
–30
72 73 74 75 76 77 78 79 80 81 82 83 84 85 86 87 88 89 90
Day of Year

(a)

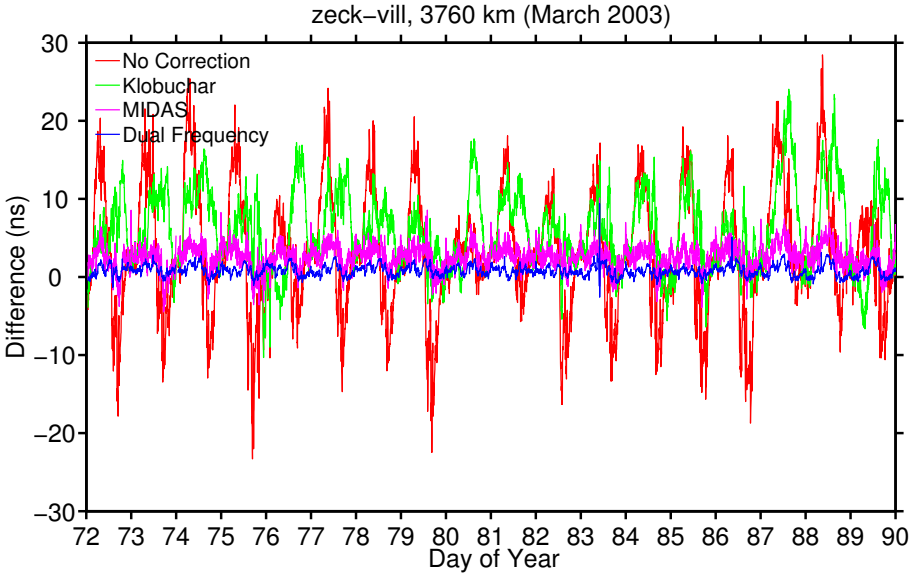
zeck–vill, 3760 km (March 2003)
No Correction
Klobuchar
MIDAS
Dual Frequency
Difference (ns)
30
20
10
0
–10
–20
–30
72 73 74 75 76 77 78 79 80 81 82 83 84 85 86 87 88 89 90
Day of Year

(b)

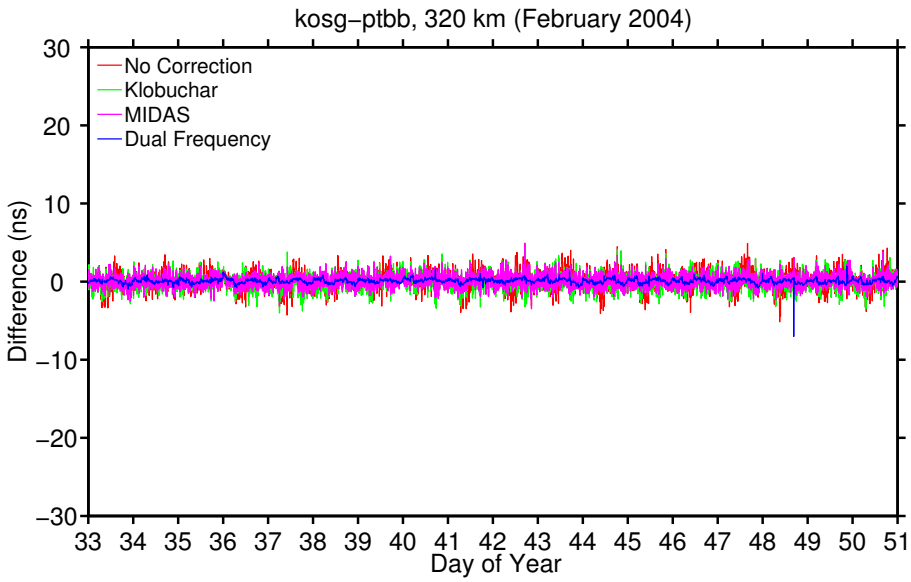

(c)

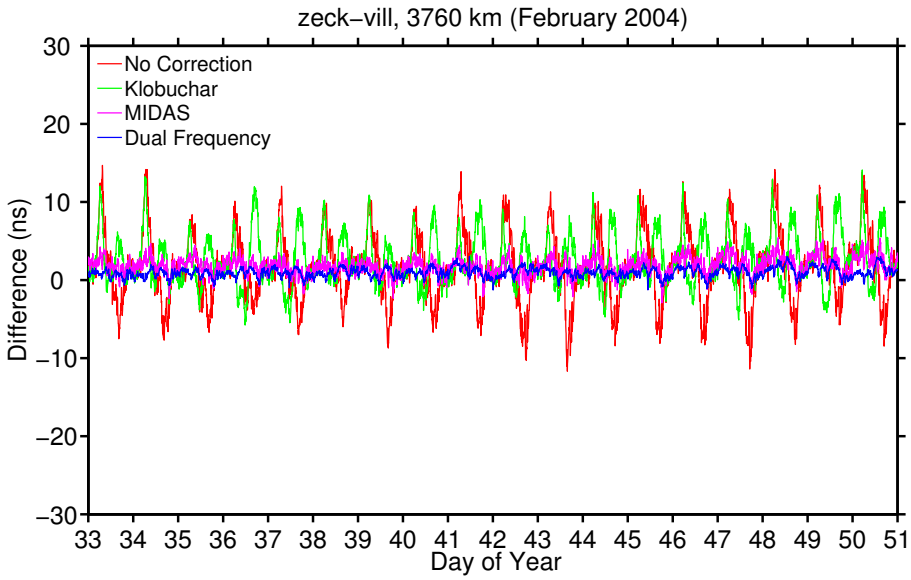

(d)

Figure 7.2 – Differences (described in Section 7.2.3) computed between **(a)** KOSG and PTBB and **(b)** ZECK and VILL for an 18 day period in March 2003 and the differences between **(c)** KOSG and PTBB and **(d)** ZECK and VILL for an 18 day period in February 2004

Figure 7.2b shows the results for the largest baseline, 3760 km, between ZECK and VILL. The 'no correction' differences are now roughly five times more variable (standard deviation of 10 ns) and greater in magnitude when compared to the results for the smallest baseline (Figure 7.2a). The differences are bounded by roughly ± 28 ns and have an RMS of 10.3 ns. Whilst the accuracy of the Klobuchar differences improves upon the former solution by only 4%, with an RMS of 9.85 ns, the variability decreases by 27% with a standard deviation of 7.28 ns. The MIDAS results offer a 71% and 84% improvement in accuracy and variability respectively, with an RMS of 2.96 ns and standard deviation of 1.64 ns. These results may be bounded by approximately 0 to 5 ns. The dual-frequency differences improve by 87%, with an RMS of 1.31 ns and by 90% in terms of variability.

Interestingly, the RMS of the differences for the no correction and Klobuchar solutions do not simply increase with increasing baseline (see Table 7.1). Links 4 to 6 inclusive have a greater RMS result for the no correction results than links 7 to 9, which have larger baselines. The RMS of link 10, the longest baseline, is the same as that of links 4 to 6: 10.3 ns. This is the largest RMS recorded in the results for the no correction technique. Similarly, the Klobuchar RMS results exhibit the same pattern. The standard deviations for both of these methods, shown in Table 7.2, concur.

However, the MIDAS and dual-frequency results generally behave as expected: the differences between the stations increases with increasing baseline. Notably, VILL is common to links 4 to 6 and 10, which suggests that the reason for the slight abnormality in the 'no correction' and Klobuchar results is due to the ionospheric delay experienced at VILL – since the abnormality is not apparent in the results that better correct for the ionosphere: MIDAS and dual-frequency.

Figures 7.2c-d represent the differences between the shortest and longest baselines respectively for the 18 day period in February 2004. This period corresponds to the latter part of solar maximum: a period of less geomagnetic activity compared to March 2003. The RMS and standard deviations of the differences of the four solution techniques for each baseline are given in Tables 7.3 and 7.4 respectively.

			RMS (ns)			
Link	**Baseline**	**Length (km)**	**SF**	**SFK**	**MIDAS**	**DF**
1	KOSG-PTBB	320	2.16	1.79	0.86	0.49
2	PTBB-ONSA	580	2.12	1.93	0.82	0.43
3	KOSG-ONSA	705	2.41	2.57	1.00	0.54
4	VILL-KOSG	1500	10.3	7.26	1.44	0.92
5	VILL-PTBB	1720	10.3	7.09	1.46	0.91
6	VILL-ONSA	2210	10.3	7.10	1.55	0.89
7	ZECK-PTBB	2500	8.33	6.25	2.30	1.19
8	ZECK-ONSA	2560	8.96	6.13	2.47	1.15
9	ZECK-KOSG	2810	8.32	6.75	2.44	1.22
10	ZECK-VILL	3760	10.3	9.85	2.96	1.31

Table 7.1 – RMS of the differences for each baseline, for each of the four solution techniques, for March 2003

			Standard Deviation (ns)			
Link	**Baseline**	**Length (km)**	**SF**	**SFK**	**MIDAS**	**DF**
1	KOSG-PTBB	320	2.15	1.71	0.85	0.49
2	PTBB-ONSA	580	1.84	1.92	0.81	0.43
3	KOSG-ONSA	705	2.24	2.45	1.03	0.54
4	VILL-KOSG	1500	9.62	7.20	1.39	0.90
5	VILL-PTBB	1720	9.69	6.93	1.39	0.89
6	VILL-ONSA	2210	9.31	6.88	1.51	0.88
7	ZECK-PTBB	2500	5.72	3.43	1.18	0.66
8	ZECK-ONSA	2560	5.43	3.56	1.28	0.67
9	ZECK-KOSG	2810	5.50	3.51	1.29	0.72
10	ZECK-VILL	3760	10.0	7.28	1.64	1.03

Table 7.2 – Standard deviations of the differences for each baseline, for each of the four solution techniques, for March 2003

			RMS (ns)			
Link	**Baseline**	**Length (km)**	**SF**	**SFK**	**MIDAS**	**DF**
1	KOSG-PTBB	320	1.10	0.97	0.80	0.30
2	PTBB-ONSA	580	2.04	1.85	1.13	0.48
3	KOSG-ONSA	705	2.03	1.75	0.97	0.50
4	VILL-KOSG	1500	3.09	2.17	0.77	0.47
5	VILL-PTBB	1720	3.40	2.34	1.05	0.45
6	VILL-ONSA	2210	4.69	3.46	1.25	0.56
7	ZECK-PTBB	2500	5.44	4.93	2.43	1.14
8	ZECK-ONSA	2560	6.70	6.04	2.90	1.34
9	ZECK-KOSG	2810	5.57	5.02	2.28	1.05
10	ZECK-VILL	3760	4.70	4.23	2.09	1.15

Table 7.3 – RMS of the differences for each baseline, for each of the four solution techniques, for February 2004

			Standard Deviation (ns)			
Link	**Baseline**	**Length (km)**	**SF**	**SFK**	**MIDAS**	**DF**
1	KOSG-PTBB	320	1.10	0.97	0.79	0.29
2	PTBB-ONSA	580	1.34	1.30	0.99	0.45
3	KOSG-ONSA	705	1.20	1.20	0.74	0.44
4	VILL-KOSG	1500	1.71	1.63	0.71	0.48
5	VILL-PTBB	1720	2.12	1.89	0.97	0.45
6	VILL-ONSA	2210	2.09	2.16	0.84	0.52
7	ZECK-PTBB	2500	3.37	2.75	1.09	0.56
8	ZECK-ONSA	2560	3.31	2.68	1.03	0.67
9	ZECK-KOSG	2810	3.67	2.84	0.92	0.53
10	ZECK-VILL	3760	4.41	3.25	1.09	0.64

Table 7.4 – Standard deviations of the differences for each baseline, for each of the four solution techniques, for February 2004

The differences for the ‘no correction’ results in Figure 7.2c are roughly bounded by ± 5 ns and have both an RMS and standard deviation of 1.10 ns. The Klobuchar method offers a 12% improvement in both accuracy and variability with respect to (wrt) the aforementioned method, with an RMS and standard deviation of 0.97 ns. The MIDAS results offer a 27% improvement with an RMS of 0.80 ns and are less variable, with a standard deviation of 0.79 ns. This method may be bounded by roughly ± 2 ns. The dual-frequency differences yield a 72% improvement in accuracy with an RMS of 0.30 ns and are less variable with a standard deviation of 0.29 ns.

Figure 7.2d shows the differences for the longest baseline. The ‘no correction’ results are more variable (standard deviation 4.41 ns) and larger in magnitude when compared to those for the shortest baseline (Figure 7.2c). The RMS is 4.70 ns and the differences may be bounded by approximately ± 14 ns. The Klobuchar differences are also quite variable with a standard deviation of 3.25 ns, yet offer a 10% improvement in accuracy wrt the no correction results. The MIDAS results offer a 55% improvement, with an RMS of 2.09 ns and may be bounded by roughly 0 to 5 ns. The dual-frequency results offer a 76% improvement, with an RMS of 1.15 ns. The MIDAS and dual-frequency techniques yield decreases in variability by 75% and 85% respectively.

7.3.2 GPS time transfer

Two GPS receiver stations, PTBB and ONSA, have been used to investigate time transfer. The baseline between the stations is 580 km in length. Four different timing solution techniques have been used.

Figures 7.3a and 7.4a show the differences between GPS Time and the clocks at PTBB and ONSA, respectively, during an 18 day period in March 2003, according to each of the four timing solutions. It can be observed from these figures that the instabilities in the 'no correction' and Klobuchar solutions are dominated by the diurnal effect of the ionosphere. The MIDAS solution reduces these effects and is similar to the dual-frequency solution.

Figures 7.3b and 7.4b show the MDEV of the differences between GPS Time and the clocks at PTBB and ONSA respectively. From the outset it is clear that the MDEV are lower for the MIDAS solutions, for both PTBB and ONSA, in comparison to the 'no correction' and Klobuchar solutions. In the short term, receiver noise appears to dominate the instabilities.

The resolution of MIDAS is not sufficient to improve the error for time periods of $\tau < 1000$ s. This is as expected because MIDAS cannot resolve the small scale transient fluctuations in the ionosphere any better than the 'no correction' or Klobuchar solutions for $\tau < 1000$ s. MIDAS has a temporal resolution of roughly 10-15 minutes (600-900 s) and for 1000 s $< \tau <$ 1E5 s, it offers a clear improvement over the 'no correction' and Klobuchar solutions and is as good as the dual-frequency solution from roughly $\tau = 20{,}000$ s (~5.5 hrs) onwards.

The 'no correction' and Klobuchar solutions tend to converge towards the dual-frequency solution when $\tau = 2.5\text{E}5$ s (~3 days). This implies that the ionosphere no longer dominates the instabilities in the long term and the limitation may now be due to clock noise and hardware instabilities.

According to Fig. 7.3b (PTBB), white Frequency Modulation (FM) dominates in the short term for each solution type. According to Fig. 7.4b (ONSA), the noise processes may be approximated as flicker PM and white PM in the short and medium terms up to roughly $\tau = 1$ day, for the single-frequency solutions. White FM appears to be the dominant noise process for the dual-frequency solution up

to τ = 1 day. In the long term, flicker FM, random walk FM and linear frequency drift may be present.

The ‘bump’ exhibited by the ‘no correction’, Klobuchar and dual-frequency techniques at τ = 30,000 s (~8.33 hrs) in both Figures 7.3b and 7.4b is indicative of periodic effects due to diurnal changes. This is most likely due to the periodic ionospheric day to night changes. Variations in temperature and hence hardware may also have some affect. Similar characteristics are exhibited in figures presented by Defraigne and Petit (2003) and Lee (2009).

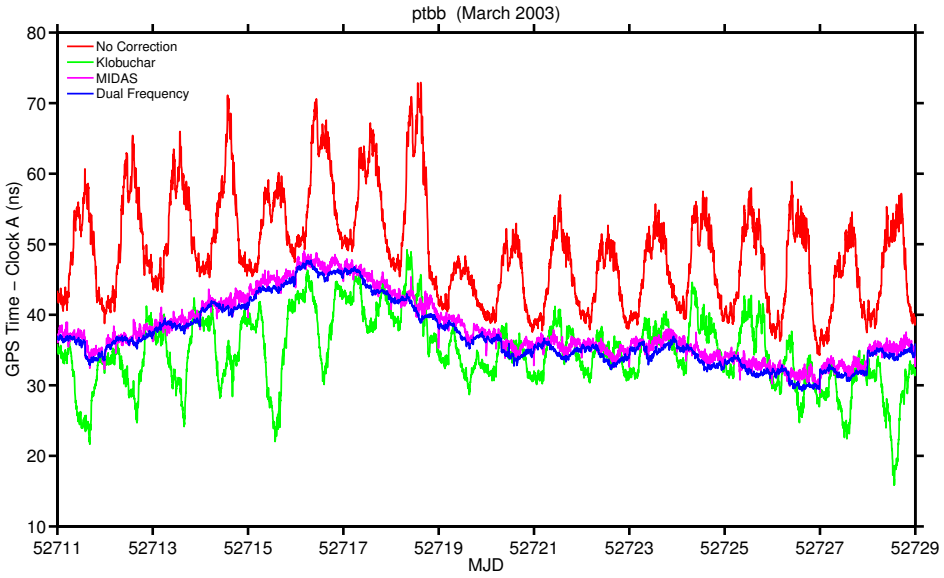

(a)

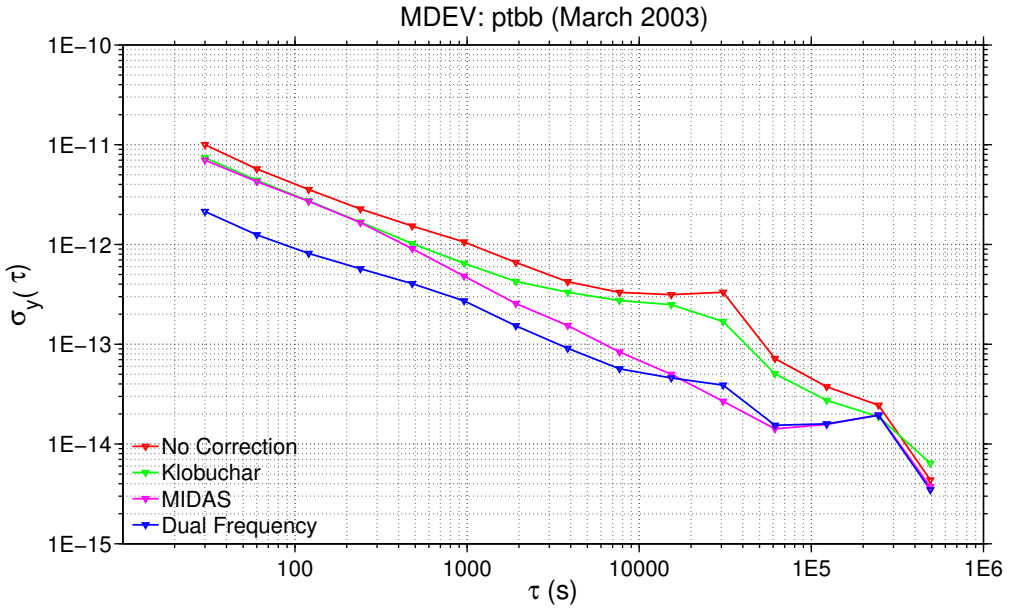

(b)

Figure 7.3 – The difference between GPS Time and the clock at PTBB **(a)** and corresponding MDEV **(b)**

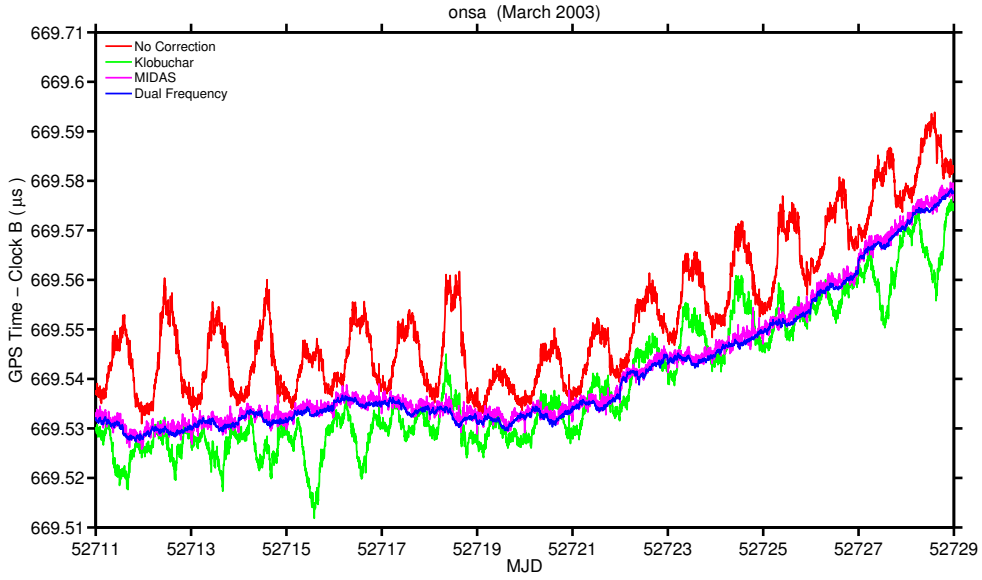

(a)

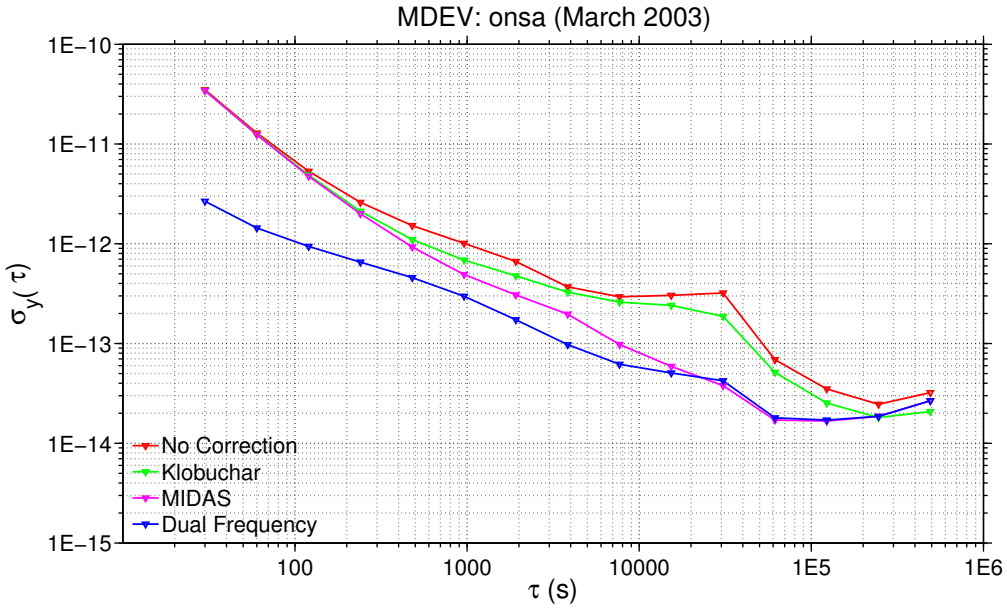

(b)

Figure 7.4 – The difference between GPS Time and the clock at ONSA **(a)** and corresponding MDEV **(b)**

Figure 7.5a represents the time transfer between PTBB and ONSA during March 2003. The diurnal effects of the ionosphere are now greatly reduced, yet still evident in the 'no correction' and Klobuchar solutions. This is to be expected because the ionosphere is less likely to vary greatly over the baseline of 580 km. The MIDAS and dual-frequency solutions are similar, yet the former exhibits more noise. GPS time transfer noise, in addition to clock noise from PTBB and ONSA, are expected to be contained within this time transfer.

Figure 7.5b shows the MDEV for the time transfer between PTBB and ONSA. From the outset it is clear that the MDEV are lower for the MIDAS solution, which shows that MIDAS may offer improvements in stability over the other single-frequency methods presented here. This also shows that the ionosphere is a limiting factor in time transfer, unless adequately compensated for.

According to Fig. 7.5b, the MIDAS solution is shown to improve the time transfer stabilities for 1000 s < τ < 1E5 s, when compared to the 'no correction' and Klobuchar solutions. The MIDAS time transfer tends to be virtually as good as the dual-frequency time transfer by τ = 7680 s (~2 hrs). The three single-frequency solutions roughly tend to converge towards the dual-frequency solution for τ > 2.5E5 s (>3 days), which implies that the ionosphere no longer dominates the instabilities in these transfers from this point.

At averaging times of roughly 2 hours the stabilities of the no correction and Klobuchar time transfers are both ~2E-13. The corresponding stabilities for the MIDAS and dual-frequency time transfers are roughly 7E-14. At averaging times of approximately 1 day, the stabilities for the no correction and Klobuchar time transfers are 2.5E-14 and 3E-14 respectively. The stabilities for the MIDAS and dual-frequency time transfers are both ~1.8E-14.

According to Fig. 7.5b, the 'no correction' time transfer noise is part flicker PM and part white PM up to τ = 2.5E5. The same is true of the time transfer using the Klobuchar method. For both the 'no correction' and Klobuchar solutions, a random walk FM process likely dominates the time transfer when τ > 2.5E5 s, according to Fig. 7.5b. The MIDAS time transfer noise appears to be partly flicker PM and white PM up to τ = 10,000 s, from which the noise appears as white FM. The dual-frequency time transfer noise appears as white FM up until

τ = 1E5 s. In the long term, there may be some flicker FM and random walk FM noise.

The ionosphere dominates the instabilities in the time transfer for both the no correction and Klobuchar solutions for longer than the solutions that better correct for it, which is as expected. In the long term, linear frequency drift becomes apparent and beyond the aforementioned times, the instabilities in the corresponding time transfers are dominated by noise from both clocks and the time transfer.

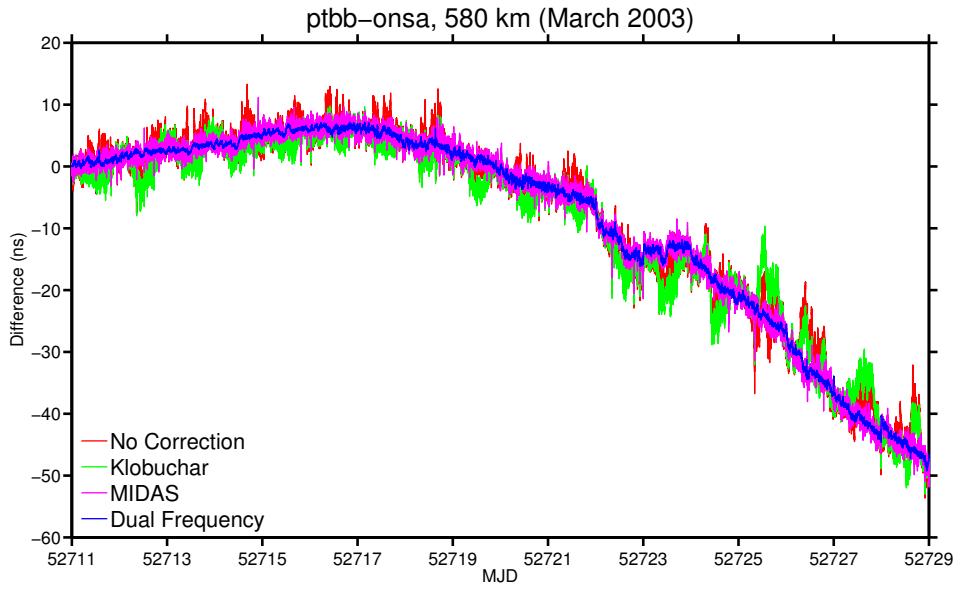

(a)

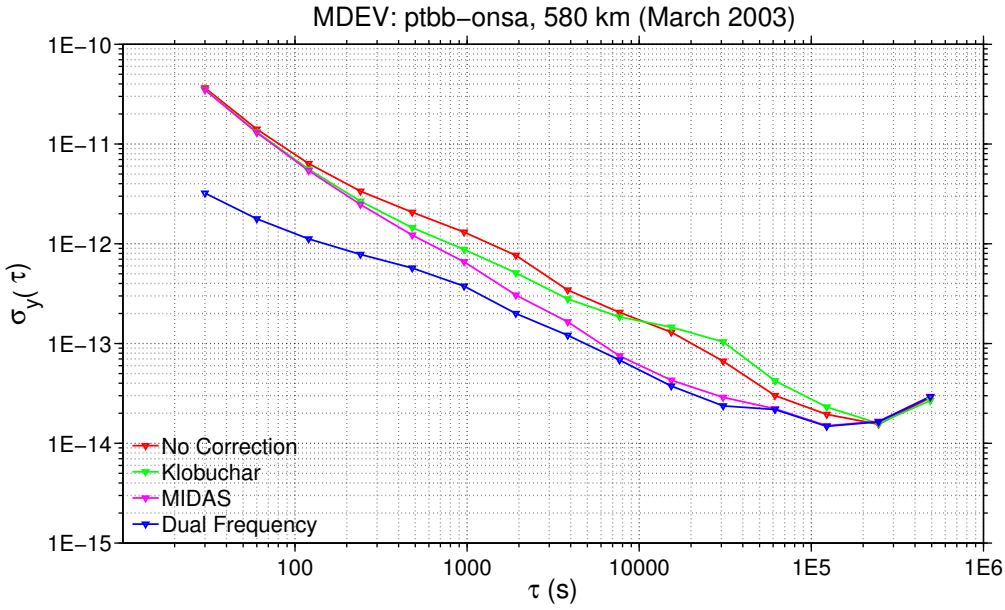

(b)

Figure 7.5 – The difference between PTBB and ONSA **(a)** and corresponding MDEV **(b)**

7.4 Conclusions and Discussion

7.4.1 Baseline comparisons

Timing comparisons have been made across baselines ranging from 320 to 3760 km using four GPS solution techniques. The differences between the RCB wrt the RCB calculated by CODE for station 1 and the same at station 2 were computed for various baselines that incorporate five test stations. The differences were computed to investigate the ionospheric impact and the performance of the 4D tomography system, MIDAS.

MIDAS provides the most accurate and least variable single-frequency GPS solutions. RMS accuracies to within 5 ns are achievable using MIDAS. Typically, the least to most accurate techniques are as follows: no correction, Klobuchar, MIDAS and dual-frequency.

Generally, the timing comparison accuracy and variability worsened as the baseline increased. The ionospheric delays are more diverse and variable between two stations with increasing baseline. This effect is most noticeable in the 'no correction' and Klobuchar results, since they least adequately compensate for the ionospheric delay. Notably, these two techniques do not always behave as expected. Tables 7.1 and 7.2 illustrate that their RMS and standard deviations are sometimes higher for baselines that are shorter than the longest baseline. This is most likely due to localised ionospheric effects.

In contrast, the MIDAS and dual-frequency techniques are much better at compensating for the ionospheric error – a trait that is most advantageous for longer baselines. These techniques can be said to essentially follow the trend, whereby the accuracy and variability are inversely proportional to the length of the baseline. These results reinforce the importance of adequately compensating for the ionospheric errors.

The improvements offered by the MIDAS and dual-frequency techniques are most significant in the 2003 results, compared to the 2004 results. This is because the ionosphere has a greater influence on the timing comparisons during the more geomagnetically stormy times in 2003, when compared to the

quieter period in 2004. Overall, MIDAS offers the most accurate and least variable single-frequency results, which are not dissimilar to the dual-frequency results.

7.4.2 GPS time transfer

The short term instabilities of the timing solutions for PTBB and ONSA are likely due to receiver noise. The medium term instabilities are dominated by the ionosphere. The long term instabilities are due to clock noise and hardware effects, which may vary according to local environmental conditions. MIDAS offers greater stabilities than the other single-frequency solutions and is not dissimilar to the dual-frequency solution. From ~20,000 s (~5.5 hrs) the MIDAS solution is as stable as the dual-frequency solution. However, it is not until nearly 2.5E5 s (~3 days) that the 'no correction' and Klobuchar solutions become roughly as stable as the MIDAS and dual-frequency techniques.

Now considering the time transfer stabilities, from 7680 s (~2 hrs) the stability of the MIDAS time transfer is roughly as stable as the dual-frequency time transfer. From 2.5E5 s (~3 days) the 'no correction' and Klobuchar time transfer solutions become as stable as the other techniques. In the medium term, the instabilities in the time transfers are due to the ionosphere. The long term instabilities in the time transfer appear to be dominated by clock noise and hardware, which is due to the characteristics of the clock and varying environmental conditions.

The benefits in terms of stability, by using MIDAS for time transfer, as opposed to the 'no correction' or Klobuchar techniques, begin after averaging times of ~500 s (~8 mins), but more notably after 1000 s (~16 mins). MIDAS offers virtually the same stabilities as the dual-frequency time transfer from ~2 hrs onwards.

Interestingly, the Klobuchar time transfer is sometimes less stable than the time transfer with no correction. This concurs with the conclusions drawn from both Chapters 5 and 6, which found that the Klobuchar model can sometimes produce a worse result than if no ionospheric model were used at all.

The ionospheric impact on the GPS time transfer is less in comparison to the impact it has upon the differences computed between GPS Time and the clocks at PTBB and ONSA. This is as expected because for a baseline of 580 km, the ionosphere is not expected to vary greatly between the stations, in comparison to a baseline of say 2000 km. Future work would include the investigation of the potential benefits of using MIDAS for transatlantic GPS time transfers, whereby MIDAS would be expected to yield time transfers similar to the dual-frequency technique and with greater stability in comparison to the 'no correction' and Klobuchar techniques.

Chapter 8

8. Conclusions and Future work

8.1 Conclusions

Single-frequency GPS receivers do not adequately compensate for the ionospheric delay, particularly during periods of severe geomagnetic storms. In general, these receivers use a broadcast ionospheric model that aims to provide at least a 50% RMS correction. This may be sufficient during periods of low ionospheric activity, such as solar minimum, but as many more applications now rely on GPS, since the last solar maximum, there is a need to explore the possible enhancement of single-frequency GPS receivers as the next solar maximum approaches.

In this project, an established ionospheric tomography system, MIDAS, has been applied to a single-frequency GPS timing system for the first time. The aim was to improve the GPS timing accuracy, using MIDAS, when compared to standard single-frequency GPS systems.

This study took place over Europe and results were presented when ionospheric delays were large and variable. Data were obtained from the last solar maximum: from 2002 to 2004, in addition to a particularly well known ionospheric stormy period in October 2003. Note that the last solar maximum (solar cycle 23) peaked between roughly 2001-2003 and 2004 lies on the downward slope (decreasing sunspot number) heading towards solar minimum. The Kp ranges from 0 to 9 during the investigated periods. Since this study looks at data during solar maximum, further improvements would be anticipated during solar minimum conditions.

The GPS data and products were sourced from the IGS/EPN network of ground-based receivers, situated across Europe and were processed to produce 4D ionospheric maps, using MIDAS. Several IGS receivers were used as test stations for the results. Various GPS timing solution techniques were presented, each with a different method of ionospheric compensation. These include two single-frequency timing solutions: one that uses the standard broadcast Klobuchar model, and the other that uses MIDAS, to correct for the ionospheric error. The solutions were compared to a dual-frequency system.

The application of 4D ionospheric imaging to improve GPS timing was investigated first in order to explore the potential of this technique and conclusions drawn as follows. MIDAS offers the most accurate and least variable single-frequency GPS timing solutions, for fixed and mobile based receiver techniques. MIDAS achieves accuracies comparable to the dual-frequency system and is in some cases more robust as it is not vulnerable to L2 losses of lock. In some cases the Klobuchar solution significantly reduces the ionospheric delays, whilst in other cases it can be highly variable over the course of a few minutes to a few hours and unreliable in severe conditions.

Next, a more extensive study was presented that builds upon the previous work by incorporating elevation masks in addition to ionospheric tomography, with the aim of improving single-frequency GPS timing. Using MIDAS, accuracies to within 10 ns are achievable using fixed GPS receiver situations, even during periods of intense geomagnetic activity. For fixed GPS receivers, the greater the elevation mask, the less variable and more accurate the timing solution will be. This relationship continues up to and including the 40° elevation mask. This is because signals from high elevation satellites are typically subject to less multipath and less ionospheric delays. Good satellite geometry is not crucial to a fixed timing solution and a balance between the number of available satellites and those at high elevations should be found. However, an elevation mask of 40° typically reduces the number of satellites in view to around 2 or 3 at any given time and since the average of all the RCB's (calculated from all of the satellites in view) forms the fixed GPS timing solution, if just one of the satellites used is subject to a fault/error then it has the potential to seriously degrade the overall solution.

For mobile GPS receivers the best choice of elevation mask lies between 10° and 20°. A mask of 10° appears to reduce multipath, whereas a mask of 20° can exasperate some errors due to the degradation of the satellite geometry. There are times when there are not any low elevation satellites in view, say between 0° and 40°. These periods adversely affect the mobile timing solution. Depending upon application, a balance must be struck between elevation mask and its effect on satellite geometry to minimise the propagation delays and optimise the timing solution. The effects of acquiring/losing a satellite signal can lead to momentary fluctuations in timing accuracy and increases in TDOP.

Timing comparisons were made across baselines ranging from 320 to 3760 km using four GPS solution techniques. The differences between the RCB wrt to the RCB calculated by CODE were calculated at each test station and then compared with each other to investigate the ionospheric impact and the performance of the 4D tomography system, MIDAS. Typically, the least to most accurate techniques were as follows: no correction, Klobuchar, MIDAS and dual-frequency. Overall, MIDAS offered the most accurate and least variable single-frequency results, which are not dissimilar to the dual-frequency results. The effect of the ionosphere increased with increasing baseline.

GPS time transfer was also investigated. The medium term instabilities were shown to be dominated by the ionosphere, whereas the long term instabilities were likely due to clock noise and hardware. The stability of the MIDAS time transfer was shown to be roughly as stable as the dual-frequency time transfer after around 2 hours averaging time. Contrastingly, the ‘no correction’ and Klobuchar time transfers required an averaging time of around 3 days to become as stable as the dual-frequency and MIDAS techniques. MIDAS offers the most stable single-frequency time transfer and improves upon the other single-frequency methods from around 8 minutes averaging time. Interestingly, the Klobuchar time transfer is less stable than the ‘no correction’ transfer between averaging times of ~4 hours and ~3 days.

MIDAS requires data from a reasonable network of GPS receivers in order to produce credible ionospheric maps. Such networks are in place across Europe, North America and parts of Asia. However these receivers are particularly sparse across Africa (and of course the oceans), which forms a limitation for MIDAS.

In summary, the application of the 4D ionospheric imaging system, MIDAS, to GPS timing has been shown to offer significant improvements in timing accuracy. These improvements have led to dual-frequency like accuracies being obtained, but from a single-frequency system. Ionospheric tomography has also been shown to reduce the variability of the timing solutions and to improve the stability in GPS time transfers.

For fixed GPS receivers, the highest possible elevation mask should be employed, provided there are a sufficient number of satellites still in view, in order to obtain the most accurate solutions. For mobile GPS receivers, a mask between 10° and 20° should be used (e.g. 15°) to ensure that the satellite geometry is not compromised.

It is important to note that solutions derived using the broadcast Klobuchar model may actually produce worse results, than if there were no ionospheric correction at all. Together with the GPS constellation, the future completion of the Galileo constellation will lead to a much larger number of satellites in view at any given time and will improve the overall satellite geometry. This will result in a more dependable and reliable GNSS era, leading to improvements in positioning and timing accuracies.

8.2 Future work

Real-time ionospheric corrections are currently generated by MIDAS and are available via the internet. It is intended that these real-time corrections will be broadcast across the UK in the near future. This opens up the possibility of synchronising devices using low-cost single-frequency GPS receivers, with greater accuracy and stability than is currently possible using the existing broadcast Klobuchar corrections (albeit with a modification that enables them to receive and make use of the MIDAS data).

An extension to this project could include the development of a warning/alarm system that could detect satellite-specific anomalies and not only prevent the erroneous satellite from being included in the solution but also dynamically lower the elevation mask to increase the number of satellites in view. Furthermore, a

new GPS timing algorithm could also incorporate elevation dependent weightings. With this in mind, the resulting GPS solutions would be influenced most by those satellites that are expected to contribute the smallest errors to the solution (eg those at high elevations, whose signals are subject to less multipath and less atmospheric effects). All this, whilst maintaining the level of satellite geometry required, according to application: fixed or mobile scenario.

Future work would be to extend the time transfer study to include transatlantic baselines. Data would be collected, using the existing networks of ground-based receivers, from across Europe and the USA. Ionospheric maps, encompassing the whole region, would be produced and hence used to mitigate the ionospheric delays for single-frequency GPS users. The time transfer accuracies and stabilities resulting from this method may then be compared to other single-frequency and dual-frequency techniques. The performance of the MIDAS derived solutions would then be tested across baselines of tens of kilometres. MIDAS would be expected to yield time transfers similar to the dual-frequency technique and with greater stability in comparison to the 'no correction' and Klobuchar techniques.

The feasibility of building a GPS timing receiver, that incorporates MIDAS, is currently being investigated. Conservatively, accuracies to within 10 ns would be achievable, even during highly variable and stormy ionospheric conditions.

Appendix A

A. TEC Maps

Maps of the ionospheric Total Electron Content (TEC) are shown here for several days in 2002 and 2003. There are 12 images per day, illustrating the TEC at 2-hour intervals. The colours represent various levels of TEC. The top left image represents the start of the day at 00:00 hrs and the image to its right shows the TEC at 02:00 hrs. The TEC at 04:00 hrs is directly below the first image and so on.

A.1 6th January 2002

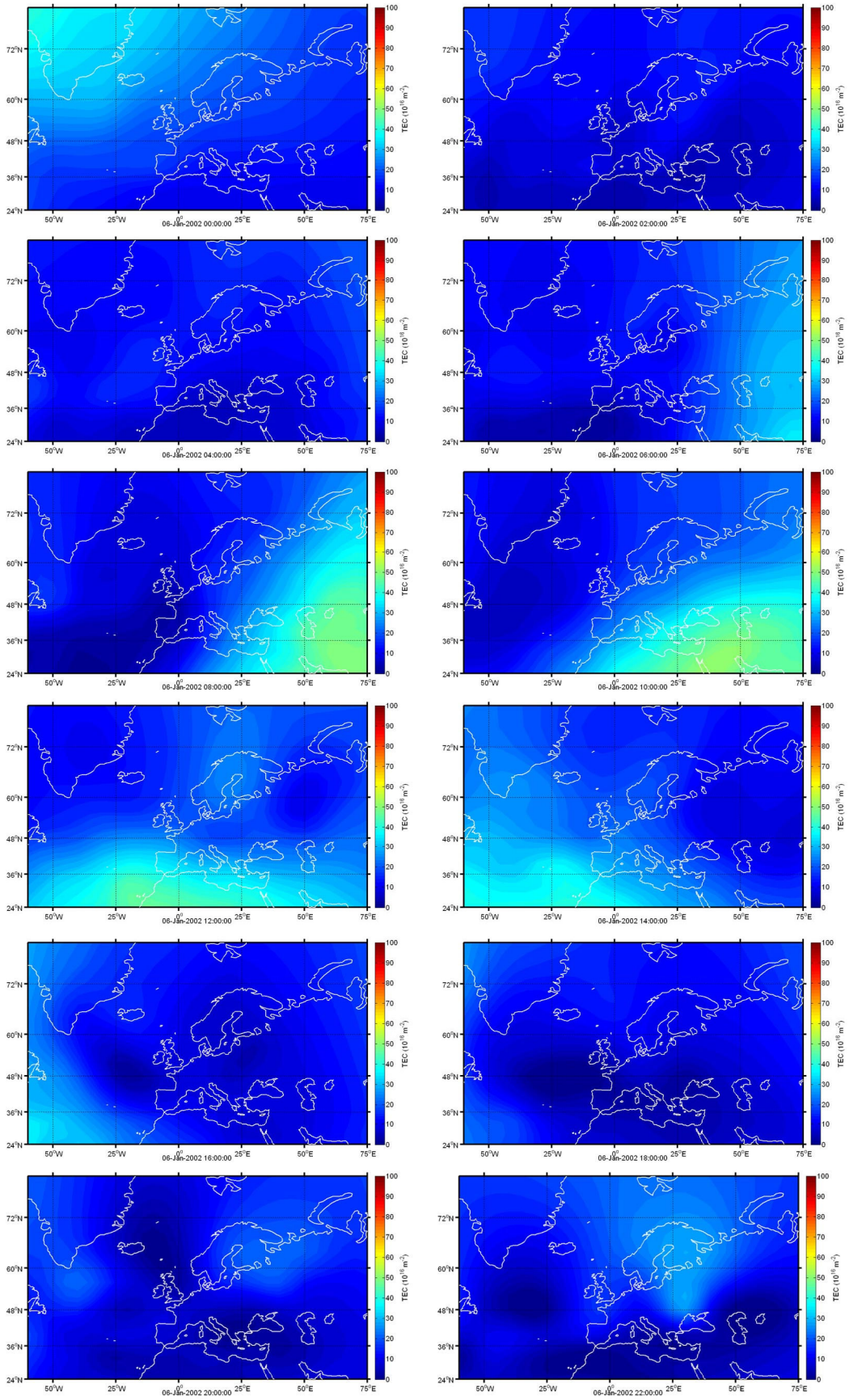

A.2 13th February 2002

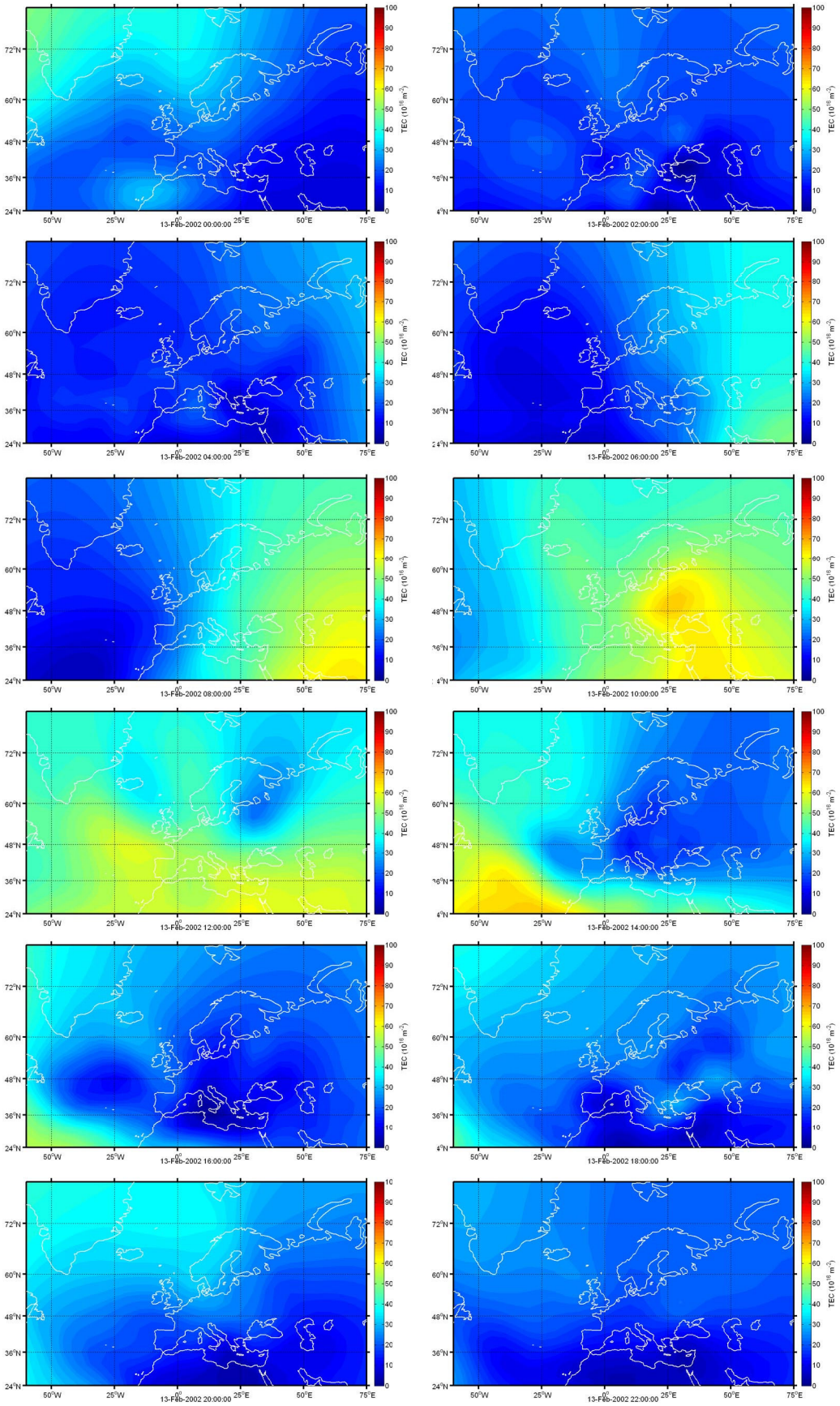

A.3 11th May 2002

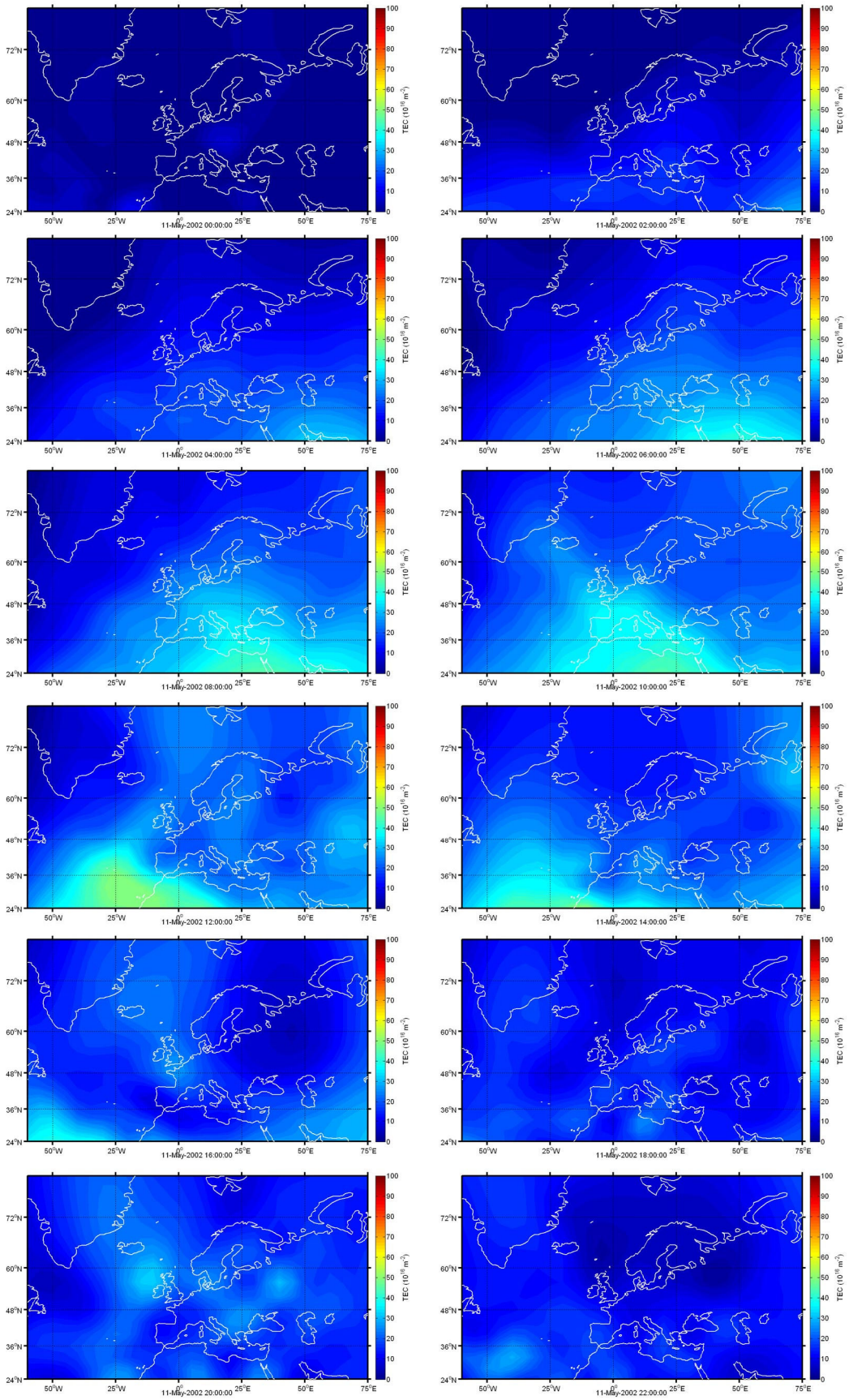

A.4 21st November 2002

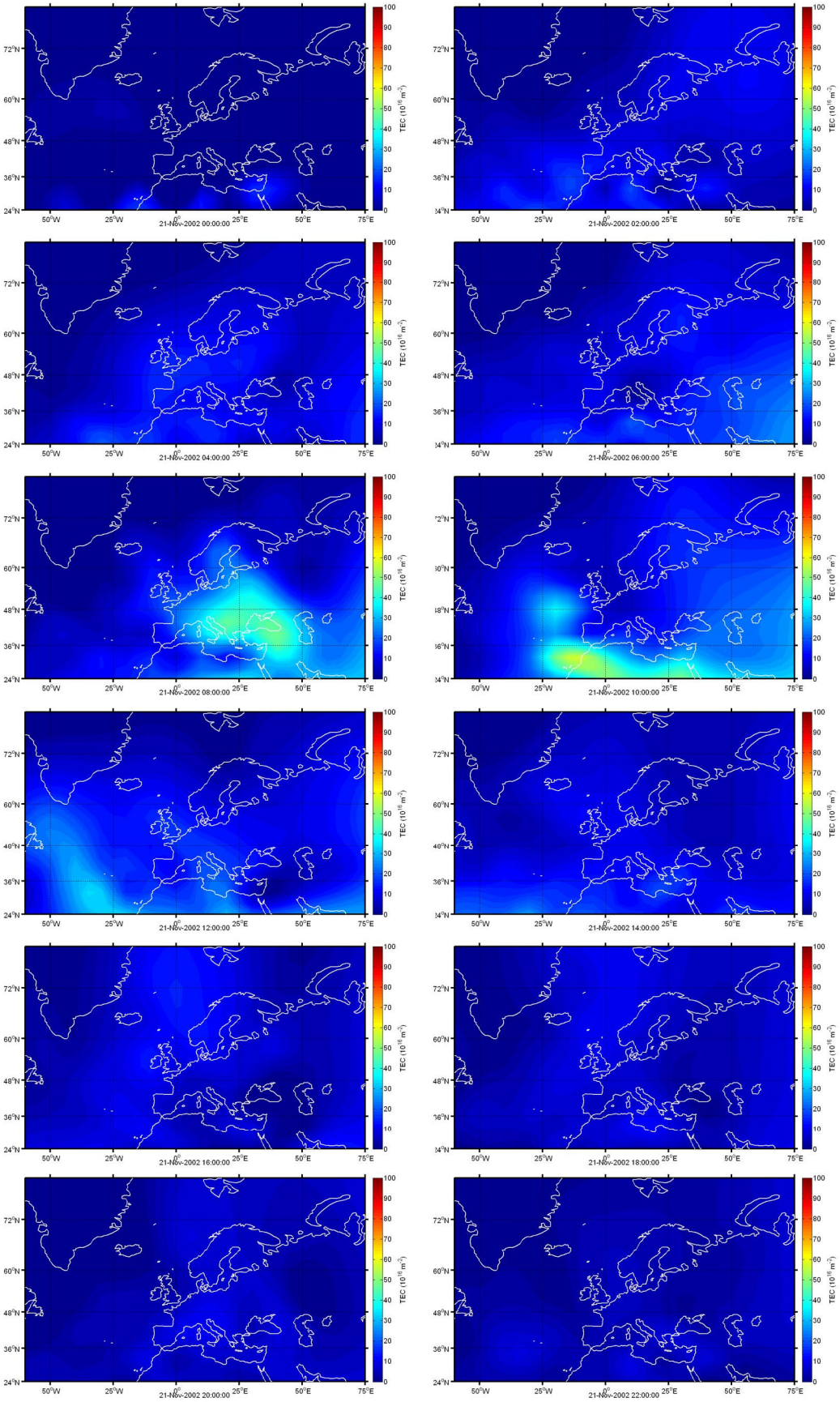

A.5 13th December 2002

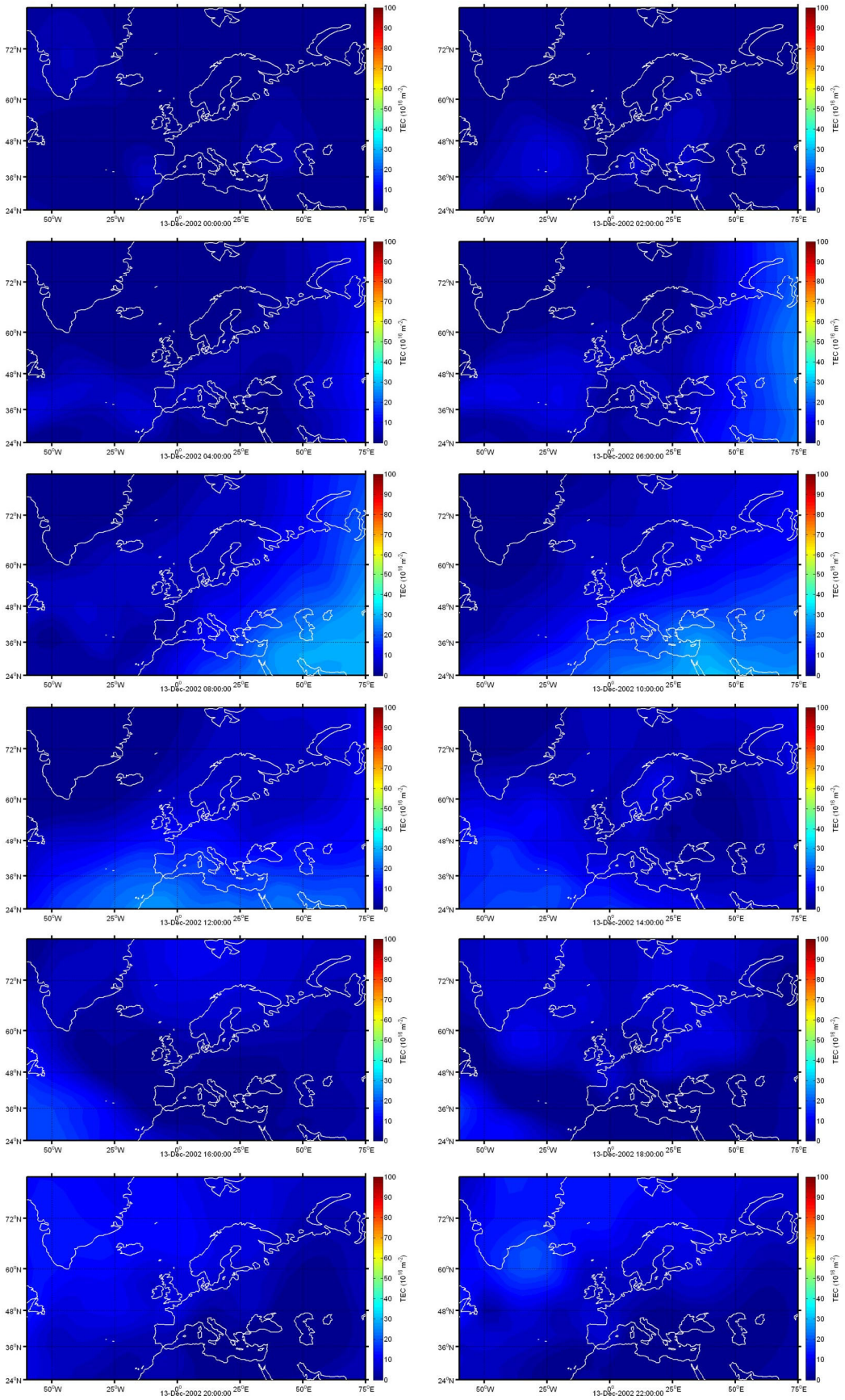

A.6 27th December 2002

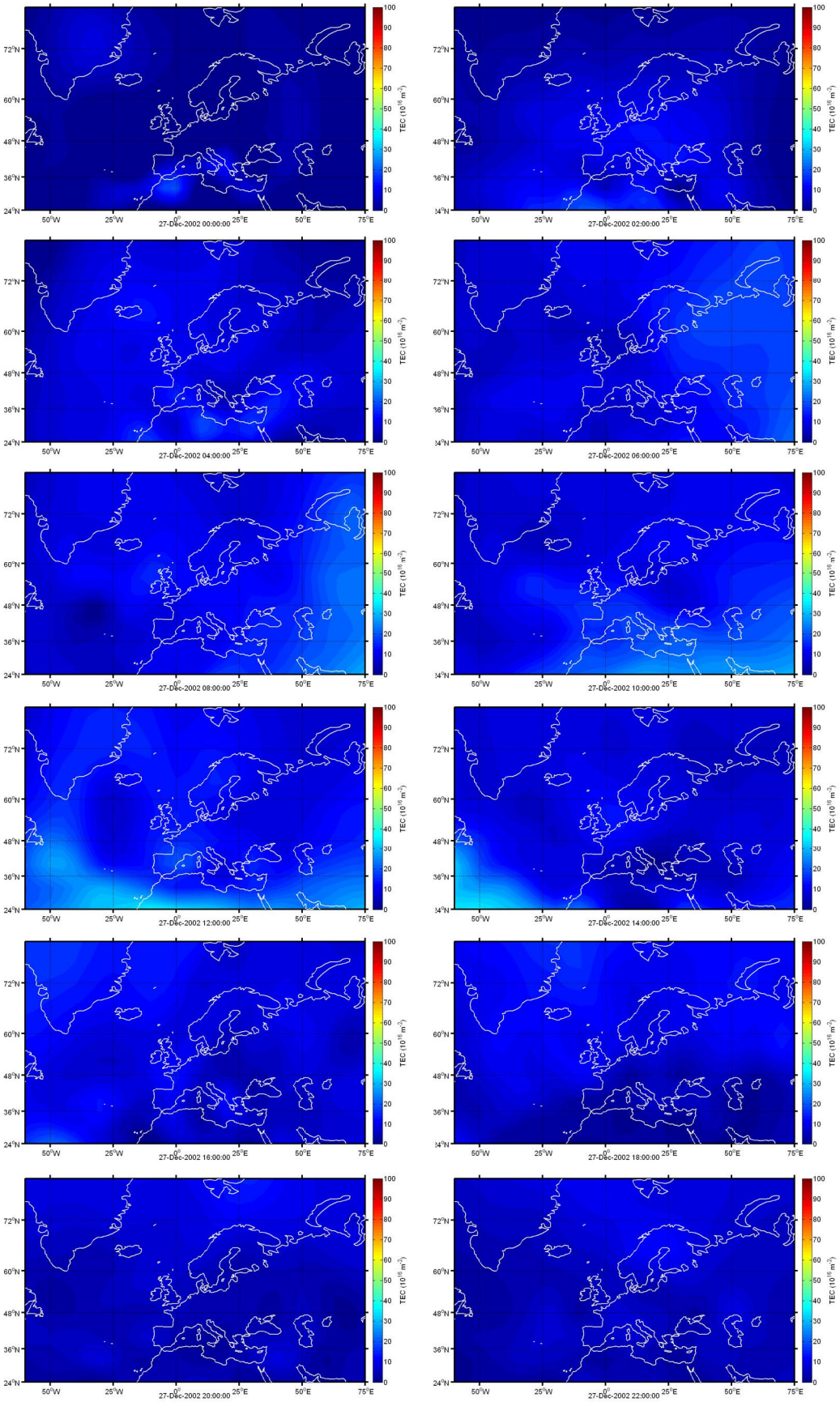

A.7 27th October 2003

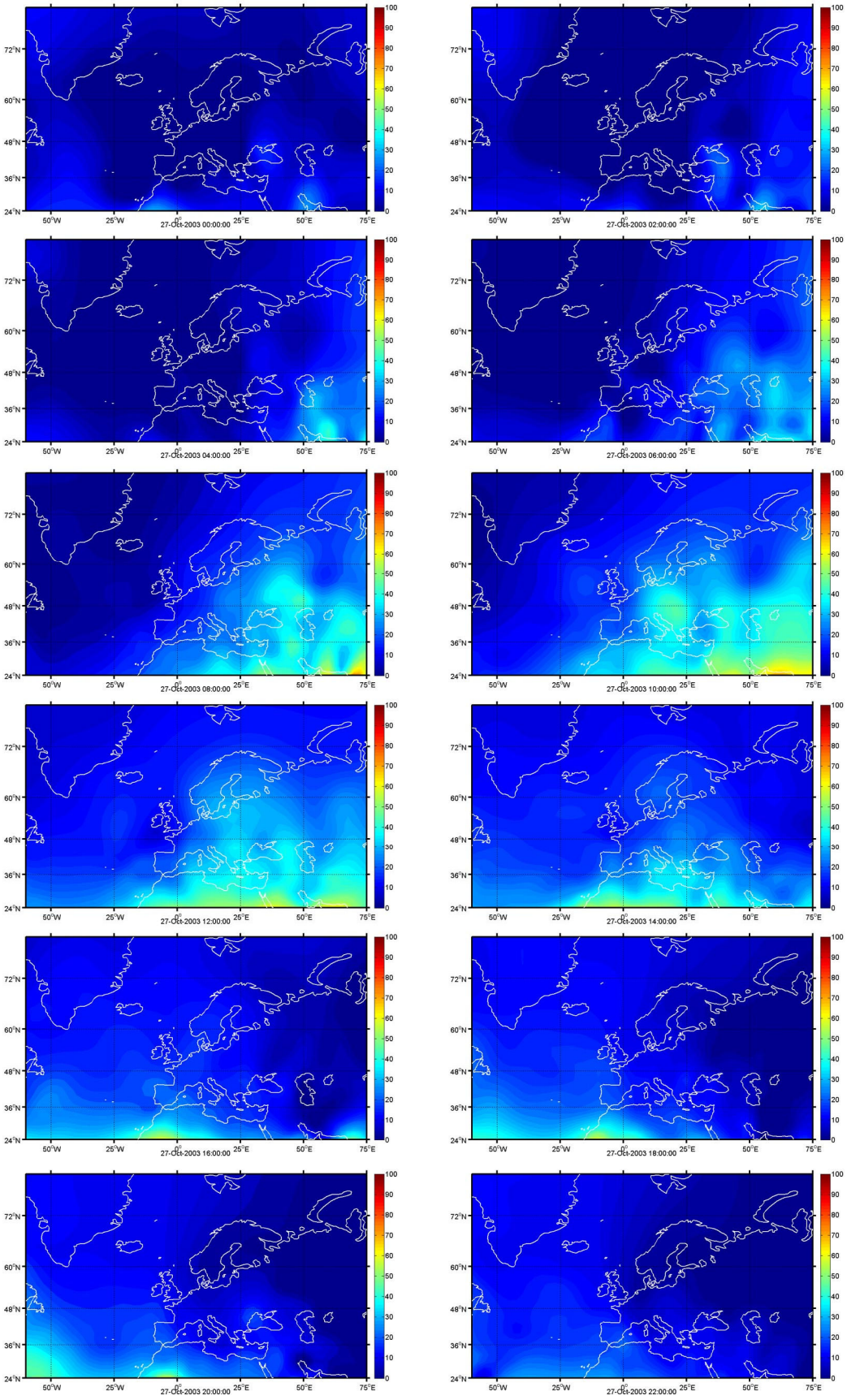

A.8 28th October 2003

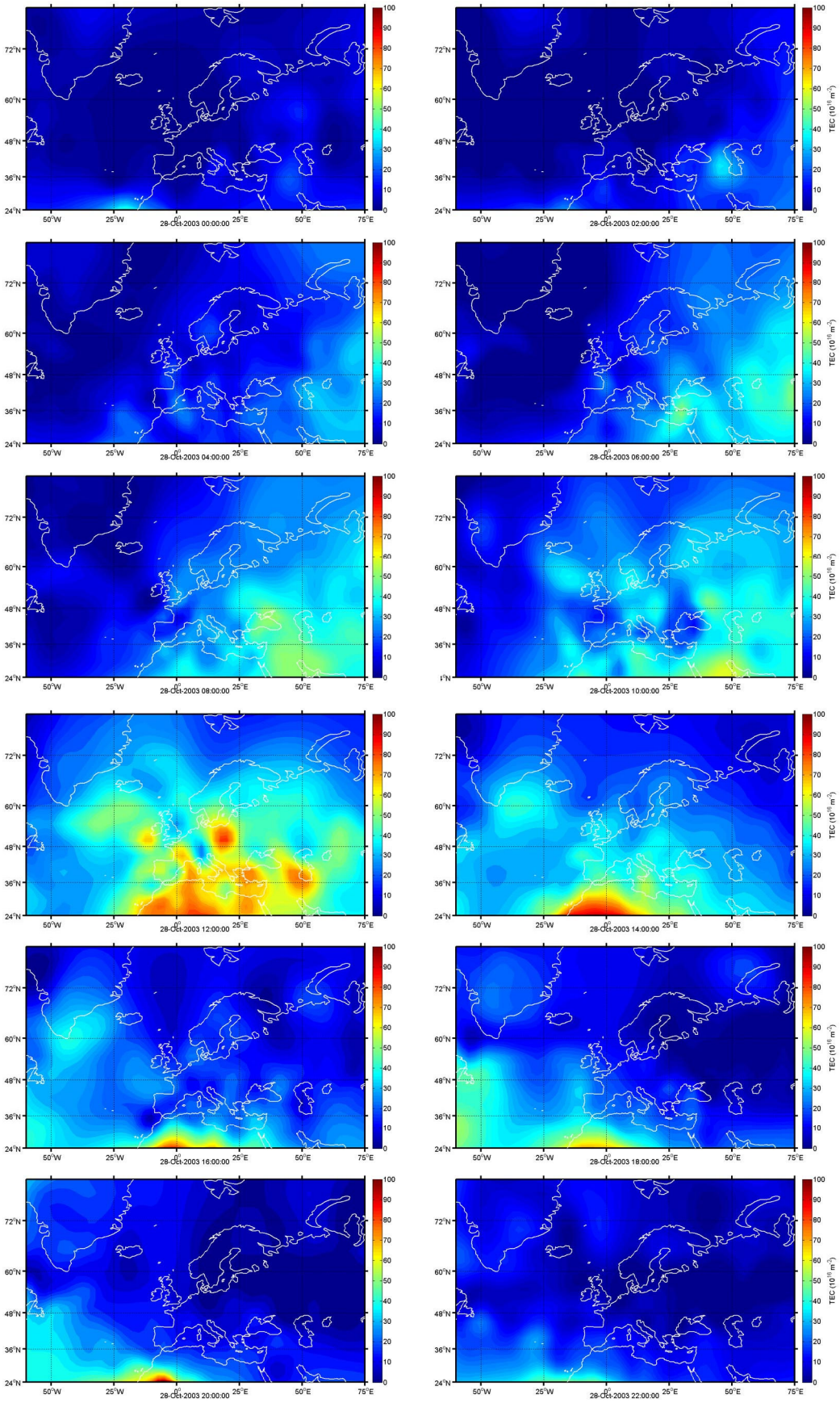

A.9 29th October 2003

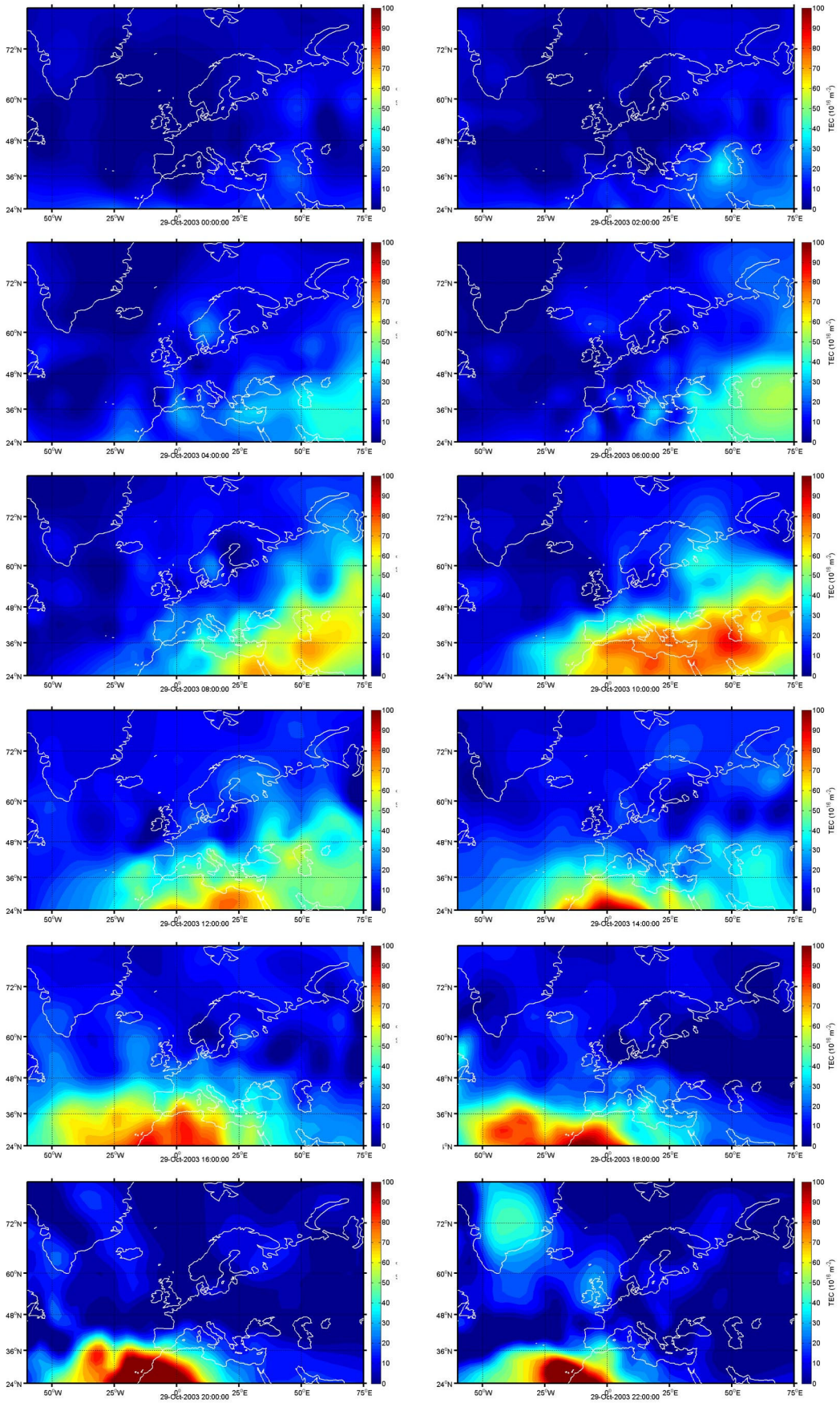

A.10 30th October 2003

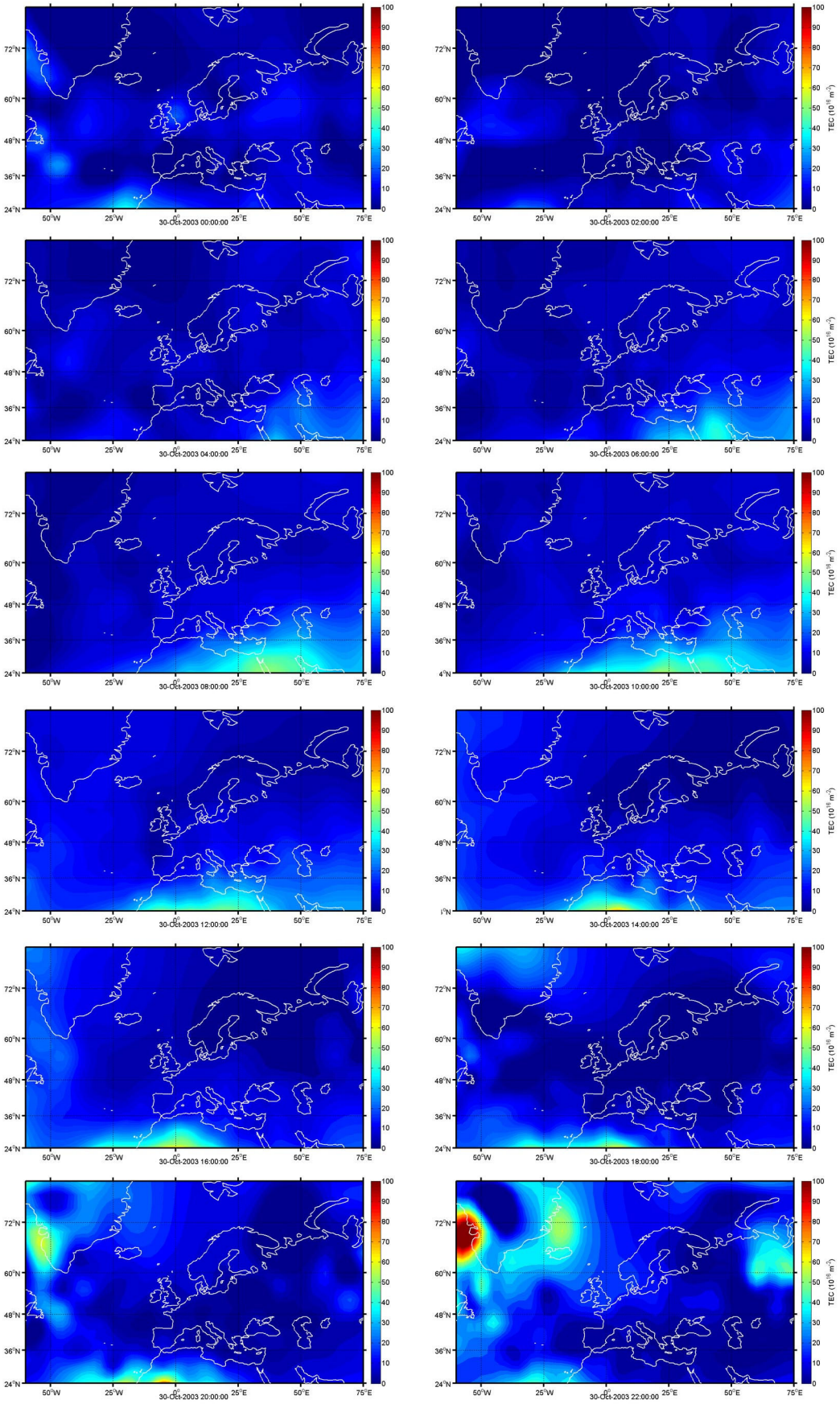

A.11 31st October 2003

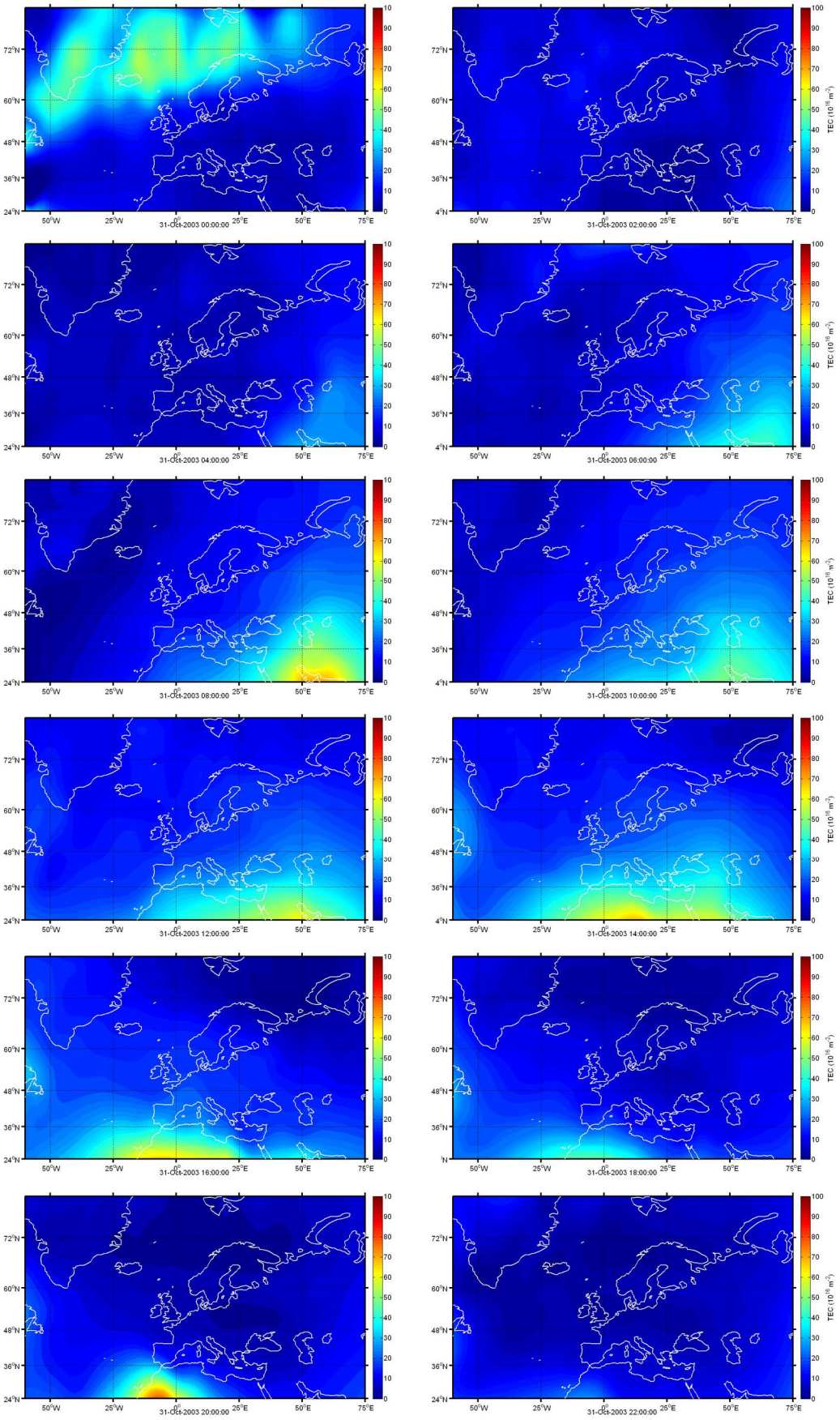

Appendix B

B. Publications

B.1 Journal Papers

1. Rose, J.A.R., Allain, D.J., and Mitchell, C.N. (2009). Reduction in the ionospheric error for a single-frequency GPS timing solution using tomography. *Ann. Geophys.* 52(5), 469-486.

2. Rose, J.A.R., Tong, J.R., Allain, D.J., and Mitchell, C.N. (2011). The use of ionospheric tomography and elevation masks to reduce the overall error in single-frequency GPS timing applications. *Adv. Space Res.* 47(2), 267-288.

B.2 Conference Proceedings

1. Rose, J.A.R., Allain, D.J., and Mitchell, C.N. (2008). *Ionospheric impact on GPS timing applications,* URSI General Assembly. Chicago, USA.

2. Rose, J.A.R., Oyeyemi, E.O., Cilliers, P., and Mitchell, C.N. (2008). *GPS Scintillations: Recent results and future plans,* HMO-UK GPS-based Space Weather Workshop. South Africa.

3. Rose, J.A.R., Tong, J.R., Allain, D.J., and Mitchell, C.N. (2009). *Relationship between GPS satellite elevations and GPS timing accuracy under variable ionospheric conditions*, COSPAR 2nd International Colloquium - Scientific and Fundamental aspects of the Galileo Programme. Padua, Italy.

4. Rose, J.A.R. (2010). *GPS, The Sun and Ionospheric Tomography: British Innovation improving GPS integrity,* SET for Britain. Houses of Parliament, London.

5. Rose, J.A.R., Allain, D.J., and Mitchell, C.N. (2010). *Reducing the Ionospheric error for GPS applications,* European Space Weather Week 2010, Bruge, Belgium.

References

Allain, DJ (2009). Ionospheric delay correction for single-frequency GPS receivers. Electronic and Electrical Engineering, University of Bath. PhD.

Allain, DJ and Mitchell, CN (2009). "Ionospheric delay corrections for single-frequency GPS receivers over Europe using tomographic mapping." GPS Solut. 13(2): 141-151.

Allan, DW (1966). "The statistics of atomic frequency standards." Proc. IEEE 54(2): 221-230.

Allan, DW and Barnes, JA (1981). "A modified Allan variance with increased oscillator characterization ability." Proc. 35th Annu. Symp. on Freq. Contrl.: 470-475.

Allan, DW and Weiss, MA (1980). "Accurate Time and Frequency Transfer During Common-View of a GPS Satellite." Frequency Control, 34th Annual Symposium on. 1980: 334-346.

Anon. (2007). "GALILEO European Satellite Navigation System." Retrieved 6 May 2008, from http://ec.europa.eu/dgs/energy_transport/galileo/index_en.htm.

Anon. (2008a). "GPS Applications." Retrieved 27 May 2008, from http://www.gps.gov/applications/.

Anon. (2008b). "Tomo." Retrieved 9 November 2008, from http://wordinfo.info/words/index.php?v=info&a=view_unit&s=tomo&page=3&u=2158&spage=1.

Austen, JR, Franke, SJ and Lui, CH (1988). "Ionospheric Imaging using Computerized Tomography." Radio Sci 23(3): 299-307.

Axelrad, P, Comp, CJ and Macdoran, PF (1996). "SNR-based multipath error correction for GPS differential phase." IEEE Trans Aerosp. and Electron. Syst. 32(2): 650-660.

Beutler, G, Rothacher, M, Schaer, S, Springer, TA, Kouba, J and Neilan, RE (1999). "The International GPS Service (IGS): An interdisciplinary service in support of Earth sciences." Adv Space Res. 23(4): 631-653.

Bilitza, D (2001). "IRI 2000." Radio Sci. 36(2): 261-276.

Borre, K (2007). A software-defined GPS and Galileo receiver: a single-frequency approach, Birkhäuser.

Braasch, MS and van Dierendonck, AJ (1999). "GPS receiver architectures and measurements." Proceedings of the IEEE 87(1): 48-64.

Bracewell, RN (1956). Strip Integration in Radio Astronomy. 9**:** 198.

Brown, A, Silva, R and Powers, E (2000). "A GPS Receiver Designed For Carrier-Phase Time Transfer." Proceeding of ION National Technical Meeting, January: 32-41.

Bruyninx, C (2004). "The EUREF Permanent Network: a multi-disciplinary network serving surveyors as well as scientists." GeoInformatics 7: 32-35.

Bust, GS and Mitchell, CN (2008). "History, current state, and future directions of ionospheric imaging." Rev of Geophys. 46(1).

Byun, SH (1998). Satellite Orbit Determination Using GPS Carrier Phase In Pure Kinematic Mode, The University of Texas at Austin.

Choi, K, Bilich, A, Larson, KM and Axelrad, P (2004). "Modified sidereal filtering: Implications for high-rate GPS positioning." Geophys. Res. Lett 31: 22.

Clarke, JD, Davis, JA and Lowe, AJ (1998). A Very-Short-Baseline Time Transfer Experiment Using Two Geodetic-Quality GPS Receivers and Carrier Phase Techniques, National Physical Laboratory, UK.

Clarke, JD, Davis, JA and Lowe, AJ (1999). "Characterisatoin of NPL's geodetic GPS time transfer receivers." IEEE Int Freq. Control Symp. 1: 225-229.

Dach, R, Beutler, G, Hugentobler, U, Schaer, S, Schildknecht, T, Springer, T, Dudle, G and Prost, L (2003). "Time transfer using GPS carrier phase: error propagation and results." Journal of Geodesy 77(1): 1-14.

Dach, R, Schildknecht, T, Hugentobler, U, Bernier, LG and Dudle, G (2006). "Continuous geodetic time-transfer analysis methods." IEEE Trans on Ultrasonics, Ferroelectrics, and Frequency Control 53(7): 1250-1259.

Dana, PH (1997). "Global Positioning System (GPS) Time Dissemination for Real-Time Applications." Real-Time Syst. 12(1): 9-40.

Davies, K (1990). Ionospheric Radio, IEE Electromagnetic Waves, Peter Peregrinus Ltd., London, U.K.

Davis, JA (1996). "Delay stability measurements made within a two-way time transfer system using satellite ranging from several locations." European Frequency and Time Forum, 1996. EFTF 96., Tenth (IEE Conf. Publ. 418): 206-211.

Davis, JA, Lewandowski, W, De Young, JA, Kirchner, D, Hetzel, D, Parker, P, Klepczynski, W, De Jong, G, Soring, A, Baumont, F, Bartle, KA, Ressler, H, Robnik, R and Veenstra, L (1996). Comparison of Two-Way Satellite Time and Frequency Transfer and GPS Common-View time transfer during the INTELSTAT field trial. European Frequency and Time Forum, 1996. EFTF 96., Tenth (IEE Conf. Publ. 418).

Defraigne, P and Petit, G (2003). "Time transfer to TAI using geodetic receivers." Metrologia 40(4): 184-188.

Dong, S, Wu, H, Li, X, Guo, S and Yang, Q (2008). "The Compass and its time reference system." 45: S47.

Dow, JM, Neilan, RE and Gendt, G (2005). "The international GPS service: celebrating the 10th anniversary and looking to the next decade." Adv. Space Res. 36(3): 320-326.

Dow, JM, Neilan, RE and Rizos, C (2009). "The International GNSS Service in a changing landscape of Global Navigation Satellite Systems." J Geod 83(3): 191-198.

El-Arini, MB, Conker, RS, Albertson, TW, Reagan, JK, Klobuchar, JA and Doherty, PH (1995). "Comparison of real-time ionospheric algorithms for a GPS Wide-Area Augmentation System(WAAS)." J. Inst. Navig. 41(4): 393-413.

FAA. (2007, 13 Jun 2007). "Navigation Services." Retrieved 11 Jun 2008, from http://www.faa.gov/about/office_org/headquarters_offices/ato/service_units/techops/navservices/gnss/.

Feng, Y (2003). "Combined galileo and GPS: a technical perspective." J. Glob. Position. Syst. 2(1): 67-72.

Foks, A (2004). Latest calibration of GLONASS P-code time receivers, Polish Academy of Sciences Warsaw (Poland) Space Research Centre.

Geier, GJ, King, TM, Kennedy, HL, Thomas, RD and McNamara, BR (1995). "Prediction of the time accuracy and integrity of GPS timing." IEEE Int Freq. Control Symp.: 266-274.

Grewal, MS, Weill, LR and Andrews, AP (2000). Global positioning systems, inertial navigation, and integration, Wiley-Interscience.

GSA. (2008). "GALILEO." Retrieved 06 May 2008, from http://www.gsa.europa.eu/go/galileo/.

Gurtner, W (2002). "RINEX: The Receiver Independent Exchange Format Version 2.10." Bull Am Meteorol Soc. 77: 1-18.

Hanson, DW (1989). Fundamentals of two-way time transfers by satellite, 43rd Annual Frequency Control Symposium: 174-178.

Hargreaves, JK (1992). The Solar-Terrestrial Environment: An Introduction to Geospace--the Science of the Terrestrial Upper Atmosphere, Ionosphere, and Magnetosphere, Cambridge University Press.

Hein, GW (2000). "From GPS and GLONASS via EGNOS to Galileo – Positioning and Navigation in the Third Millennium." GPS Solut. 3(4): 39-47.

Hernández-Pajares, M, Zornoza, JMJ, Subirana, JS and Colombo, OL (2003). "Feasibility of wide-area subdecimeter navigation with GALILEO and Modernized GPS." IEEE Trans. Geosci. Remote Sens. 41(9): 2128-2131.

Hlavac, R and Stacey, PW (2004). Evaluation of Loran Timing Receivers at NPL, National Physical Laboratory (NPL).

Hochegger, G, Nava, B, Radicella, S and Leitinger, R (2000). "A family of ionospheric models for different uses." Phys. Chem. Earth 25(4): 307-310.

Jefferson, DC and Bar-Sever, YE (2000). Accuracy and consistency of broadcast GPS ephemeris data, ION GPS 2000.

Jin, XX and de Jong, CD (1996). "Relationship between satellite elevation and precision of GPS code observations." J. Inst. Navig. 49(2): 253-265.

Kaplan, ED and Hegarty, CJ (2006). Understanding GPS: Principles And Applications, Artech House.

Kintner, PM, Ledvina, BM and de Paula, ER (2007). "GPS and ionospheric scintillations." Space Weather 5(9): S09003.

Kirby, RC and Comm, IRC (1995). History and trends in international radio regulation: 141-146.

Kirchner, D (1991). "Two-way time transfer via communication satellites." Proc. of the IEEE, Special Issue on Time and Frequency 79(7): 983-990.

Klobuchar, JA (1987). "Ionospheric time-delay algorithm for single-frequency GPS users." IEEE Trans. Aerosp. Electron. Syst. 23(3): 325-331.

Kouba, J and Heroux, P (2001). "GPS precise point positioning using IGS orbit products." GPS Solut. 5(2): 12-28.

Kouba, J and Springer, T (2001). "New IGS Station and Satellite Clock Combination." GPS Solut. 4(4): 31-36.

Langley, RB (1997). "The GPS Error Budget." GPS World 8(3): 51-56.

Larijani, LC (1998). GPS for Everyone: How the Global Positioning System Can Work for You, AIAA (American Institute of Aeronautics & Astronautics).

Larson, KM and Levine, J (1999). "Carrier-phase time transfer." Ultrasonics, Ferroelectrics and Frequency Control, IEEE Transactions on 46(4): 1001-1012.

Lee, SW (2009). "Real-time formation of a time scale using GPS carrier-phase time transfer network." Metrol. 46: 693-703.

Lewandowski, W and Azoubib, J (2000). "Time transfer and TAI." Frequency Control Symposium and Exhibition, 2000. Proceedings of the 2000 IEEE/EIA International: 586-597.

Lewandowski, W, Azoubib, J and Klepczynski, WJ (1999). GPS: primary tool for time transfer, Proc. of the IEEE.

Lewandowski, W and Thomas, C (1991). "GPS time transfer." Proceedings of the IEEE 79(7): 991-1000.

Lombardi, MA, Ed. (2002). Fundamentals of time and frequency, CRC Pr LLC.

Matsunaga, K, Hoshinoo, K and Igarashi, K (2003). "Observations of ionospheric scintillation on GPS signals in Japan." J. Inst. Navig. 50(1): 1-7.

McNamara, LF (1991). The ionosphere: communications, surveillance, and direction finding, Krieger Pub. Co., Malabar, Fla.

Meggs, RW and Mitchell, CN (2006). "A study into the errors in vertical total electron content mapping using GPS data." Radio Sci. 41(1).

Meggs, RW, Mitchell, CN and Spencer, PSJ (2004). "A comparison of techniques for mapping total electron content over Europe using GPS signals." Radio Sci. 39.

Mitchell, CN, Alfonsi, L, De Franceschi, G, Lester, M, Romano, V and Wernik, AW (2005). "GPS TEC and scintillation measurements from the polar ionosphere during the October 2003 storm." Geophys. Res. Lett. 32(12): L12S03.

Mitchell, CN and Spencer, PSJ (2003). "A three-dimensional time-dependent algorithm for ionospheric imaging using GPS." Ann. Geophys. 46(4): 687-696.

NASA. (2008). "Magnetosphere Rendition." Retrieved 12 June 2008, from http://sec.gsfc.nasa.gov/popscise.jpg.

NIST. (2008a). "Time and Frequency Transfer Using the Phase of the GPS Carrier." Retrieved 25 January 2008, from http://tf.nist.gov/timefreq/time/carrierphase.htm.

NIST. (2008b). "Two Way Time Transfer." Retrieved 23 January 2008, from http://tf.nist.gov/time/twoway.htm.

Parkinson, BW and Spilker, JJ (1996). Global Positioning System: Theory and Applications, vol 1, AIAA.

Petit, G and Jiang, Z (2008). "GPS All in View time transfer for TAI computation." Metrol. 45: 35-45.

Petit, G and Thomas, C (1996). "GPS frequency transfer using carrier phase measurements." Frequency Control Symposium, 1996. 50th., Proceedings of the 1996 IEEE International.: 1151-1158.

Radicella, SM and Leitinger, R (2001). "The evolution of the DGR approach to model electron density profiles." Adv. Space Res. 27(1): 35-40.

Ragheb, A, Clarke, P and Edwards, S (2007). "GPS sidereal filtering: coordinate- and carrier-phase-level strategies." J Geod 81(5): 325-335.

Ray, J and Senior, K (2003). "IGS/BIPM pilot project: GPS carrier phase for time/frequency transfer and timescale formation." Metrol. 40(4): 205-205.

RCR. (2008). "Common terms." Retrieved 9 November 2008, from http://www.rcr.ac.uk/content.aspx?PageID=489.

Riley, WJ (2008). Handbook of Frequency Stability Analysis, US Dept. of Commerce, National Institute of Standards and Technology.

Rose, JAR, Allain, DJ and Mitchell, CN (2009). "Reduction in the ionospheric error for a single-frequency GPS timing solution using tomography." Ann. Geophys. 52(5): 469-486.

Rose, JAR, Tong, JR, Allain, DJ and Mitchell, CN (2011). "The use of ionospheric tomography and elevation masks to reduce the overall error in single-frequency GPS timing applications." Adv. Space Res. 47(2): 267-288.

Roth, GL, Schick, P, Jacoby, J, Schweitzer, C, Gervasi, D and Wiley, E (2005). Enhanced or eLoran for time and frequency applications. Frequency Control Symposium and Exposition, 2005. Proceedings of the 2005 IEEE International.

Schmid, R, Steigenberger, P, Gendt, G, Ge, M and Rothacher, M (2007). "Generation of a consistent absolute phase-center correction model for GPS receiver and satellite antennas." J Geod. 81(12): 781-798.

Senior, K and Ray, J (2001). "Accuracy and Precision of GPS Carrier Phase Clock Estimates." Proc. 33rd Annual Precise Time and Time Interval (PTTI) Applications and Planning Meeting (Long Beach, CA, 27–29 November 2001: 199–217.

Shemar, LS and Davis, JA (1999). "A study of delay instabilities within a two-way satellite time and frequency transfer Earth station." IEEE Int Freq. Control Symp. 1: 208-212.

Skoug, RM, Gosling, JT, Steinberg, JT, McComas, DJ, Smith, CW, Ness, NF, Hu, Q and Burlaga, LF (2004). "Extremely high speed solar wind: 29–30 October 2003." J Geophys Res. 109(A9): A09102.

Smith, DA, Araujo-Pradere, EA, Minter, CF and Fuller-Rowell, TJ (2008). "A comprehensive evaluation of the errors inherent in the use of a two-dimensional shell for modeling the ionosphere." Radio Sci 43: RS6008.

Spencer, PSJ and Mitchell, CN (2007). "Imaging of fast moving electron-density structures in the polar cap." Ann. Geophys. 50(3): 427-434.

Steele, JMA, Markowitz, W and Lidback, CA (1964). "Telstar time synchronization." IEEE Trans. Instrum. Meas. 13(4): 164-170.

Takahashi, F, Imamura, K, Kawai, E, Lee, CB, Lee, DD and Chung, NS (1993). "Two-way Time Transfer Experiments Using an INTELSAT Satellite in a Inclined Geostationary Orbit." IEEE Transactions on Instrumentation and Measurement 42(2).

Tascione, TF (1994). Introduction to the space environment, Krieger Publishing Co.

Weiss, MA, Petit, G and Jiang, Z (2005). A comparison of GPS Common-View time transfer to All-in-View. Frequency Control Symposium and Exposition, Proc. IEEE Int.